Graduate School Form 30
Updated 1/15/2015

PURDUE UNIVERSITY
GRADUATE SCHOOL
Thesis/Dissertation Acceptance

This is to certify that the thesis/dissertation prepared

By Dana Bors

Entitled

Development of Total Vaporization Solid Phase Microextraction and Its Application to Explosives and Automotive Racing

For the degree of Doctor of Philosophy

Is approved by the final examining committee:

John Goodpaster
Chair

Christine Picard

Paul Shepson

Graham Cooks

To the best of my knowledge and as understood by the student in the Thesis/Dissertation Agreement, Publication Delay, and Certification Disclaimer (Graduate School Form 32), this thesis/dissertation adheres to the provisions of Purdue University's "Policy of Integrity in Research" and the use of copyright material.

Approved by Major Professor(s): John Goodpaster

Approved by: Eric Long

Head of the Departmental Graduate Program Date

DEVELOPMENT OF TOTAL VAPORIZATION SOLID PHASE MICROEXTRACTION AND ITS APPLICATION TO EXPLOSIVES AND AUTOMOTIVE RACING

A Dissertation

Submitted to the Faculty

of

Purdue University

by

Dana E. Bors

In Partial Fulfillment of the

Requirements for the Degree

of

Doctor of Philosophy

December 2015

Purdue University

West Lafayette, Indiana

For my parents. Thank you for encouraging me to chase my dreams and reminding me to put on my crown.

ACKNOWLEDGMENTS

First, I would like to thank my advisor John Goodpaster for his unending support and guidance. I would also like to thank Sergeant Leonard Langland and the members of the Indiana State Police Bomb Squad for initiating all explosive devices. Tim White and Bob Lang of the National Hot Rod Association were generous in providing insight into the drag racing community. Finally, I would like to thank all students at IUPUI who made my graduate experience a memorable one.

TABLE OF CONTENTS

Page

Page

LIST OF TABLES

LIST OF FIGURES

Figure Page

Figure Page

ABSTRACT

Bors, Dana E. Ph.D., Purdue University, December 2015. Development of Total Vaporization Solid Phase Microextraction and Its Application to Explosives and Automotive Racing. Major Professor: John V. Goodpaster.

Pipe bombs are a common form of improvised explosive device, due in part to their ease of construction. Despite their simplistic nature, the lethality of pipe bombs should not be dismissed. Due to the risk of harm and their commonality, research into the pipe bomb deflagration process and subsequent chemical analysis is necessary.

The laboratory examination of pipe bomb fragments begins with a visual examination. While this is presumptive in nature, hypotheses formed here can lead to subsequent confirmatory exams. The purpose of this study was to measure the mass and velocity of pipe bomb fragments using high speed video. These values were used to discern any trends in container type (PVC or black/galvanized steel), energetic filler (Pyrodex or double base smokeless powder), and ambient temperature (13°C and -8°C). The results show patterns based on container type, energetic filler, and temperature.

The second stage of a laboratory exam is chemical analysis to identify any explosive that may be present. Legality calls for identification only, not quantitation. The purpose of this study is to quantitate the amount of explosive residue on post-blast pipe bomb fragments. By doing so, the instrumental sensitivities required for this type of analysis will be known. Additionally, a distribution of the residue will be mapped to provide insight into the deflagration process of a device. This project used a novel sampling technique called total vaporization solid phase microextraction. The method was optimized for nitroglycerin, the main energetic in double base smokeless powder.

Detection limits are in the part per billion range. Results show that the concentration of residue is not uniform, and the highest concentration is located on the endcaps regardless of container type.

Total vaporization solid phase microextraction was also applied to automotive racing samples of interest to the National Hot Rod Association. The purpose of this project is two-fold; safety of the race teams in the form of dragstrip adhesive consistency and monitoring in the form of fuel testing for illegal adulteration. A suite of analyses, including gas chromatography mass spectrometry, infrared spectroscopy, and evaporation rate, were developed for the testing of dragstrip adhesives. Gas chromatography mass spectrometry methods were developed for both nitromethane based fuel as well as racing gasolines. Analyses of fuel from post-race cars were able to detect evidence of adulteration.

Not only was a novel technique developed and optimized, but it was successfully implemented in the analysis of two different analytes, explosive residue and racing gasoline. TV-SPME shows tremendous promise for the future in its ability to analyze a broad spectrum of analytes.

CHAPTER 1. THE ANATOMY OF A PIPE BOMB EXPLOSION: MEASURING THE MASS AND VELOCITY DISTRIBUTIONS OF CONTAINER FRAGMENTS

1.1 Introduction

Pipe bombs are a common type of Improvised Explosive Device (IED) that can be constructed from readily available materials found at local hardware and sporting goods stores. Pipe bombs typically contain deflagrating low explosive powders (i.e., black powder, black powder substitutes, and smokeless powder). As pipe bombs utilize low explosives as the main charge, the pipe serves as a rigid container that confines the deflagration until the pipe expands and eventually fails, resulting in an explosion. Although pipe bombs are crude in design, they can also be lethal. For example, during a demonstration of civil unrest in Northern Ireland, a pipe bomb killed a 16 year old boy as he raised his arm to throw it. His hand was severely mangled and nearly amputated. Shrapnel gashed the back of his head exposing fractured skull and brain matter[1]. Ted Kaczynski, commonly known as the Unabomber, killed Hugh Scrutton using a pipe bomb packed with nails[2]. Furthermore, pipe bombs constitute the bulk of the United States' bombing incidents. Since 1978, the U.S. Bureau of Alcohol, Tobacco, Firearms and Explosives (ATF) has reported 25,000 bombings and attempted bombings, as well as 21,000 incidents with recovered explosives or devices[3].

The pipes used in pipe bombs are typically made of polyvinyl chloride (PVC), chlorinated polyvinyl chloride (CPVC), black steel, or galvanized steel. Given that such pipes are intended for use in plumbing applications, they conform to a number of standards and conventions. For example, the outer diameters of all commercially available pipes must conform to Nominal Pipe Size (NPS) that does not always match the actual outer diameter (e.g., a 2.54 cm nominal diameter pipe is actually 3.34 cm outer

diameter). In addition, the wall thickness of pipe is dictated by schedules, with one of the most common being Schedule 40 (e.g., a 2.54 cm nominal diameter Schedule 40 pipe must have walls that are 0.338 cm thick).

The protocols for the laboratory examination of a pipe bomb that has either been rendered safe or functioned as designed will vary depending upon the laboratory involved. However, one can generalize these protocols into three main stages: an initial visual/microscopic exam to photograph and document the evidence, chemical analyses to identify any intact explosive particles or residues that may be present, and an examination of any device components that may be present.

Much time and attention has been focused on the second stage of this process. For example, chemical and instrumental methods for identifying low explosives and their post-blast residues are well established and described in various books and book chapters[4-7]. The third stage, the identification and comparison of IED components, is also well-established as it involves many of the same analytical techniques applied to items such as tape, fuses, wires, batteries, etc. In contrast, only a small amount of published research is available that is focused on the first stage of this process. This stage, although necessarily presumptive in nature, is no less important given that the type of analyses required for different explosive fillers can vary dramatically. A well-formed hypothesis can help direct subsequent exams and adds probative value by linking direct observations with instrumental results.

In particular, during a visual/microscopic exam, one can begin to formulate a hypothesis as to the explosive filler based upon the size, shape and number of container fragments that are present. For example, steel pipe bombs containing black powder or black powder substitutes will produce few large fragments. The end cap face plates are often blown out and fragments will exhibit square, 90° edges. Heavy grey or black residue will be present on the interior surfaces of the pipe. Finally, the pipe may be rusted due to the formation of corrosive by-products. In contrast, steel pipe bombs containing double-base smokeless powder (DBSP) will have no apparent residue.

There will be extensive fragmentation, including 90° breaks as well as 45° reversing slants on edges (this is known as "stepping"). Finally, the pipe fragments may be thinned due to the force of the explosion.

These characteristics are based upon the extensive experience of forensic chemists, but they also draw support from many decades of research into the behavior of cylindrical explosive devices. Although many of these studies were focused on military high explosives, their general conclusions are still useful and many of their observations are also seen in pipe bombs filled with highly energetic low explosives like double-base smokeless powder. For example, Taylor et al investigated the effect of tensile and compressive stress on fracture radii, concluding a proportional relationship[8,9]. Tensile stress is the tension that results when materials resist elongation as equal and opposite forces are applied to them. Compressive stress is tension in multiple directions acting on a material causing shortening. These stresses both influence the extent to which a tube can expand before it begins to fracture. With the inclusion of detonation pressure as a variable, it was found that the diameter of a tube expands to nearly twice the original size before fragmentation occurs. This, in turn, leads to thinning of the container walls. The first fractures appear along planes of maximum shear stress, usually along the longitudinal axis[10]. Stepping, also called a shear lip fracture, is also present when high pressures are generated inside the device[10].

Computational modeling of cylinders by Anderson et al explains that the majority of the velocity of casing fragments is obtained before fragmentation occurs[11]. In other words, the acceleration of the tube material is most active when the tube is still intact. Furthermore, following fragmentation of a cylindrical device, a correlation exists between a fragment's projection angle and its speed, as well as the detonation velocity of the bomb:

$$\theta = \sin^{-1}\left(\frac{V_0}{2U}\right) \qquad \text{(Equation 1-1)}$$

where Θ is the angle relative to the normal to the surface, V_0 is the speed, and U is the detonation velocity[12]. This formula is valid when flow is largely one dimensional, common with long artillery projectiles. Finally, Gurney developed an equation that relates initial fragment velocity to properties of the explosive and container:

$$V_0 = (2E')^{\frac{1}{2}} \times \left(\frac{\frac{W}{W_c}}{1+\frac{W}{2W_c}}\right)^{\frac{1}{2}} \quad \text{(Equation 1-2)}$$

where V_o is the initial fragment velocity, $(2E')^{\frac{1}{2}}$ is the Gurney constant, W is the weight of the explosive, and W_c is the weight of the casing[13]. The Gurney energy constant varies with explosive type, and is usually about one-third of the value of the detonation velocity[14]. This equation is also only effective for one dimensional flow and some circumstances require more detailed calculations.

Overall, this summary highlights that while the investigation of fragmentation patterns and velocities is not new, there is a need to apply these and other methods to low explosive devices used by amateurs. One the other hand, attempts to characterize IED's using the mass of post blast fragments with respect to container type and filler energy has been demonstrated, most notably by J.C. Oxley et al[15]. FWDM's (Fragment Weight Distribution Maps), used by Oxley, were employed to characterize the distribution of fragment masses. To construct a FWDM, the relative mass of a given fragment versus the mass of that fragment divided by the mass of all fragments of higher mass were plotted[15]. Equation 1-3 is the equation for FWDM's where M_r=the mass of the n*th* fragment plus all fragments heavier than the n*th* fragment, M_n=the mass of the n*th* fragment, M_{total}= the total mass of all fragments collected, and m=slope. In practice, a value of two was added to the y-axis component of the equation to assure that FWDM's reside in the first quadrant graphically.

$$\log(M_r/M_{total}) = m(\,M_n/M_{total}) \quad \text{(Equation 1-3)}$$

It is important to note that Oxley's experiments utilized secondary containers to recover as much of the pipe fragments as possible. However, an FWDM is intended to be relatively insensitive to fragment recovery percentage, making this an attractive characterization method.

The use of FWDMs as a forensic tool has been challenged by Dean et al, who claims that the proportion of fragments recovered should not be used as a quantitative measure[16]. In other words, since both the ordinate and abscissa of the FWDM are normalized by the total number of fragments recovered, the slope is still considered to be slightly dependent on the total recovery. Because of this, bias will be present based on the

total fragments recovered; therefore, using a proportion of fragments for characterization purposes is inaccurate. Following this reasoning, the Held equation, specifically the constant B, is rejected as a valid quantitative method as well. The constant B is a function of the total mass recovered in addition to the mass of the largest fragment, yielding misleading data if the total recovery is reduced[16]. The Held equation is:

$$M(n) = M_0 * [1 - e^{-Bn^{\lambda}}] \qquad \text{(Equation 1-4)}$$

where M(n) is the cumulative fragment mass, or the overall mass of the heaviest n fragments, M_o is the total mass of all fragments, n is the cumulative fragment number beginning with the heaviest fragment, and B and λ are constants[17]. Besides mass, other physical characteristics of container fragments have been examined. This has included microstructure deformation and hardness, in order to correlate explosive properties with material response. Walsh et al concludes that as the detonation pressure and velocity increase, microstructure deformation increases as well, to the point of localized recrystallization in some cases[18]. At low detonation velocities and pressure, the hardness increased immediately, compared to a plateau at medium velocities and a decrease in hardness with high energy fillers. Gregory et al expanded on Walsh's qualitative study, in an attempt to produce quantitative results. Work hardening was monitored by microhardness, specifically in the form of Knoop hardness values. Values increased with increasing energy fillers, also causing a large aspect ratio due to pearlite deformation[19]. Pipe thinning was directly correlated to the amount of plastic deformation caused by the resulting pressure wave, therefore the use of a high energy filler would result in a decrease of pipe thickness.

Overall, it is our opinion that the potential for pipe bomb fragments to injure or kill is not fully appreciated. In addition, the lethality of pipe bombs that do not contain shrapnel is largely based upon the velocity and mass of container fragments leaving the site of a pipe bomb explosion. Hence, we have measured the velocity and mass of pipe bomb container fragments using a high speed video camera and an analytical balance, respectively. The aim of this chapter is to demonstrate the major trends that exist for various container types (i.e., PVC, black steel and galvanized steel) as well as filler (i.e., Pyrodex and double-base smokeless powder). Pyrodex and double base smokeless

powder are both low explosives, however DBSP is more energetic because of higher gas and heat production. In particular, our hypothesis is that fragment mass distributions (expressed as either simple histograms or FWDM slopes) can indicate the explosive filler and that the velocity of fragments will be proportional to the explosive power of the filler. We will also display velocity data in the form of novel Particle Velocity Vector Maps (PVVM) which are displayed as the paths or tracks taken by the fragments overlaid on top of a representation of the pipe bomb. In addition, our results include a surprising anomaly in the slopes of our FWDM plots as well as a larger than expected distribution of fragment velocities.

1.2 Materials and Methods

A total of seven devices were exploded. For all devices, the explosive filler was either Hodgdon Pyrodex or Alliant Red Dot double-base smokeless powder (DBSP) purchased from sporting goods stores. All devices were constructed from 20.32 cm lengths of 2.54 cm nominal diameter Schedule 40 pipe purchased from hardware stores. These pipes were constructed from galvanized steel, black steel (steel pipe with a black lacquer coating), and PVC, respectively. All devices were capped at both ends with the corresponding material type. For the metal devices, endcaps were composed of cast iron, rather than milled steel. One end cap was drilled on each device with a 0.48 cm hole to accommodate the igniter wires.

All devices were assembled and initiated via electric match (seen on the right in all stepwise frames). The Indiana State Police Bomb Squad assembled and exploded the devices in a gravel pit in Noblesville, IN. Two containment structures, one for each filler type, were constructed with dimensions of approximately 2.44 m x 2.44 m x 1.22 m from 1.91 cm plywood. Each device was suspended from a lumber strut via fishing line so that the IED was approximately 0.6 m from the ground (Figure 1-1).

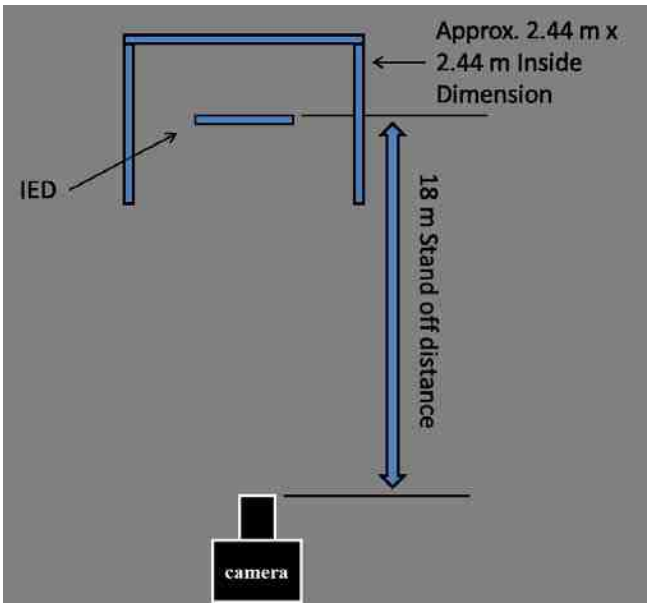

Figure 1-1 Schematic of experimental setup.

The first two devices consisted of a PVC pipe filled with double-base smokeless powder. These were used to validate the frame rate (10,000 frames per second) and shutter speed (19.6 ms) of the high speed video camera. These parameters were then used on each of the successive devices. The videos that captured the explosions were analyzed using ProAnalyst software (Xcitex, Cambridge, MA). Individual fragments were tracked within the software and their velocity was calculated by plotting the XY position (in pixels) of the fragment as a function of time to yield a velocity in pixels per second. The velocities were then converted from pixels/s to cm/s by calculating the number of pixels/cm for the outer diameter of the pipe (3.340 cm), which was visible in the footage prior to the blast. The velocities of individual fragments were then plotted using particle velocity vector maps (PVVM). PVVMs depict a two dimensional representation of the improvised explosive device, along with numerous fragments whose trajectories could be tracked in the high speed video footage. It is important to note that due to the geometry of the camera setup, all fragments were tracked only in two dimensions. Given that fragments can travel in and out of the plane of focus for the camera, all velocity values are minimum estimates. The following equation depicts the relationship between velocities obtained from the high speed imaging and the actual velocities:

$$Actual = measured/\cos\theta \qquad \text{(Equation 1-5)}$$

In future work, it is hoped to utilize two cameras to simultaneously record the event and then reconstruct a three dimensional trajectory for container fragments, thereby avoiding this source of error.

Post blast fragments were collected and placed into cans corresponding to pipe material type and filler. All personnel wore latex gloves to prevent cross contamination. Post blast fragment masses were recorded using a Fisher Scientific analytical balance (Accuseries-124; Pittsburgh, PA). The distribution of fragment masses was visualized using histograms and FWDM's with respect to container and filler type.

1.3 Results and Discussion

1.3.1 Visual and Microscopic Examination

The fragment edge profiles were analyzed via visual inspection and photography either by digital camera or stereomicroscope when greater magnification was needed. The PVC IED's regardless of filler generated many small fragments and all containers were completely destroyed. However, there was a difference between the size of fragments between the low power and high power fillers with smaller fragments for the Alliant Red Dot Devices than for the Pyrodex devices.

The metallic devices filled with Pyrodex produced fragments that were relatively large, thus leaving fewer to collect. Many of these devices only generated end cap fragments and very small number of body fragments typically leaving a large portion of the device intact. The edge profiles of these fragments for the most part demonstrated a 90° break with respect to the exterior surface of the device.

In contrast, the higher energy filler, Alliant Red Dot, generated much smaller fragments and destroyed most of the device upon explosion. The fragment edge profiles for these devices were jagged and demonstrated a classic saw-tooth like pattern typically seen in high explosive container fragments known as *stepping*.

Transitions between smooth 90° edges and stepped edges on some of the larger fragments can be seen in some of these metallic fragments.

1.3.2 Velocity Measurements

Histograms were used to graphically display the distribution of fragment velocities from devices constructed from PVC, black steel and galvanized steel (Figures 1-2 through 1-4). For example, Figure 1-2 shows the distribution of velocities for the three PVC devices. The two PVC devices with DBSP filler exhibited a near Gaussian distribution of velocities with similar means. In contrast, the PVC device with Pyrodex filler had more fragments traveling at lower velocities as well as a wider range of overall velocities. Figures 1-3 and 1-4 show the distribution of velocities for the black steel and galvanized steel devices respectively. In both cases, Pyrodex filler generated fragments with lower velocities, whereas the devices with DBSP filler generated fragments with higher average velocities that spanned a very wide range. In comparison, the Pyrodex filler generated lower velocities that were more clustered around a central point.

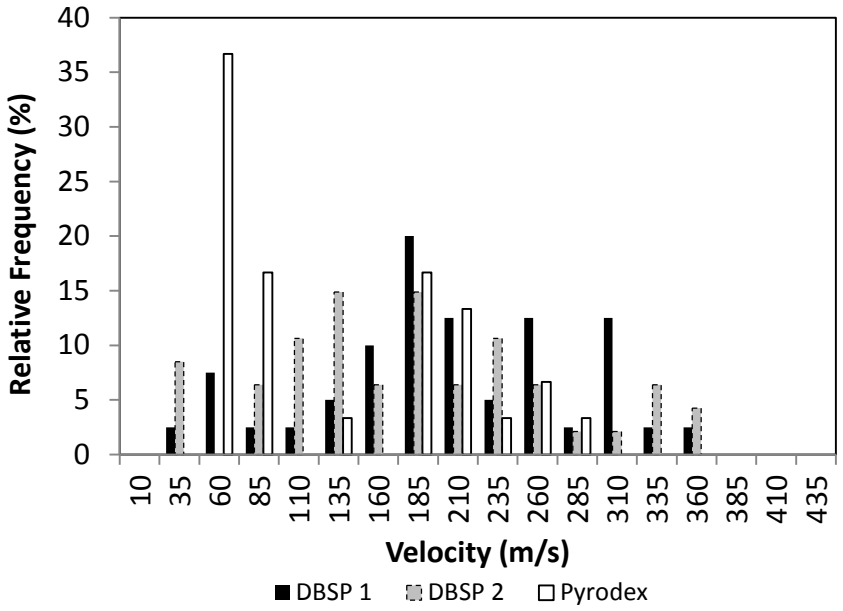

Figure 1-2 Velocity histogram of PVC devices with two different energetic fillers.

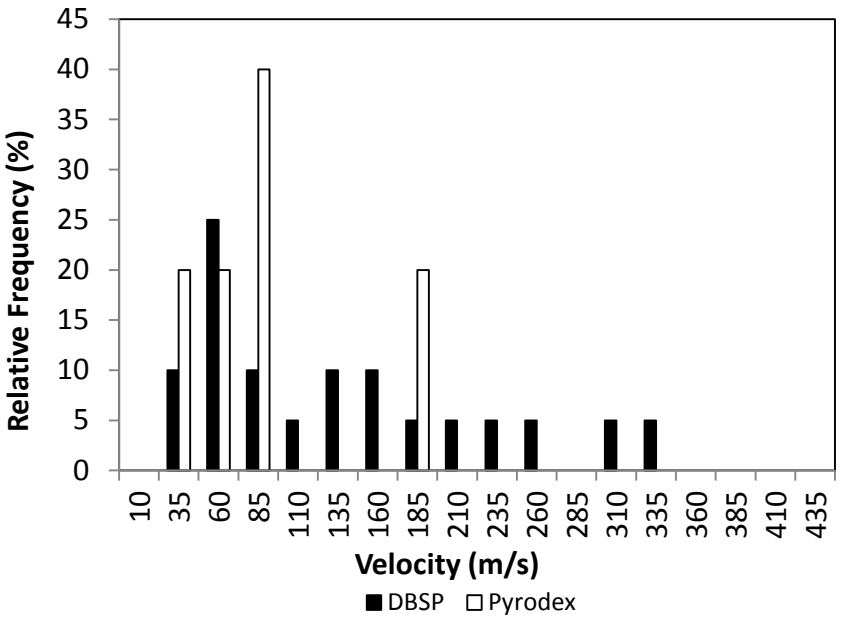

Figure 1-3 Velocity histogram showing black steel devices filled with DBSP and Pyrodex.

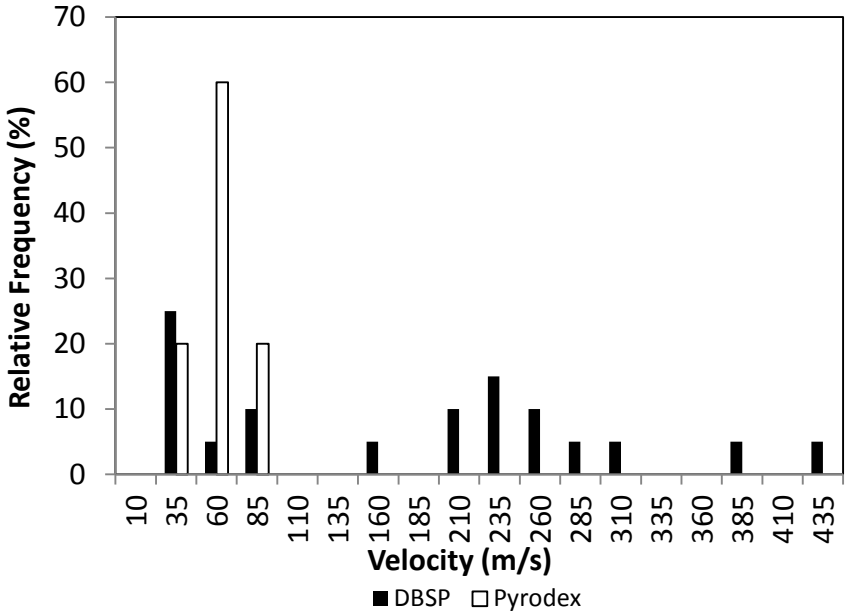

Figure 1-4 Velocity histogram showing galvanized steel devices with two energetic fillers.

Given that high speed photography was used to capture the explosion event, a stepwise sequence of the bombs exploding was able to be captured. Figures 1-5 and 1-7 show the PVC DBSP devices over a time period of 1500 µs. The point of first failure was along the body of the pipe at a time equal to approximately 600µs for both devices. The paths of specific fragments were then mapped using particle velocity vector maps. Figures 1-6 and 1-8 show the PVVMs of the two PVC DBSP devices, where the devices exhibit severe fragmentation with a wide range of velocities. Note that a cluster of slower moving fragments appear at positions and trajectories suggesting they emanated from the right endcap, in which the igniter wires were inserted.

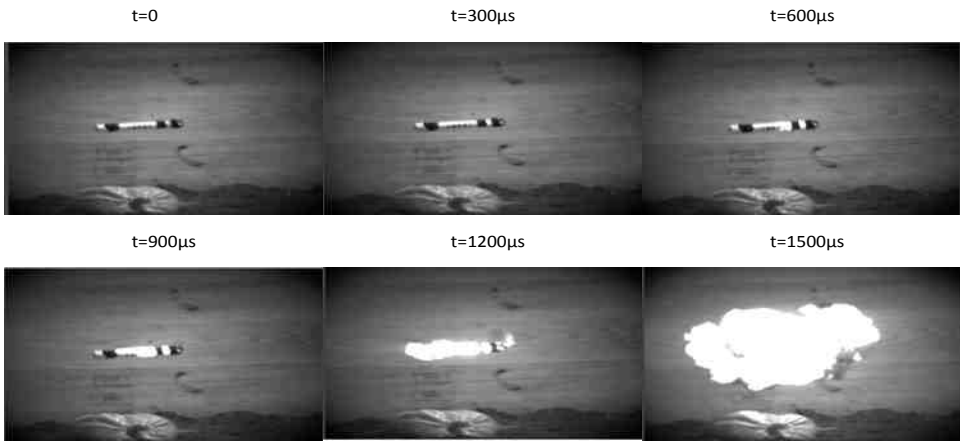

Figure 1-5 Stepwise frames of the PVC DBSP device exploding over 1500 µs.

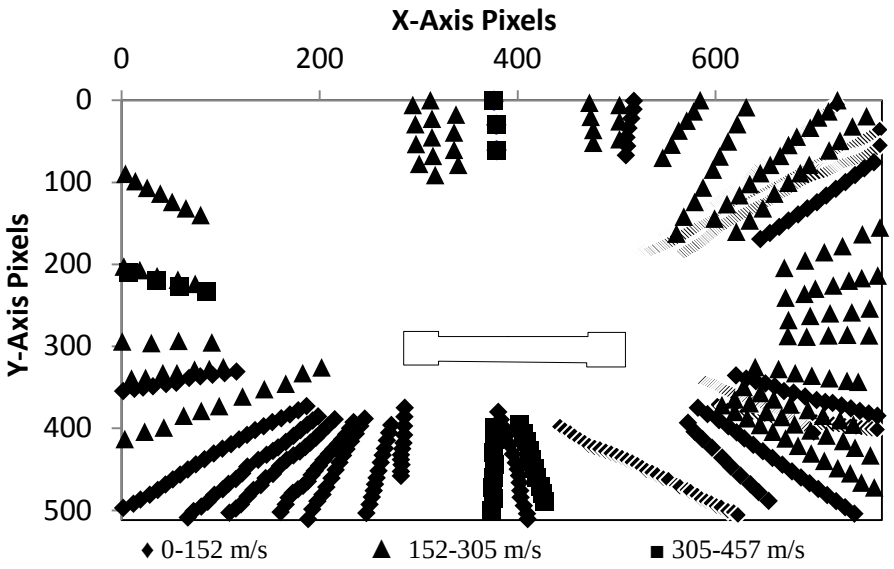

Figure 1-6 A particle vector velocity map of PVC pipe filled with DBSP.

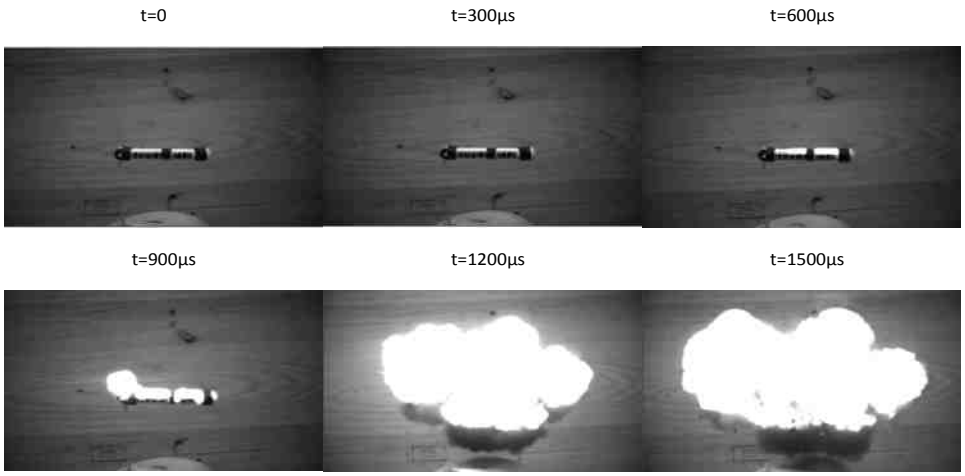

Figure 1-7 Stepwise frames of the second PVC DBSP device exploding over 1500 µs.

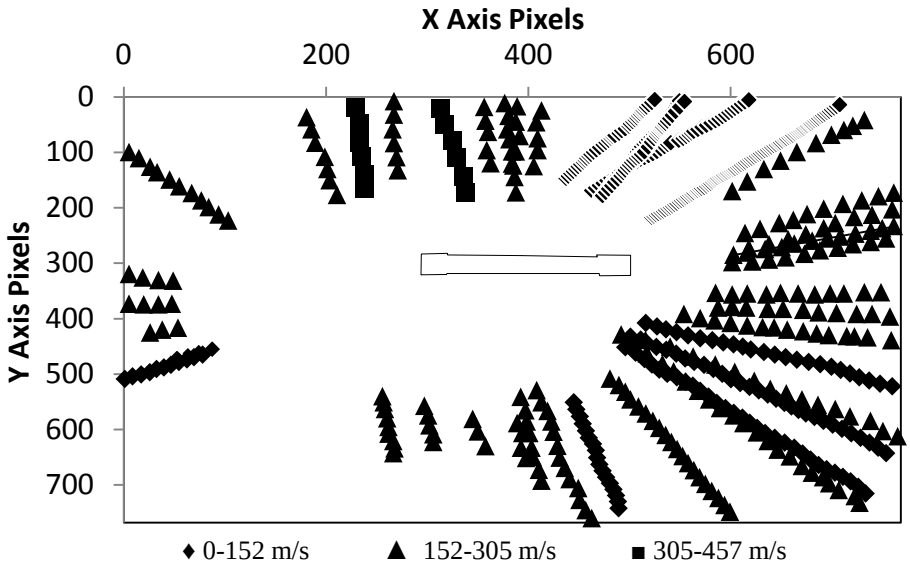

Figure 1-8 A PVVM of the second PVC DBSP device.

Figure 1-9 illustrates the photographic sequence of the explosion of black steel with DBSP. The point of first failure can be seen as the endcap opposite the igniter wires, with the entire explosion event occurring within 500 µs. The PVVM for this device, shown in Figure 1-10, demonstrates a wide range of fragment velocities and trajectories. As was seen previously, a cluster of slow moving fragments appear to track back to the right endcap. In addition, one of the fragments in the video sequence had a distinctive shape so that it could be tracked as well as recovered and weighed. The trajectory for this fragment is labeled in the PVVM (see below for more discussion on this fragment).

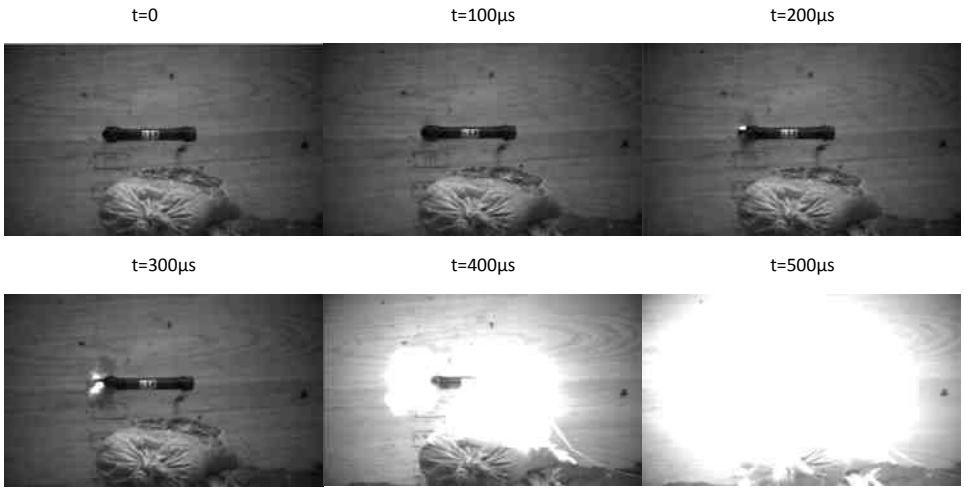

Figure 1-9 Stepwise frames of the black steel DBSP device exploding over 500 µs.

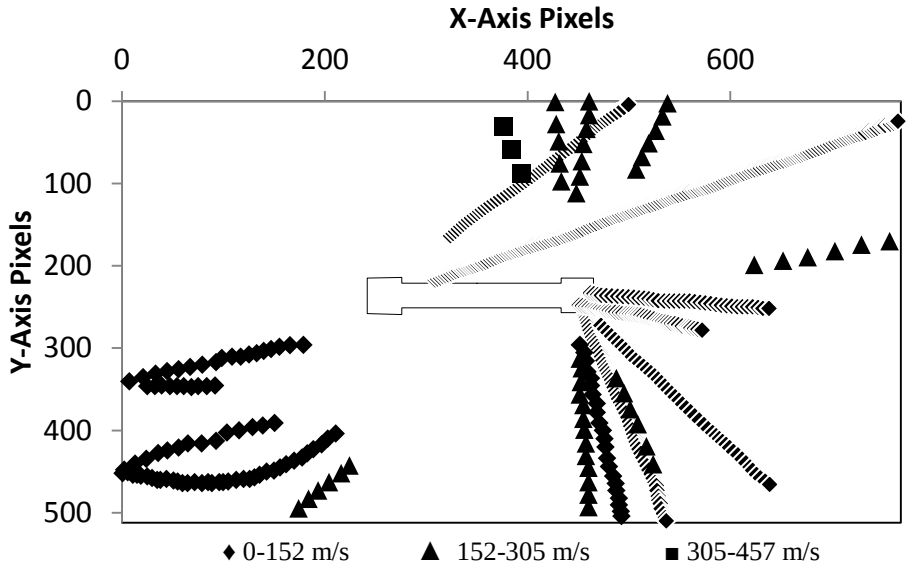

Figure 1-10 PVVM of black steel pipe with DBSP filler.

Figure 1-11 displays the galvanized steel DBSP device, which begins to fail at 100 µs and the explosion is complete within 500 µs. As was seen with the black steel device, the point of first failure was at the endcap (although in this case it was the end cap with the igniter wires). Figure 1-12 shows the path of the fragments in all directions from

the pipe, as well as velocities falling between 20-435 m/sec. The pattern of slow moving fragments emanating from the drilled end of the device is also evident.

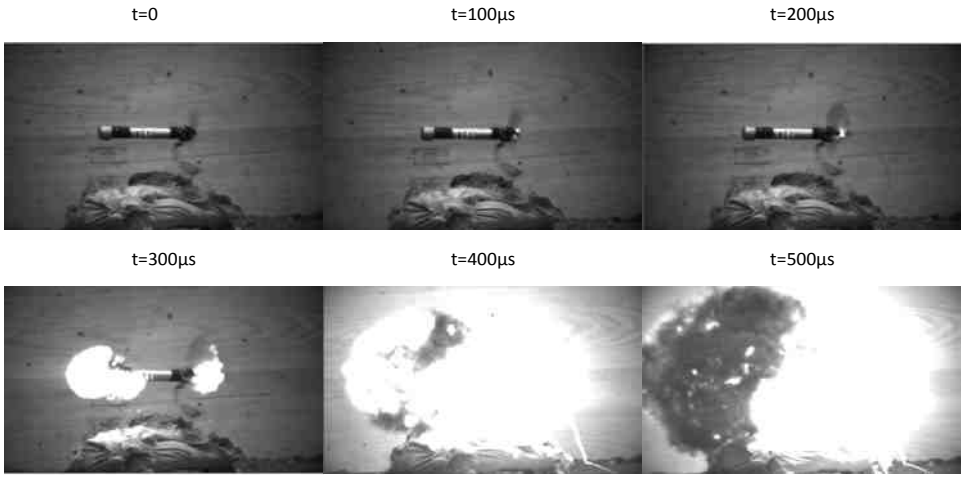

Figure 1-11 Stepwise frames of the galvanized steel DBSP device exploding over 500 µs.

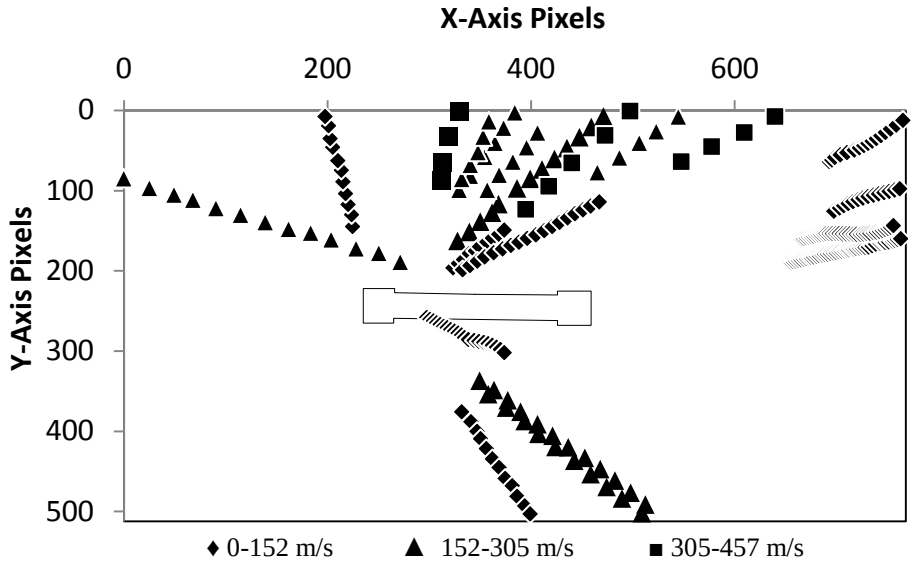

Figure 1-12 PVVM for galvanized steel device containing DBSP.

Figure 1-13 displays the PVC Pyrodex device explosion with the first failure of the pipe body shown in the second frame. Figure 1-14 shows the PVVM of the same device, with fragments escaping in all directions, including many originating from the right endcap (Figure 1-14). These fragments were positively identified in the video as multiple fragments of the right end cap. Figure 1-15 depicts the progression of the black steel Pyrodex explosion. Note the first failure at time 100 μs on the right endcap. It is evident from Figure 1-16 that a smaller number of fragments were able to be traced, due to the less complete fragmentation caused by the lower energy filler. The pipe body itself was tracked due to its large size and slow velocity. Figure 1-17 shows the progression of the galvanized steel Pyrodex explosion. Note the first failure at the right endcap, as well as the subsequent failure at the other endcap. Once again, few particles were tracked in the lower energy filler devices. Figure 1-18 shows a “banana peel” fragment, which is a characteristic fragmentation pattern for low energy explosives such as Pyrodex.

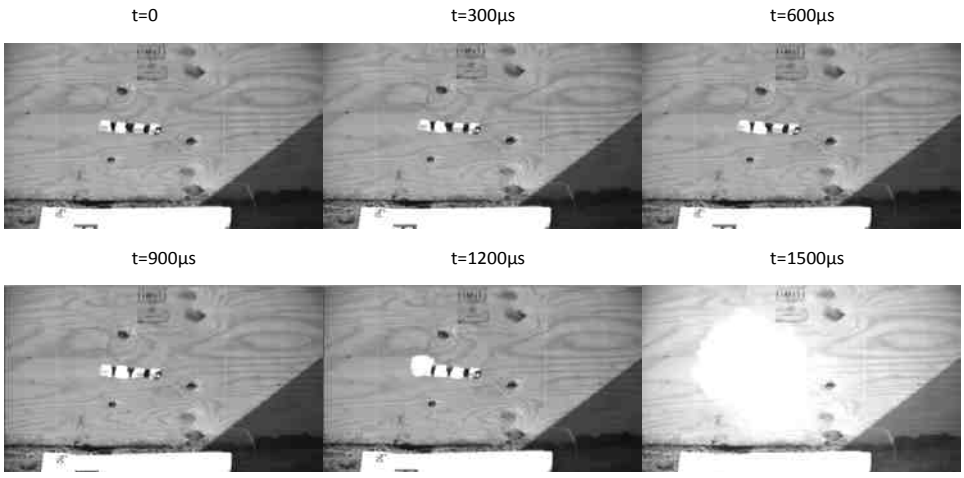

Figure 1-13 Stepwise frames of the PVC Pyrodex device exploding over 500 μs.

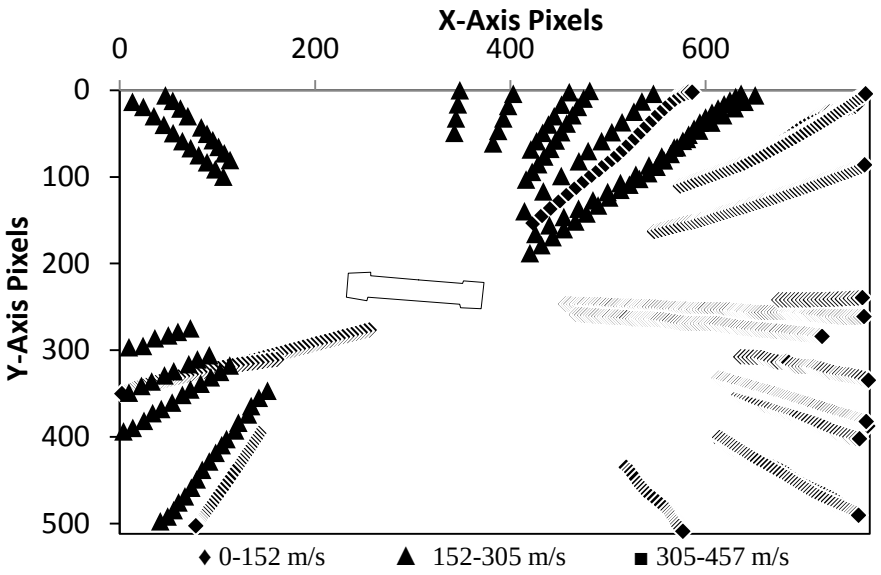

Figure 1-14 Particle vector velocity map for the PVC Pyrodex device.

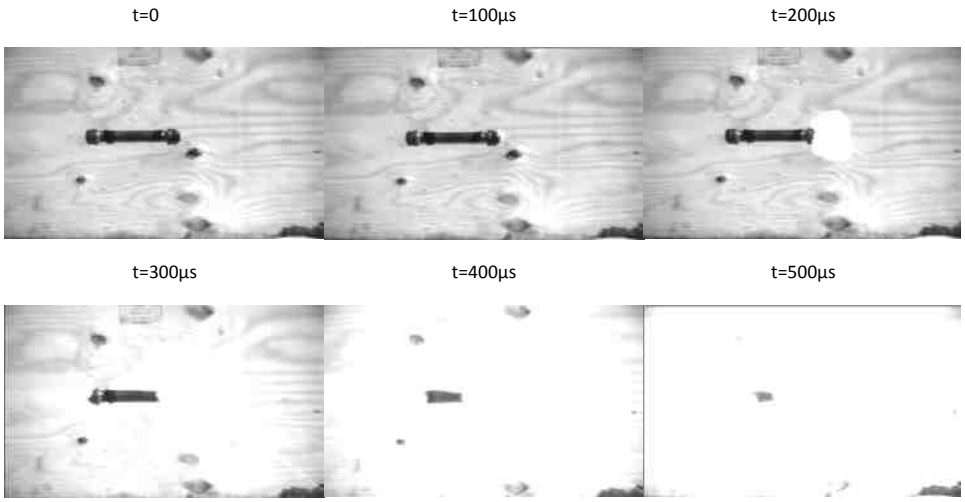

Figure 1-15 Stepwise frames of the black steel Pyrodex device exploding over 500 µs.

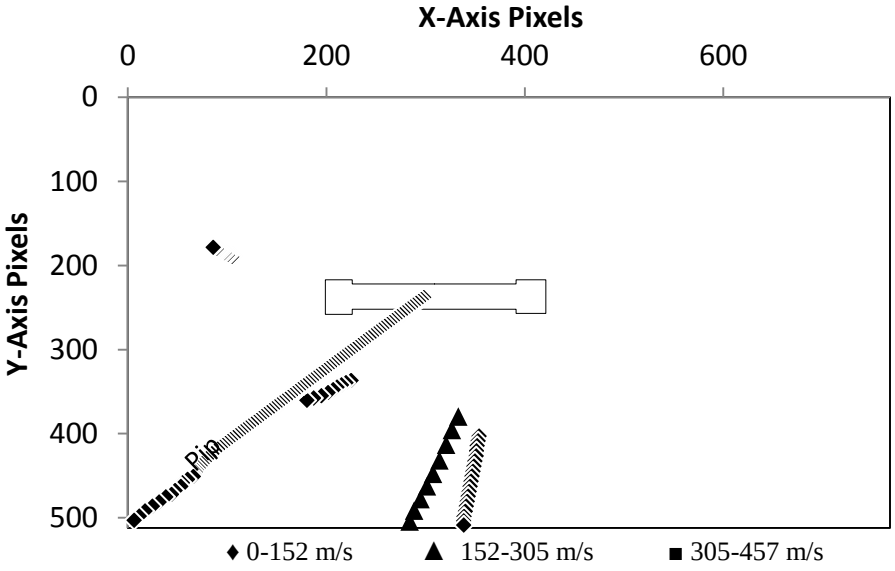

Figure 1-16 PVVM for Pyrodex in a black steel pipe.

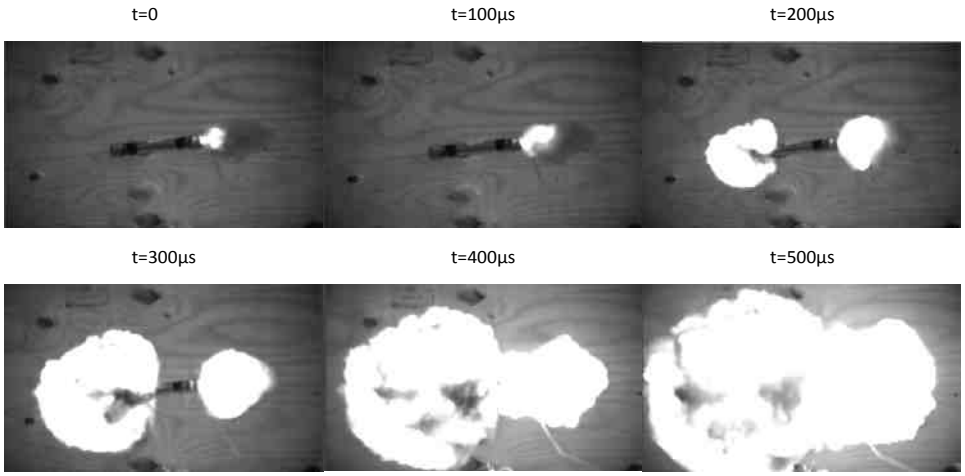

Figure 1-17 Stepwise frames of the galvanized steel Pyrodex device exploding over 500 µs.

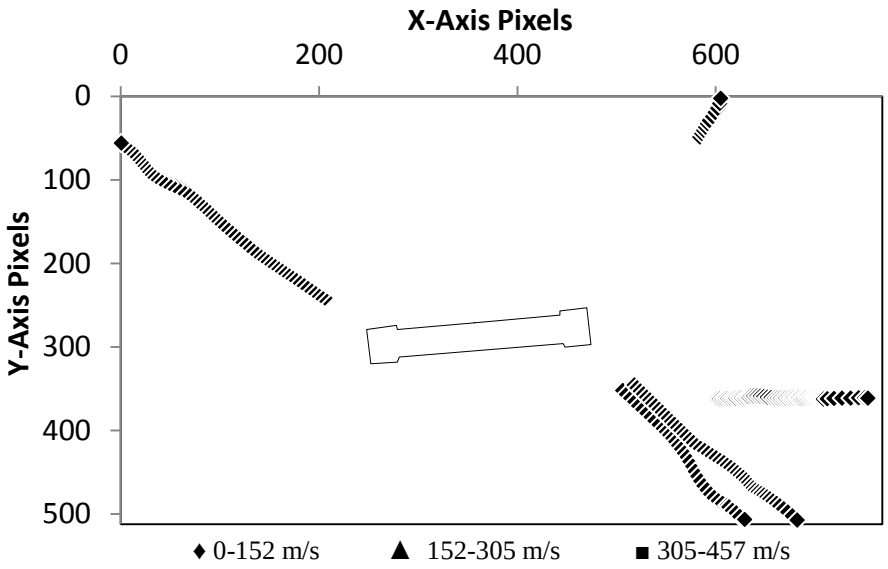

Figure 1-18 PVVM for the galvanized steel Pyrodex device.

1.3.3 Mass Measurements

Table 1-1 summarizes the slopes of the FWDM plots of the various devices, along with the corresponding R^2 values. Fitting a FWDM to a line is problematic due to significantly larger fragments, which tend to dictate the slope. Regardless, when including all fragments in the slope determination, the behavior of the energetic fillers agrees with previously published results[15]. For example, DBSP has a much steeper slope demonstrating more fragmentation overall, indicating a higher energy filler. On the other hand, Pyrodex exhibits a shallow slope caused by the presence of large fragments, characteristic of lower energy fillers. For the PVC DBSP slope calculation, two devices were included, however the results still follow Oxley's model. The metal Pyrodex devices also corresponded with Oxley, despite exceptionally low linearity values of 0.6401 and 0.5162 for black steel and galvanized steel respectively. Incomplete fragmentation of these devices produced relatively large fragments; therefore, this produced a wide range of masses and ultimately poor linearity. Removing these points dramatically improved the correlation values to near 0.97. However by doing so, the black steel devices deviated from Oxley's model, with the Pyrodex device having a steeper slope than the double base smokeless powder device.

Table 1-1 Comparison of slopes of FWDMs for all devices.

Type of Pipe	Type of Filler	Slope of FWDM (including all points)	R^2	n
PVC (2 devices)	DBSP	-47.4 ± 0.9	0.8642	393
Black Steel	DBSP	-1.48 ± 0.07	0.9587	24
Galvanized Steel	DBSP	-2.5 ± 0.2	0.8826	18
PVC	Pyrodex	-14.1 ± 0.3	0.9426	190
Black Steel	Pyrodex	-0.27 ± 0.06	0.6401	11
Galvanized Steel	Pyrodex	-0.14 ± 0.05	0.5162	11

In addition to the FWDMs, histograms were generated to show fragment mass distribution. The plots reinforce the information gained from the FWDM slope values. The PVC histogram (Figure 1-19) showed the heaviest fragment from the DBSP device was located at 5% by mass, signaling complete fragmentation. The Pyrodex fragments were concentrated near the lowest bin, with decreasing amounts in each of the successive bins with the heaviest fragment being 9% by mass. Once again the histogram comparing the fillers in a black steel pipe (Figure 1-20) supports the information from the FWDM. Both the DBSP and Pyrodex produced a fragment considerably larger than the others, 32% and 65% by mass respectively. The significant difference in these values is shown by the histogram as well as the photographs. The galvanized steel pipe filled with Pyrodex produced a large fragment that showed peeling, easily seen in the photograph in Figure 1-21, which heavily influenced the slope of the FWDM. In comparison, the masses of the DBSP pipe were all relatively similar, with the heaviest fragment being 20% by mass.

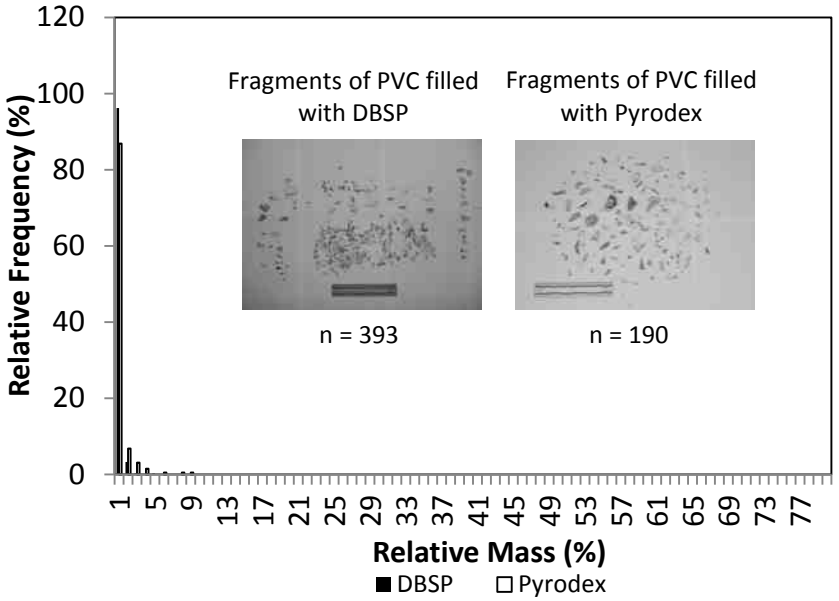

Figure 1-19 Mass histogram for PVC devices filled with DBSP and Pyrodex.

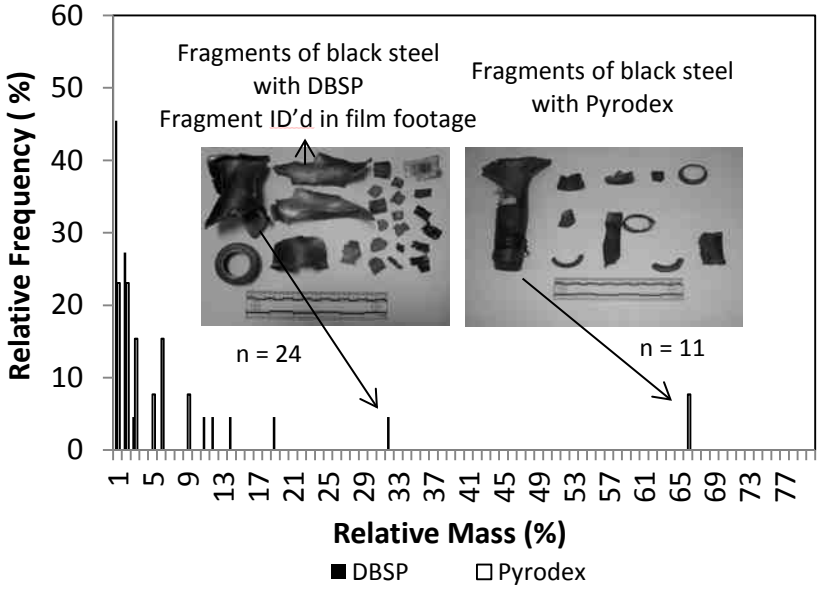

Figure 1-20 Mass histogram of black steel devices filled with various energetic fillers.

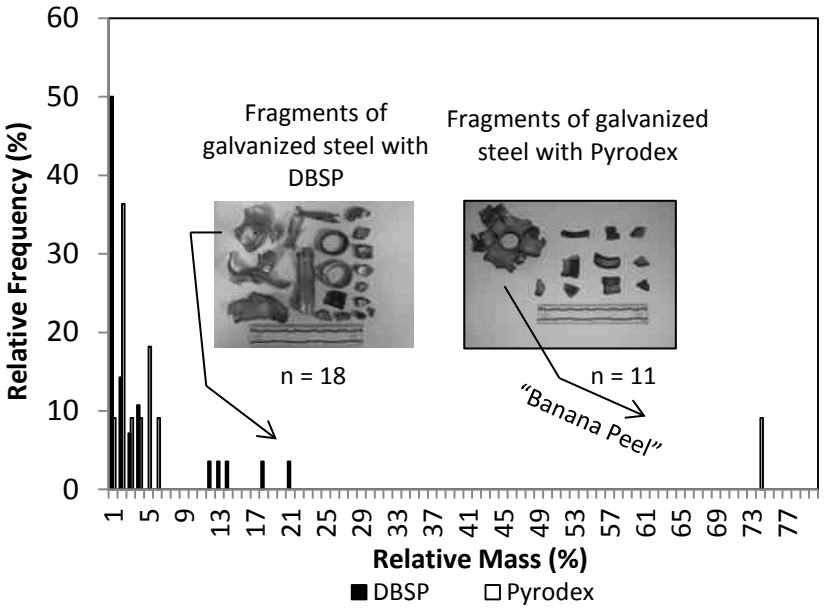

Figure 1-21 Mass histogram of galvanized steel devices with two different fillers.

1.3.4 Momentum and Kinetic Energy Calculations

Fortunately, the DBSP black steel device contained a fragment whose unique shape allowed for it to be easily recognized in the video. The same fragment was then recovered from one of the walls of the enclosure and weighed. As a result, both the velocity and mass of the fragment were known (104.9 m/sec and 48.76 g, respectively). Therefore, the momentum and kinetic energy of the fragment could be calculated, bringing together individual aspects of this study. For example, the momentum of this fragment was 5.11 kg-m/sec and its kinetic energy was 268 J. By way of comparison, a 0.45 caliber bullet weighs much less but travels faster. As a result, such a bullet yields less momentum (3.79 kg-m/sec) but more kinetic energy (483 J). Finally, this particular fragment was also spinning as it flew away from the site of the explosion at 25,000 revolutions per minute (rpm), which vastly exceeds the rpm of an automobile engine and is more comparable to tools like metal grinders. While locating this fragment was quite fortuitous, we were not able to identify any other fragments for which velocity and mass were known.

1.4 Conclusions

Based upon high speed videography, and with all pipe types, the highest overall velocities were observed with the double base smokeless powder filler. In fact, the velocities of the fastest fragments in this study are comparable to the muzzle velocities of handgun ammunition. In addition, all devices except the metal devices containing Pyrodex had clusters of low velocity fragments near the right endcap. This could be characteristic of endcap material that did not experience the same internal pressure. This would occur if a small but significant amount of gas was allowed to escape through the drill hole. For metal devices, the first failure occurred at the endcaps, but for the PVC devices the pipe body was the point of failure. Additionally, the PVC devices took nearly three times as long to explode compared to the metal devices. In general, the Pyrodex devices exhibited lower overall velocities clustered in a narrow range. This is in stark contrast to DBSP, which produced higher velocity fragments over a broad range. The mass of the fragments was a clear indication of filler both in terms of the FWDM but also some general trends in metal pipes, where the Pyrodex devices were the only ones that contained a fragment that represented more than 50% of the total mass recovered.

CHAPTER 2. THE ANATOMY OF A PIPE BOMB EXPLOSION: THE EFFECT OF EXPLOSIVE FILLER, CONTAINER MATERIAL, AND AMBIENT TEMPERATURE ON DEVICE FRAGMENTATION

2.1 Introduction

Pipe bombs are composed of two basic components, the container and the filler. Containers are usually metal or plastic pipe, and fillers can have various energies and compositions. Once the filler is ignited and begins to deflagrate, the rapid increase of internal pressure ultimately causes the pipe to fail, thus generating an explosion. While deflagration is a well-known concept, a factor that has not been well-researched is the influence of environmental factors (i.e., temperature) on this process in actual pipe bombs.

Several studies have evaluated pipe materials (not pipe bombs) for their mechanical and tensile properties under varying conditions. Germain et al tested two plastics composed of poly-12-amino dodecanoic acid with high and low plasticizer content over a range of temperatures. He concluded that the hoop stress, defined as the circumferential stress required to increase the pipe diameter, is proportional to the plasticizer amount and inversely proportional to temperature[20]. It was also noted that the properties of these specific polymers are insensitive to the manufacturing process. In contrast, similar studies on PVC have shown that variability in manufacturing affects the behavior of the PVC. This raises the question of reproducibility between batch samples. Fluctuation of conditions during manufacturing can affect how the PVC responds to certain stimuli. Merah et al conducted tensile property tests on high density polyethylene (HDPE) and chlorinated polyvinylchloride (CPVC) pipes at temperatures ranging from -10°C to 70°C. He found that for both types of pipe, yield stress and the modulus of elasticity exhibited a linear decrease as temperature increased[21-23]. Numerical data

depicting this trend in CPVC is shown in Table 2-1[23]. This is expected since yield stress is the amount of stress required to stop the material from behaving elastically. Modulus of elasticity relates this stress to the resultant strain on the material. This value remains constant for a certain range of stress. However, deviations from constancy will occur, which is called yield strength. Since yield strength is directly proportional to the modulus of elasticity, this property followed the same pattern. Temperature appeared to have little effect on yield strain, or change in shape of the material, as it only slightly increased over the entire temperature range. One apparent difference in the two polymers was that at all temperatures, HDPE fractured in a ductile manner, meaning it showed substantial permanent deformation before breaking, whereas the CPVC exhibited ductile fracture above room temperature and brittle fracture, which exhibits little or no plastic deformation, below room temperature[21-23].

Table 2-1 Average values of CPVC mechanical properties obtained from weld specimens at different temperatures[21-23].

Temperature (°C)	Number of Tests	Yield Strength	Elastic Modulus	Fracture Strain
-10	3	57	3360	2.3
0	3	53	3077	2.1
23	4	47	2823	2.4
50	3	37	2506	1.6
70	3	30	2322	1.7

The effect of temperature on low explosives such as are found in pipe bombs has not been as extensively studied. McAbee and Chmura tested four double-base propellant formulations to observe the reactions of materials to forces applied under tension, known as tensile properties, over a temperature range of -60°C to 80°C. A general trend was that the duration of the explosion was pointedly longer as temperature increased. Also, the modulus and tensile strength were indirectly proportional to temperature. This means the resistance of the material to tearing increased as temperature decreased and vice versa. Irregularities were present however, leading to the overall conclusion stating, "…there is

no simple way of predicting performance at one temperature from performance at another temperature"[24]. Hence, temperature-dependent changes in the pipe material itself may be more important in this case.

Overall, it is evident that effect of temperature on pipe bombs should not be ignored. The aim here is to focus on various pipe materials containing low explosives, where the behavior of similar devices at different temperatures is investigated. The use of high speed video to capture pipe bomb explosions is novel, as is using motion tracking software to extract information from the videos.

2.2 Materials and Methods

In general, the experimental setup was modeled after Bors et al[25]. Devices were constructed from galvanized steel (Mueller Global brand), black steel (Mueller Global brand), or PVC, and were all purchased at Home Depot. The pipes were Schedule 40 with 20.32 cm pipe bodies and a 2.54 cm nominal diameter. The metal pipes had scarf marks on the inside of the pipe body indicating that they were manufactured using an electric resistance weld**.** The two energetic fillers used were Hodgdon Pyrodex and Alliant Red Dot double-base smokeless powder (DBSP). All devices were capped at each end with one end cap having a 0.476 cm diameter hole for inserting igniter wires. The devices were assembled inside of a vehicle and then suspended approximately one foot off of the ground within an outdoor wooden containment structure.

On the date of the first spring event, the minimum temperature in Indianapolis, IN was 8°C and the maximum temperature was 21°C. The average dew point was 7°C and the mean sea level pressure was 1.016 bar[26]**.** In contrast, on the date of the second winter event, the minimum and maximum temperatures were -9°C and -3°C respectively (with an estimated wind chill of -15^{o}C). On this day, the mean dew point was -9°C and the average pressure was 1.009 bar. Both events occurred in the morning, with an hourly temperature breakdown shown in Figure 2-1.

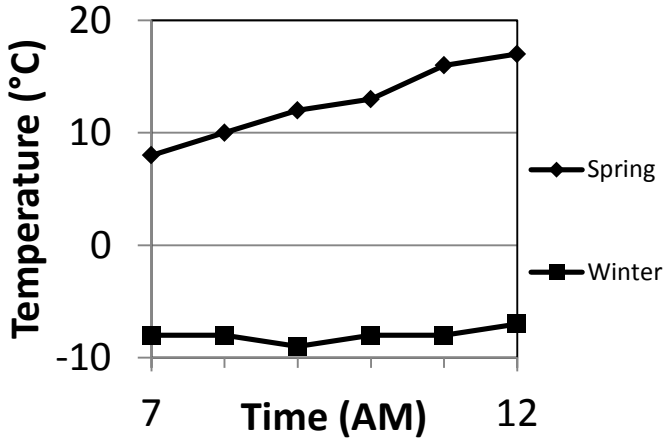

Figure 2-1 Hourly temperature breakdown for both testing days.

The amount of time that elapsed between the construction of the winter devices inside a vehicle at the test site and the initiation of the devices was not specifically monitored. However, after the set-up of the device, configuring the camera and clearing the area, devices were exposed to the outside air temperature for a minimum of 20 minutes. Calculations of the rate of conductive and convective heat loss from a 20.32 cm galvanized steel pipe under these environmental conditions yield an estimated equilibration time of less than 10 minutes.

High speed video, using a frame rate of 30,000 frames per second, captured the explosions for the winter devices filled with DBSP. Photron FASTCAM (Photron, San Diego, CA) and ProAnalyst software (Xcitex, Cambridge, MA) were used to analyze the footage. Note that in the spring event, the camera was started at the same time as the activation of the electric igniter but only a set amount of frames before and after the start of the camera were saved. In the winter, the camera saved all frames beginning with the start of the camera, which coincided with the initiation of the device. Therefore, only the footage from the winter had a true “time zero” and it was analyzed to determine the time to explosion, which is the time elapsed between initiation of the device and the first breach of the container. The duration of the explosion, or the time elapsed between the first breach of the container to complete failure, was determined for all devices. Histograms and particle vector velocity maps (PVVM) were generated to show the distribution of fragment velocities for all devices.

Due to the inherent legal and safety issues in this experiment, all devices were assembled and deployed one at a time and only by personnel from the Indiana State Police Bomb Squad. Post blast fragments from each device were collected and placed into individual paint cans. Masses of the fragments were obtained using an analytical balance. The masses were plotted as histograms and FWDMs to depict the distribution in relation to pipe and energetic filler type. This study will only focus on the behavior of six devices (three different pipe materials with two different fillers) and how they compare to the same type of device exploded in the spring (Chapter 1). Statistical analyses were performed in order to directly compare the data obtained (velocity and mass) between the two temperatures.

2.3 Results and Discussion

2.3.1 Effect of Container Material and Filler Type (Winter Devices)

High speed video was used to capture the explosions of three devices filled with DBSP. ProAnalyst software provided tracking of individual fragments and allowed for the calculation of fragment velocities. The distributions of fragment velocities for the three DBSP devices are depicted graphically using histograms (Figure 2-2). The distribution of fragment velocities for the PVC device appears Gaussian in nature, compared to the more uniform distribution of the metal devices. Figure 2-3 contains frames representing a stepwise sequence of the explosion of the PVC DBSP device. The second frame depicts the point of first failure of the pipe (located on the pipe body), hence the time to explosion for this device was 8.1 ms. Figure 2-4 shows the trajectories of specific fragments mapped in a particle velocity vector map (PVVM), where the vast majority of the fragments are traveling at less than 305 m/s. An advantage of a PVVM is that it depicts fragment trajectory and fragment velocity, which are clearly not independent in this case. For example, there is a group of slower moving fragments clustered in the lower left corner, opposite the point of first failure on the pipe body.

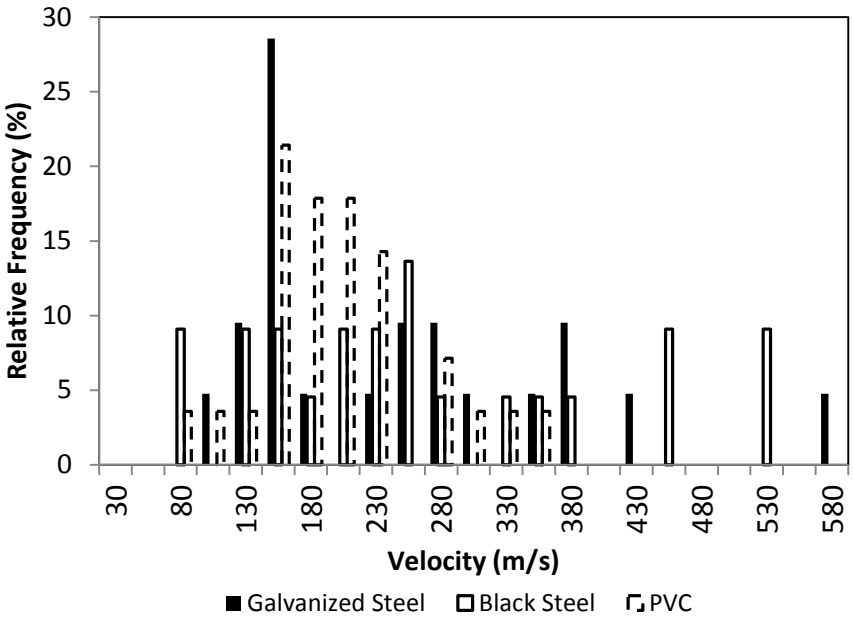

Figure 2-2 Combined velocity histogram for DBSP devices.

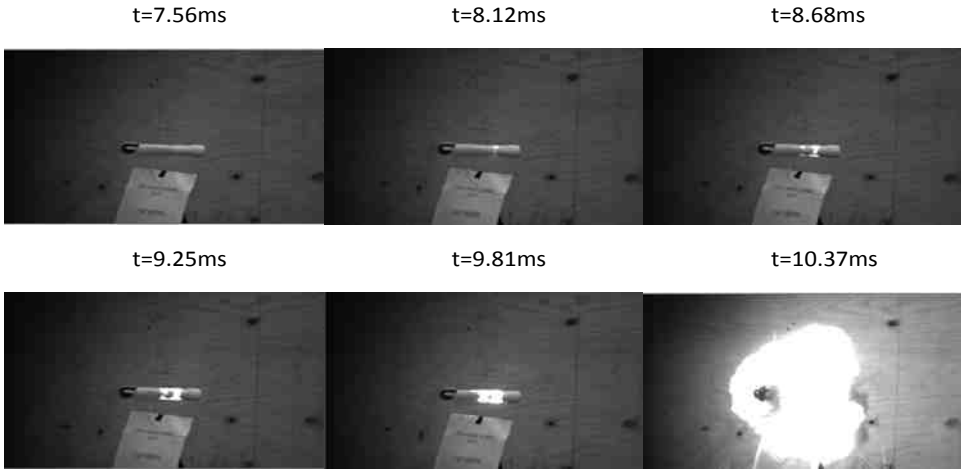

Figure 2-3 Stepwise frames of PVC DBSP exploding.

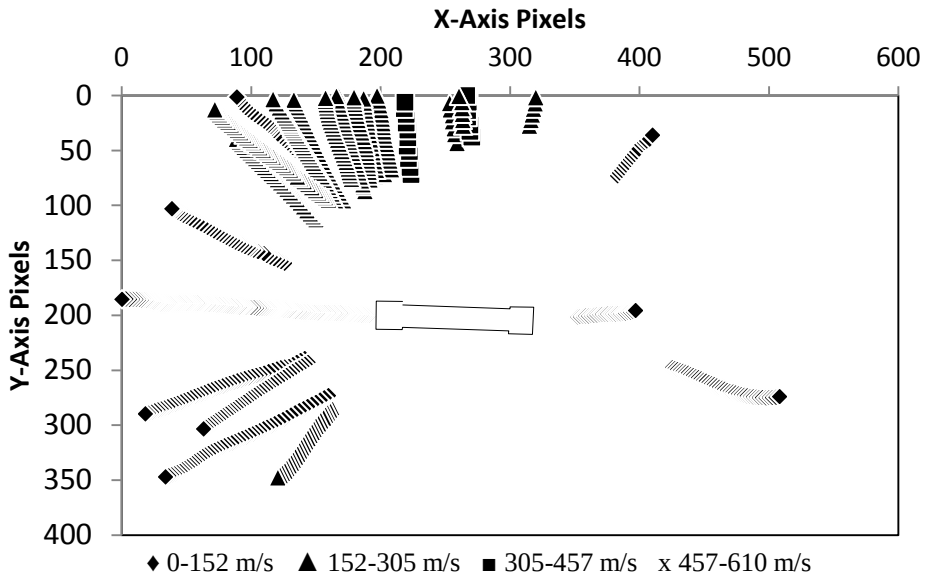

Figure 2-4 A PVVM of PVC DBSP.

Figure 2-5 contains frames representing a stepwise sequence of the explosion from the black steel DBSP device. The second frame depicts the point of first failure of the pipe (located on the right end cap) with a time to explosion of 5.8 ms. The location of first failure is consistent with our prior observations of metal devices [27]. Note that the total time elapsed in Figure 2-5 is only 170 μs. In Figure 2-6, the PVVM for this device shows a broad range of fragment trajectories and velocities. Two fragments indicated in this plot were easily identified in the video and recovered post-blast. Given that their mass and velocity were known, it was possible to calculate momentum (26.5 kg·m/s and 5.8 kg·m/s) and kinetic energy (4681 J and 210 J) for fragments 1 and 2, respectively.

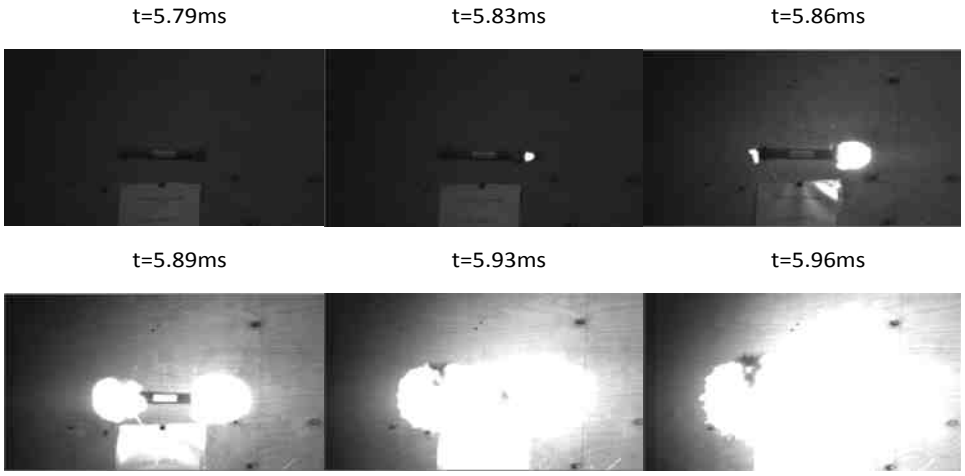

Figure 2-5 Stepwise frames of black steel DBSP exploding.

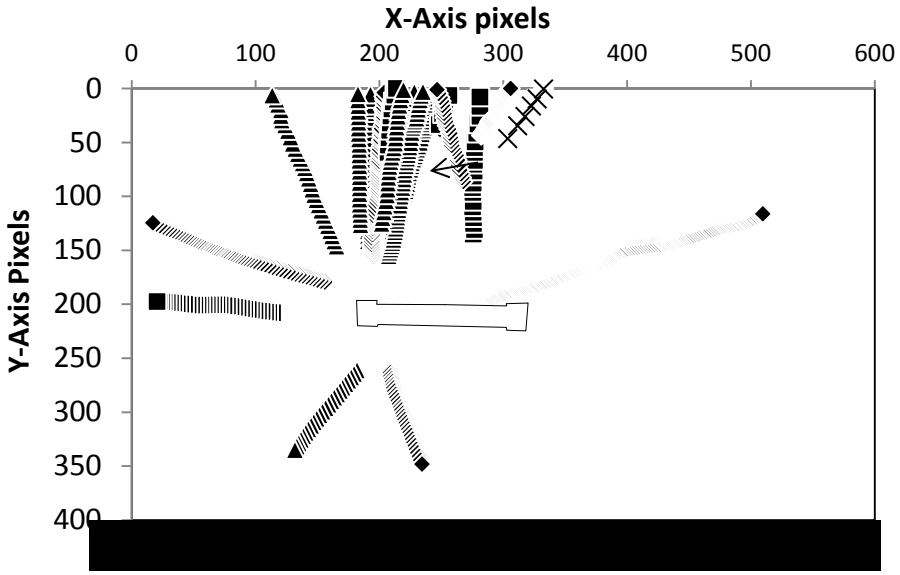

Figure 2-6 A PVVM of the black steel DBSP device.

Figure 2-7 contains frames representing a stepwise sequence of the explosion from the galvanized steel DBSP (total time elapsed is 160 µs). Once again, the point of first failure is the right endcap at t = 5.35 ms. Figure 2-8 is the PVVM of the galvanized steel DBSP device. In this case, the highest velocity fragments all had upward trajectories, where slower traveling fragments were evident in all directions.

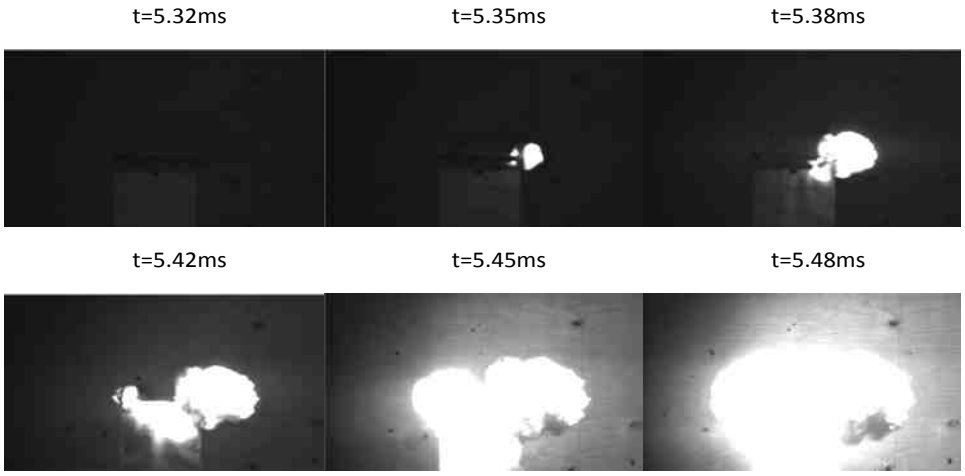

Figure 2-7 Stepwise frames of galvanized steel DBSP exploding.

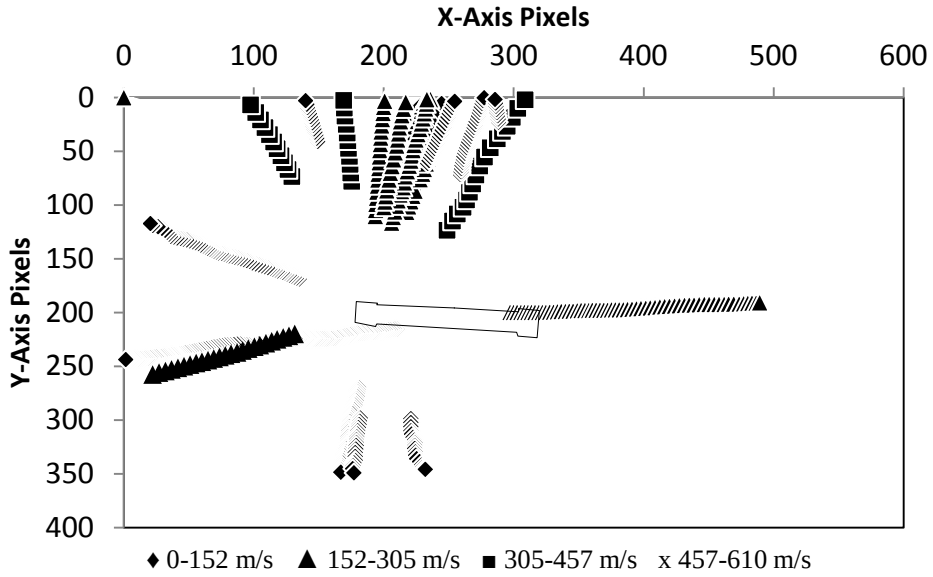

Figure 2-8 A PVVM of the galvanized steel DBSP device.

Oxley has pioneered the use of fragment weight distribution maps (FWDM) as a way to characterize the distribution of fragment masses in post-blast debris[15]. FWDM's represent the ratio of the relative mass of a specific fragment to the mass of that same fragment divided by the total mass of all heavier fragments[15]. In general, highly energetic fillers are expected to cause more complete fragmentation, resulting in a steeper slope in

the FWDM. Following this reasoning, DBSP should yield a steeper slope than Pyrodex for a given container type. Although the galvanized steel devices followed this trend, the black steel and PVC devices did not (Table 2-4). In both cases, the devices filled with Pyrodex gave the steepest slopes. The mass histograms agree with the conclusions drawn from the FWDMs. Figures 2-9 – 2-11 are the mass histograms for the PVC, black steel, and galvanized steel devices, respectively. The largest fragments by mass in all devices were generated in the steel devices. It was expected that DBSP would generate the smallest fragments by mass due to the more complete fragmentation. However, only the galvanized steel device behaved this way.

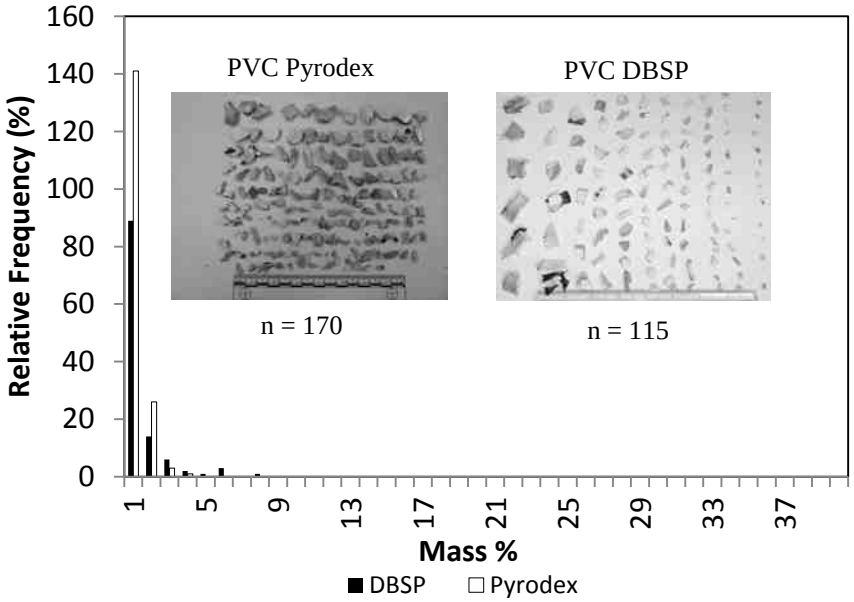

Figure 2-9 Histogram of fragment masses from the PVC devices.

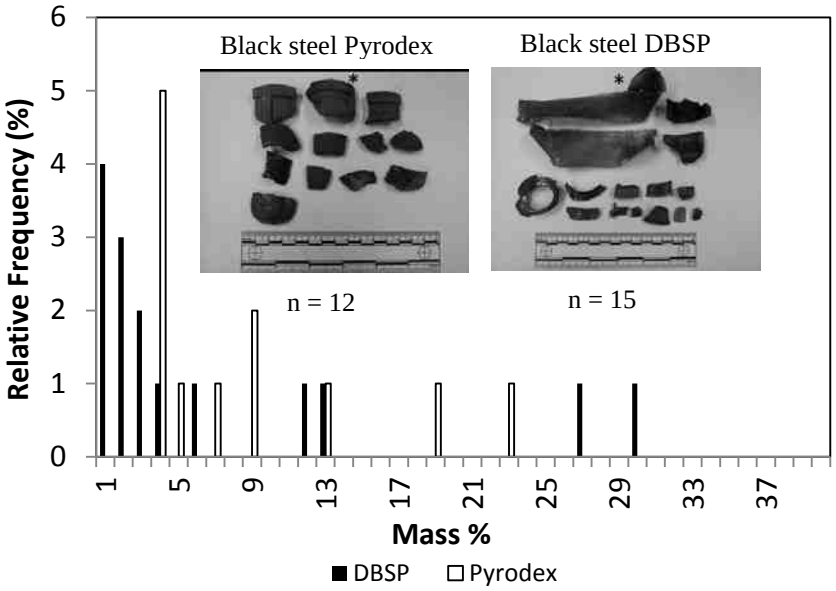

Figure 2-10 Histogram of fragment masses from the black steel devices. *Denotes largest fragment by mass.

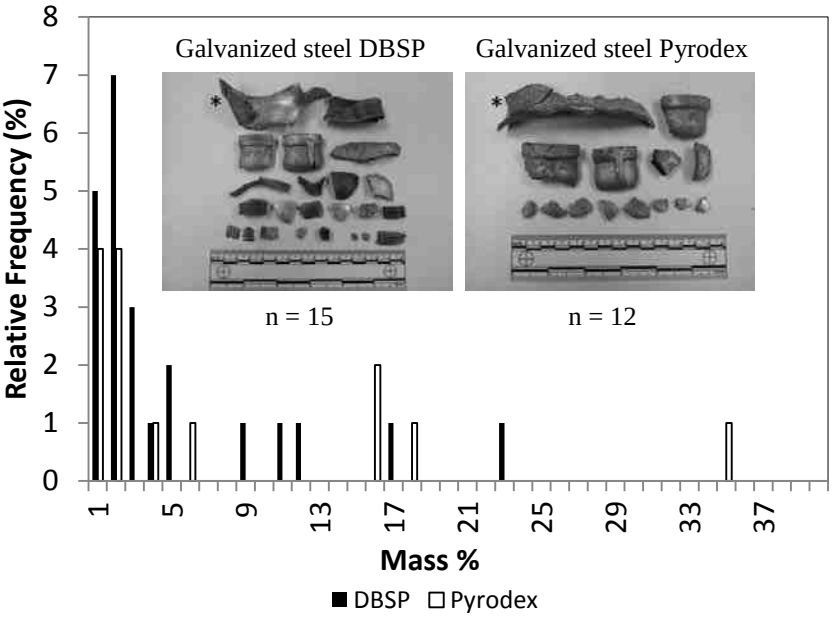

Figure 2-11 Histogram of fragment masses from the galvanized steel devices. *Denotes largest fragment by mass.

2.3.2 On the Effect of Ambient Temperature

Maximum and minimum velocities as well as time to and duration of the explosion for all of the devices are listed in Table 2-2. There are several similarities between the winter and spring data. High speed video showed that the highest overall fragment velocities for all pipe materials were from those devices filled with double base smokeless powder filler. The velocities of the high energy devices were also uniformly distributed. Higher energy fillers produced faster fragments regardless of season. Also, the points of first failure were consistent (i.e., the end caps for the metal pipes, and the pipe bodies for the PVC pipe). The PVVMs showed fragments traveling in all directions, with velocities of the metal fragments having the widest range. The momentum and kinetic energy of one of the winter black steel DBSP fragments (5.8 kg·m/s and 210 J) was similar to that for a black steel fragment from the spring study (4.52 kg·m/s and 209 J).

However, there are several differences in fragment velocities that were found to be statistically significant (Table 2-3). For example, the fragment velocities from the winter PVC DBSP and the winter black steel DBSP device were significantly higher than a similar device exploded in the spring. In fact, the fragment velocities from all of the winter devices were significantly higher than the spring black steel DBSP device.

Table 2-2 Velocity comparison of pipe bombs with DBSP filler. *Spring data from Chapter 1 devices.

			Velocity (m/s)					
Season	**Material**	**n**	**Min**	**Max**	**Mean**	**s**	**Time to Explosion (ms)**	**Duration of Explosion (ms)**
Spring	PVC	40	34	351	191.4	79.4	-	1.5
	PVC	48	17	340.5	160.3	77.4	-	1.5
	Galvanized Steel	20	15.1	423.6	169.2	126.9	-	0.5
	Black Steel	20	29.4	318.7	130	89.5	-	0.5
Winter	PVC	28	76.8	331.9	190	63.2	8.12	2.24
	Galvanized Steel	21	80.8	567.4	234.2	122.7	5.35	0.13
	Black Steel	22	61.3	450.4	255.9	136.6	5.82	0.13

Table 2-3 p values from two-sample t-tests comparing all fragment velocities from DBSP devices. Direct comparisons of the same device type in two different seasons are shaded in gray.

		Spring				Winter		
		PVC DBSP	PVC DBSP	Galvanized DBSP	Black DBSP	PVC DBSP	Galvanized DBSP	Black DBSP
Spring	PVC DBSP		**<0.001**	>0.05	**<0.05**	>0.05	>0.05	>0.05
	PVC DBSP	**<0.001**		**<0.001**	**<0.01**	**<0.001**	**<0.001**	**<0.001**
	Galvanized DBSP	>0.05	**<0.001**		>0.05	>0.05	>0.05	>0.05
	Black DBSP	**<0.05**	**<0.01**	>0.05		**<0.05**	**<0.01**	**<0.05**
Winter	PVC DBSP	>0.05	**<0.001**	>0.05	**<0.05**		>0.05	**<0.05**
	Galvanized DBSP	>0.05	**<0.001**	>0.05	**<0.01**	>0.05		>0.05
	Black DBSP	>0.05	**<0.001**	>0.05	**<0.05**	**<0.05**	>0.05	

The fragment masses and slopes of all the FWDMs are summarized in Table 2-4. As shown in Table 2-5, differences in the mean fragment mass between different devices were generally not significant – including between devices with the same pipe material and different filler. These results are not surprising given the breadth of the mass distributions, indicating that the shape of the distribution (as reflected in a histogram or FWDM) is more important than its mean value. The majority of the winter devices exhibited steeper FWDM slopes than their spring counter-parts (e.g., PVC/Pyrodex, Galvanized Steel/DBSP, Galvanized Steel/Pyrodex, and Black Steel/Pyrodex). As mentioned above, the FWDM slopes for the spring devices increased as expected when DBSP was used as filler. However, the FWDM slopes for the winter PVC and black steel devices did not increase as expected with DBSP filler.

Table 2-4 Comparison of fragment masses for all devices. *Note that the fragments from two PVC devices in the spring were pooled prior to weighing.

				Mass					
Season	**Material**	**Filler**	**n**	**Min (%)**	**Max (%)**	**Mean (%)**	**s (%)**	**FWDM**	**R^2**
Spring	PVC	DBSP	394*	2.00E-04	4.93	0.25	0.38	-47.4	0.9
	PVC	Pyrodex	191	0.002	8.14	0.52	1.04	-14.1	0.9
	Galvanized Steel	DBSP	28	0.01	20.4	3.57	5.75	-2.5	0.9
	Galvanized Steel	Pyrodex	11	0.01	74	9.09	21.6	-0.1	0.5
	Black Steel	DBSP	22	0.07	31.9	4.55	7.96	-1.5	1
	Black Steel	Pyrodex	13	0.05	65.2	7.69	17.5	-0.3	0.6
Winter	PVC	DBSP	116	0.01	7.16	0.86	1.27	-14.1	1
	PVC	Pyrodex	117	0.02	3.37	0.58	0.56	-42.9	1
	Galvanized Steel	DBSP	23	0.08	22.4	4.35	5.87	-2.6	1
	Galvanized Steel	Pyrodex	14	0.48	35	7.14	10.2	-1.3	0.9
	Black Steel	DBSP	15	0.56	29.1	6.67	9.38	-1.4	0.9
	Black Steel	Pyrodex	12	3.17	22.7	8.33	6.53	-2.8	1

Table 2-5 Results of two-sample t-tests comparing all fragment masses. Direct comparisons of the same device type in two different seasons are shaded in gray. Direct comparisons of the same container type with different fillers are shaded in black. *Note the fragments from two PVC devices in the spring were pooled prior to weighing.

		Spring						Winter					
		PVC DBSP (2)	PVC Pyrodex	Galvanized DBSP	Galvanized Pyrodex	Black DBSP	Black Pyrodex	PVC DBSP	PVC Pyrodex	Galvanized DBSP	Galvanized Pyrodex	Black DBSP	Black Pyrodex
Spring	PVC DBSP (2)		>0.05	**<0.01**	>0.05	**<0.05**	>0.05	**<0.05**	>0.05	**<0.01**	**<0.05**	**<0.05**	**<0.01**
	PVC Pyrodex	>0.05		**<0.05**	>0.05	**<0.05**	>0.05	>0.05	>0.05	**<0.01**	**<0.05**	**<0.05**	**<0.01**
	Galvanized DBSP	**<0.01**	**<0.05**		>0.05	>0.05	>0.05	**<0.01**	**<0.01**	>0.05	>0.05	>0.05	>0.05
	Galvanized Pyrodex	>0.05	>0.05	>0.05		>0.05	>0.05	>0.05	>0.05	>0.05	>0.05	>0.05	>0.05
	Black DBSP	**<0.05**	**<0.05**	>0.05	>0.05		>0.05	**<0.05**	**<0.05**	**<0.05**	>0.05	>0.05	>0.05
	Black Pyrodex	>0.05	>0.05	>0.05	>0.05	>0.05		>0.05	>0.05	>0.05	>0.05	>0.05	>0.05
Winter	PVC DBSP	**<0.05**	>0.05	**<0.01**	>0.05	**<0.05**	>0.05		>0.05	**<0.05**	<0.05	**<0.05**	**<0.01**
	PVC Pyrodex	>0.05	>0.05	**<0.01**	>0.05	**<0.05**	>0.05	>0.05		**<0.05**	**<0.05**	**<0.05**	**<0.01**
	Galvanized DBSP	**<0.01**	**<0.01**	**<0.05**	>0.05	**<0.05**	>0.05	**<0.05**	**<0.05**		>0.05	>0.05	>0.05
	Galvanized Pyrodex	**<0.05**	**<0.05**	>0.05	>0.05	>0.05	>0.05	**<0.05**	**<0.05**	>0.05		>0.05	>0.05
	Black DBSP	**<0.05**	**<0.05**	>0.05	>0.05	>0.05	>0.05	**<0.05**	**<0.05**	>0.05	>0.05		>0.05
	Black Pyrodex	**<0.01**	**<0.01**	>0.05	>0.05	>0.05	>0.05	**<0.01**	**<0.01**	>0.05	>0.05	>0.05	

2.4 Conclusions

Overall, we suggest that there were significant differences in the behavior of pipe bombs at different ambient temperatures. These changes are likely rooted in the mechanical properties of the pipes themselves (versus the energetic properties of explosive fillers). This is supported by prior studies as well as our observation of significant changes in the distribution of the velocity and mass of container fragments. That being said, future work in this area that includes additional replicate devices is warranted.

There are several implications of these findings for explosives investigations. Firstly, several devices generated fragments with higher velocities in the winter. Higher fragment velocities increase the overall lethality of the device. In addition, higher velocity fragments will travel greater distances and investigators must establish larger search areas at a post-blast scene. Furthermore, we noted anomalous behavior in the fragment mass distributions between devices filled with either Pyrodex or DBSP. This calls into question the use of fragment mass distributions as a means to presumptively differentiate explosive fillers under extreme environmental conditions.

CHAPTER 3. TOTAL VAPORIZATION SOLID-PHASE MICROEXTRACTION THEORY, OPTIMIZATION, AND APPLICATION TO MAPPING EXPLOSIVE RESIDUE

3.1 Introduction

Solid phase microextraction (SPME) is a sampling technique in which components are pre-concentrated onto a fiber coated with a sorbent and then subsequently desorbed in the inlet of a gas or liquid chromatograph[28-31]. Traditional SPME is conducted by either headspace or immersion, where the fiber extracts the vapor above a sample or the fiber is placed directly into a liquid sample, respectively. Both headspace and immersion SPME methods have been developed for a wide variety of analytes. In contrast, total vaporization is a technique that has been used in simple headspace sampling[32]. Matrix effects that result between two phases in headspace sampling are of particular concern. One way to eliminate matrix effects is to completely evaporate both the analyte and its matrix. Examples of applications of total vaporization headspace include determination of methanol in wood pulp, ethanol in fermentation liquor, volatile organic compounds in biological samples and odor compounds in aqueous samples[33-36]. Matrix effects can also be eliminated in SPME by quantitatively extracting analytes from complex matrices. This method is known as cooled fiber SPME and it has been used to extract polycyclic aromatic hydrocarbons (PAHs) from heated soil samples[37-39]. Alternatively, solvent extracts of urine have been evaporated to dryness in a headspace vial and the residue heated until analytes vaporize, derivatize and sorb to a SPME fiber[40].

In this chapter, we report a different technique - total vaporization SPME (TV-SPME). In this approach, analytes are extracted from a sample by a solvent. Then, a

portion of the solvent extract is completely vaporized inside a headspace vial into which is inserted a SPME fiber. This results in a simple two-phase system. In particular, partitioning of the analyte between the extract and the headspace is eliminated and the analyte partitions directly between the vapor phase and the SPME fiber (see Figure 3-1).

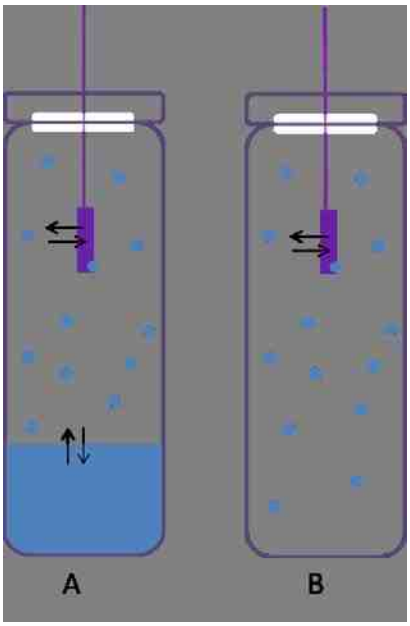

Figure 3-1 Depiction of headspace SPME of a liquid sample (A) and of a totally vaporized sample after heating (B).

Overall, combining total vaporization of a sample extract with the ability of SPME to pre-concentrate analytes onto the fiber has several distinct advantages. For example, it is difficult to determine an organic analyte in an organic solvent by either headspace or immersion SPME. Vaporizing the solvent allows the analyte to be extracted from the vapor phase by the SPME fiber. As the distribution of the analyte in TV-SPME occurs at a vapor/solid interface, we have found that extraction time is less important than extraction temperature and sample volume for efficient recovery of analytes.

In comparison to liquid injection, sample extracts do not need to be filtered in TV-SPME. Any solids or non-volatile compounds that may be present in a sample extract will remain on the surface of the vial. This can greatly reduce the amount of buildup and contamination that may occur in the inlet and GC column. Furthermore, the selectivity of the GC inlet in liquid injection is primarily based upon the boiling point of the analytes.

TV-SPME can add an additional level of chemical selectivity because the properties of the fiber can be selected to target specific analytes. Finally, liquid injection volumes are typically around one microliter; therefore, only a small fraction of the sample extract is injected. Large-volume injection (LVI) techniques have thus been developed for GC. However, LVI requires modifications to the instrument and its parameters. TV-SPME requires no change in instrumentation, allows for large sample volumes to be analyzed and, ultimately, results in greater sensitivity than liquid injection.

3.1.1 Theory of Total Vaporization Solid-Phase Microextraction

TV-SPME is most analogous to immersion SPME, where there is a single partition between the sample and the fiber coating. The amount of analyte on a SPME fiber that is directly immersed into a liquid sample can be described by the following equation[28]:

$$n = \frac{K_{fs}V_sV_fC_0}{K_{fs}V_f+V_s} \approx K_{fs}V_fC_0 \qquad \text{(Equation 3-1)}$$

where n is the mass of analyte on the fiber, K_{fs} is the distribution coefficient between the fiber and the sample, V_s is the volume of sample, V_f is the volume of fiber coating and C_0 is the initial concentration of analyte in the sample. Since the sample volume is typically much greater than the fiber volume (i.e., $V_s \gg V_f$) and when there is negligible depletion of the analyte in the sample, this equation can be simplified so that n depends solely on K_{fs}, V_f, and C_0. The equation describing TV-SPME utilizes Equation 3-1, with slight modification:

$$n \approx K_{fs}V_fC_v = K_{fs}V_fC_0\frac{V_0}{V_v} \qquad \text{(Equation 3-2)}$$

where C_v is the concentration of the totally vaporized analyte in the vial. This concentration is determined by the original concentration of the analyte in the liquid sample (C_0) multiplied by the ratio of the volume of the liquid sample (V_0) and the volume of the vial (V_v). Note that the temperature must be high enough to completely vaporize the solvent as well as any volatile or semi-volatile analytes that are present. The octanol water partition coefficient (log P) represents the ratio of distribution of analyte in

two immiscible phases. The log P for nitroglycerin (1.6), diphenylamine (3.5), and ethyl centralite (3.6) show that the lowest value is for NG[41]. Since NG is more hydrophilic than the other two analytes, the extraction of NG using immersion SPME in water would be less efficient than using TV-SPME because TV-SPME eliminates the matrix effect and forces the analyte into the headspace.

Two key parameters in TV-SPME are the volume of the sample extract and the temperature at which the sample is vaporized. The amount of liquid sample that can be completely vaporized inside a vial can be estimated by using the ideal gas law to calculate the number of moles of the solvent times the molar volume of the liquid as shown in the following equation:

$$V_0 = \left(\frac{PV_v}{RT}\right)\left(\frac{M}{\rho}\right) \qquad \text{(Equation 3-3)}$$

where V_0 is the volume of sample (mL), P is the vapor pressure of the solvent (bar), V_v is the volume of the vial (L), R is the ideal gas constant (8.3145×10^{-2} L bar/K mol), T is temperature (K), M is the molar mass of the solvent (g/mol), and ρ is the density of the solvent at the temperature at which it was placed in the vial (e.g., room temperature) (g/mL).

The vapor pressure of the solvent is strongly influenced by temperature, which can be accounted for using the Antoine equation[42]:

$$\log_{10} P = A - \frac{B}{T+C} \qquad \text{(Equation 3-4)}$$

where T is the temperature and A, B, and C are Antoine constants for the solvent (available from various sources, including the NIST Chemistry WebBook). Substituting Equation 3-4 into Equation 3-3 fully describes the volume of sample that can be totally vaporized as a function of temperature:

$$V_s = \left(\frac{\left(10^{A-\frac{B}{T+C}}\right)V}{RT}\right)\left(\frac{M}{\rho}\right) \qquad \text{(Equation 3-5)}$$

This relationship can be seen in Figure 3-2 for several organic solvents in a 20 mL SPME vial. As implied by Equation 3-5, volatile solvents that have a high vapor pressure and a large molar volume (M/ρ) can be vaporized at temperatures and in quantities suitable for TV-SPME analyses.

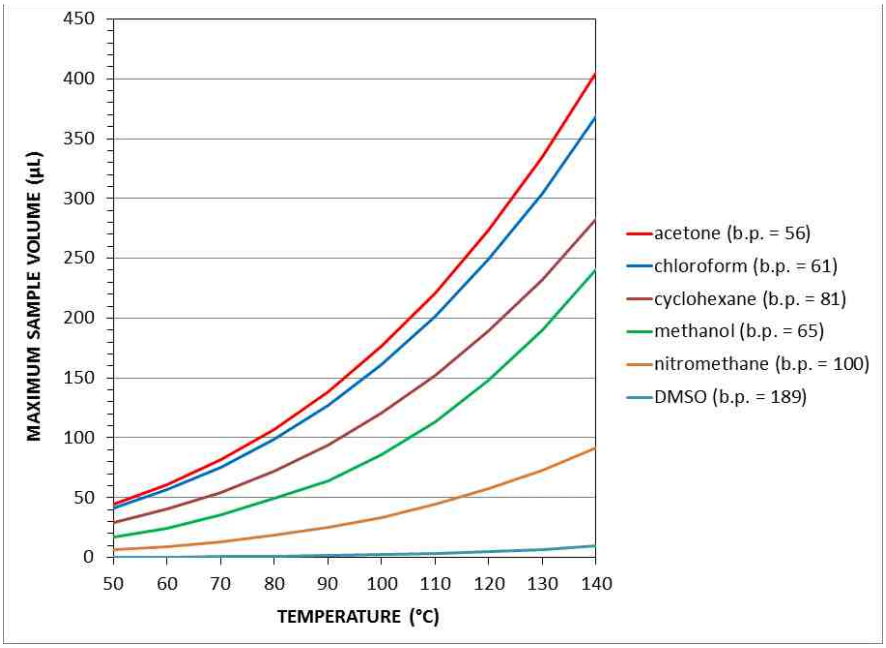

Figure 3-2 The calculated volume of various organic solvents that can be totally vaporized in a 20 mL headspace vial as a function of temperature.

Although increased temperature allows for larger sample volumes in TV-SPME, temperature will also have a major effect on the ability of a SPME fiber to sorb analytes. For example, an increase in temperature will typically result in a decrease in K_{fs} and a decrease in the amount of analyte that will absorb onto the fiber. However, in total vaporization, increasing the temperature will also result in an increase in V_s and, therefore, an increase in C_v because larger samples are able to be vaporized. Temperature has a greater influence on vapor pressure than it does on the partition coefficient, hence, an optimized temperature can be found that balances these two factors.

3.1.2 Limitations of TV-SPME

Depending on the choice of fiber coating and solvent, there may be some inherent fiber swelling in TV-SPME[29]. When an absorbent SPME fiber (e.g., polydimethylsiloxane (PDMS), polyethylene glycol (PEG) and polyacrylate (PA)) is exposed to a solvent, the fiber will absorb the solvent and therefore the diameter of the fiber will increase. An extreme example is a PA fiber immersed in chloroform, where the

overall diameter of the fiber (core + coating) increases by greater than 20%. However, any absorbent fiber coating can swell in the presence of non-polar solvents or high concentrations of their vapors. To some extent, this could be an advantage in TV-SPME in the same way that the "solvent effect" helps analytes condense on a GC stationary phase that has swelled due to exposure to the injection solvent. As the SPME fiber absorbs some of the solvent vapor and swells (i.e., V_f increases), it has a greater capacity for analyte absorption and therefore greater analyte response[28,29]. However, a swollen fiber coating may also have a lower partition coefficient, which would be counter-productive[28,29]. Of course, excessive swelling could lead to the fiber coating being stripped when the fiber is retracted inside its metal sheath.

In general, we have found that some combinations of fiber coating and solvent do result in swelling that shortens fiber lifetimes (e.g., using a PA fiber with chloroform) whereas other combinations that have been utilized in our laboratory have not exhibited any problems (e.g., using a PDMS/DVB fiber with chloroform and using a PEG fiber with methylene chloride).

3.1.3 Optimization of the TV-SPME Method

There are numerous parameters that are incorporated into a TV-SPME method, including SPME fiber type, extraction temperature, extraction time, desorption temperature, desorption time, and sample volume. In this case, using a statistical experimental design is the best way to determine the optimal values for the parameters without performing every possible variable combination, or a "vary-one-parameter-at-a-time" approach.

Response surface methodology (RSM) and central composite design (CCD) are commonly used techniques to optimize parameters (variables) in analytical chemistry[43-45]. RSM uses mathematical and statistical techniques to model and analyze responses which are dependent on many variables with the ultimate goal being to optimize the response[46]. When there are multiple responses, it becomes important to find the best compromise of the variables so that all responses are optimized[47]. RSM is useful to understand changes

in response by adjusting the design variables. In this case, a second order RSM model was used that contained quadratic and interaction terms[43,46]:

$$y = \beta_0 + \sum_{i=1}^{k} \beta_i x_i + \sum_{i=1}^{k} \beta_{ii} x_i^2 + \sum \sum_{i<j} \beta_{ij} x_i x_j + \in \quad \text{(Equation 3-6)}$$

where y is the response, β_0 is a constant, β_i is the coefficient of the linear term, x_i is the linear variable, β_{ii} is the coefficient of the square term, x_i^2 is the square variable, β_{ij} is the coefficient of the interaction terms, $x_i x_j$ is the interaction variable term, $\in$ is the error in the response, and k is the number of variables. The variable terms are coded on a scale from -1 to +1 to represent low and high values[46].

In order to get the most efficient approximation of the polynomials, a proper experimental design must be used to collect the data[47]. Many different experimental designs can be used to fit response surfaces and CCD is the most popular design[46]. CCD generally contains 2^k factorial runs and 2k axial runs, where k is the number of variables. In CCD, two parameters can be chosen which will determine the design for fitting the model: α, which is the distance of the axial points from the center and n_c, which is the number of center points. The parameter n_c is chosen so as to give enough experimental runs to provide good variance of the predicted response (e.g., >3). In this work, a face-centered CCD with α=1 and n_c=6 was used[46].

3.1.4 Explosives Analysis

Both headspace and immersion SPME have been used to analyze various explosives. For example, headspace SPME with ion mobility spectrometry was used to analyze various plastic-bonded explosives (PBX)[48]. Ethylene glycol dinitrate (EGDN), nitroglycerin (NG), pentaerythritol tetranitrate (PETN), trinitrotoluene (TNT), and cyclotrimethylenetrinitramine (RDX) have also been analyzed using headspace SPME gas chromatography mass spectrometry (GC-MS)[49]. In addition, separate studies using headspace SPME-GC/MS have been used to determine the volatiles that are associated with explosives such as smokeless powder, PETN-based sheet explosive, Composition C-4 and TNT[50-55].

Explosives can also be present in the environment, hence, the detection of organic explosives in water and/or aqueous soil extracts has been achieved using direct immersion SPME coupled with GC-MS and GC-electron capture detection[56,57]. Some examples of explosives that have been identified in this way include 2,6-dinitrotoluene, TNT, PETN, dynamite and Composition C-4[58-60].

The identification of high explosive residues at bombing scenes has parallels to environmental analysis in that soil samples are gathered and analyzed. In addition, the identification of low explosive particles or residues of low explosives on post-blast debris plays an important role in explosives investigations. This can determine what explosive was originally present, which may link the device to a particular suspect. In the absence of intact explosive particles, the standard methodology involves extracting one or more pieces of debris with an organic solvent (e.g., dichloromethane and/or acetone) and then analyzing the extract(s) via infrared spectroscopy and/or liquid injection GC/MS[61]. Specific guidelines on the analysis of post-blast debris have been established by the Technical Working Group on Fires and Explosions (TWGFEX)[62,63].

Although the use of SPME in forensic science has been well-established for many years[64], SPME is not routinely applied to the analysis of post-blast debris. Previous reports include the analysis of single particles of smokeless powder[65] or extraction of explosive residues from soil samples gathered from the blast seat following an explosion[60,66]. The analysis of low explosive residues from post-blast debris has not been reported.

The samples of interest to this study originate from pipe bombs, which consist of a rigid container (the pipe with end caps), a low explosive filler and a chemical fuse. Given their simplicity and ease of construction, pipe bombs are a common form of improvised explosive device (IED) in the United States. For example, materials such as pipes and endcaps are found in most hardware stores, and low explosive propellants are widely available at sporting goods stores. In particular, double-base smokeless powder (DBSP) is a popular propellant that is based on nitrocellulose and nitroglycerin (NG). DBSP also contains stabilizers and burn-rate modifiers such as diphenylamine (DPA) and ethyl centralite (EC).

Residue from the explosive filler in a pipe bomb can be identified on post-blast container fragments using a variety of spectroscopic, chromatographic or mass spectrometry methods[67]. In particular, smokeless powder constituents can be identified using liquid chromatography/mass spectrometry (LC/MS)[68], gas chromatography coupled to either a thermal energy analyzer (GC/TEA) or a mass spectrometer (GC/MS)[69], and capillary electrophoresis (CE)[70].

Regardless of the method used, the amount of residue is not quantified because explosives investigators wish to know what explosive is present, not necessary how much. This project does not seek to contradict that view. Instead, we present a quantitative approach to understand, in a general sense, the distribution of explosive residue on pipe bomb fragments. In turn, this "residue mapping" may indicate what portion of the device is most likely to yield higher levels of residue. In addition, the actual concentration of residue on device fragments dictates the sensitivity and detection limit of any analytical scheme that is applied. Lastly, mapping of the residue may shed light on the specific process by which a pipe bomb container fails and then fragments. Thus far, this has only been studied using high-speed filmography[71,72].

Overall, this chapter reports several novel findings: the use of SPME (TV-SPME in particular) to analyze trace residues of low explosives, the quantitation of these residues on device fragments, and the determination of how these residues are distributed within the device itself.

3.2 Materials and Methods

3.2.1 Materials

Nitroglycerin (1 mg/mL) was purchased from Restek. Diphenylamine (ACS grade) was purchased from Acros Organics. Methylene chloride (HPLC grade), ethyl centralite (99%) and all SPME fibers were purchased from Sigma Aldrich. Galvanized steel and PVC pipe (8" x 1"diameter) and cast iron and PVC endcaps (1" diameter) were

purchased at Home Depot, and the Alliant Red Dot double-base smokeless powder was obtained from Gander Mountain. SPME vials and caps were acquired from Gerstel.

3.2.2 Instrumental Analysis

A Thermo Trace Ultra GC with a DSQ II MS and a TriPlus Autosampler was used for all analyses. Samples were incubated for 5 minutes at the desired extraction temperature. Various extraction temperatures and times were used and are discussed below. After extraction, the SPME fibers were desorbed in the GC inlet for 1 minute. A PTV inlet ramp was used with the initial temperature at 200°C for 0.21 minutes, ramped 10°C/s to 250°C and held for 0.21 minutes. The fiber was then conditioned offline at 240°C for 3 minutes. The column used was a Zebron ZB5-MS with dimensions of 10 m x 0.18 mm x 0.18 µm. Helium was used as the carrier gas with a flow rate of 1.5 mL/min. The oven program began at 40°C for 1 min, then it was ramped at 45°C/min to 250°C, immediately set to 300°C, and then held for 1 min. The transfer line to the MS and the ion source were both held at 250°C. Pulsed positive ion negative ion chemical ionization (PPINICI) was used with a methane reagent gas flow of 1.3 mL/min. Selected ion monitoring (SIM) was used to detect nitroglycerin (m/z 62 in negative mode), diphenylamine (m/z 170 in positive mode) and ethyl centralite (m/z 269 in positive mode). The total scan time was 0.1 s and the dwell times were 5 ms.

3.2.3 Effect of Fiber Chemistry

Preliminary experiments were conducted to compare several SPME fiber chemistries. A set of calibrants consisting of 5 ppb-5 ppm nitroglycerin in dichloromethane were prepared. Four fibers were evaluated: polydimethylsiloxane (PDMS), polydimethylsiloxane-divinyl benzene (PDMS-DVB), polyethylene glycol (PEG) and polyacrylate (PA). In each case, 50 µL of each calibrant was extracted at 50^{o}C for 30 min. The fibers were desorbed at 200°C in the inlet for 1 min. The fiber was conditioned offline at 240°C for 2 min. The column used in this study was a Zebron ZB5-

MS with dimensions of 60 m x 0.25 mm x 0.25 µm. Hydrogen was used as the carrier gas with a flow rate of 2.0 mL/min. The oven program began at 40°C and was ramped 20°C/min to 320°C and held 1 min. The transfer line was 220°C and the ion source was 200°C. Electron impact ionization was used in SIM mode with m/z values of 46 and 76 (NG).

3.2.4 Effect of Sample Volume

A study of the effect of sample volume with either a constant concentration (0.5 ppm) or a constant mass of NG, DPA and EC (50 ng) was completed. Sample volumes of 50 µL, 60 µL, 70 µL, 80 µL, 90 µL and 100 µL were analyzed in 20 mL SPME vials. The extraction time was 20 min and the extraction temperature was 60°C.

3.2.5 Optimization

Many parameters are incorporated into a TV-SPME method, including SPME fiber type, extraction temperature, extraction time, desorption temperature, desorption time, and sample volume. The effect of some of these variables in headspace and immersion SPME of explosives has been explored[73]. For this project, response surface methodology (RSM) and central composite design (CCD) were utilized to optimize the system[43-45]. RSM uses statistical techniques to analyze responses that are dependent on numerous variables. The ultimate goal is to optimize the response. A second order RSM model was used, as shown in Equation 3-6.

In order to get the most effective results, a proper experimental design must also be used. CCD is the most popular design used to fit response surfaces. In CCD, two parameters are chosen which will determine the design for fitting the model: α, which is the distance of the axial points from the center value and n_c, which is the number of center points. The parameter n_c is selected to provide adequate experimental data to properly model the response (e.g., >3)[9].

In this case, a face-centered CCD with α=1 and n_c=6 was used. The three parameters and ranges studied were incubation temperature (40-120°C), extraction time (5-30 min) and sample volume (10-50 µL). A constant mass of NG was used in all studies (50 ng). This required 20 experimental runs. In all cases, a polyethylene glycol (PEG) SPME fiber was used.

3.2.6 Sensitivity Comparison

Comparison to liquid injection involved preparing a series of nitroglycerin calibrants in DCM ranging from 1 pg/mL-1 µg/mL. These were analyzed using the optimized TV-SPME method with an extraction time of 20 min at 60°C. The same solutions were also analyzed via liquid injection, with 1 µL of each calibrant injected with a total splitless time of 1 min.

3.2.7 Pipe Bomb Study

Assembling and functioning of the pipe bombs was completed by the Indiana State Police Bomb Squad.

Prior to assembly, the exterior of the pipe and endcaps were color coded with paint so that the assembled devices had five distinct sections: left end cap (4.57 cm x 3.05 cm), left pipe body (3.05 cm x 6.78 cm), center pipe body (3.05 cm x 6.78 cm), right pipe body (3.05 cm x 6.78 cm), and right end cap (4.57 cm x 3.05 cm). In the device, the overlap of the endcap over the threaded portion of the pipe was 0.889 cm at each end.

Blast cages constructed of a welded steel frame and two layers of metal grating were used to trap as many fragments as possible. Approximately 50 g of DBSP was used in each device. A time fuse inserted through a hole in the right endcap was used to initiate each device. After the explosions, fragments from within the cages were collected by gloved personnel and placed in paint cans specific to each device. The pipe bomb fragments were then transported to the laboratory and stored at room temperature until needed. Prior to extraction, the fragments were sorted by pipe location/color and

photographed as a whole. Each fragment was assigned an identification number according to the convention, device number – location – number. Fragments were also photographed individually, weighed, and placed in plastic bags.

3.2.8 Extraction of Fragments

Each pipe bomb fragment was placed in a small, medium or large screw-top glass jar depending upon the fragment's size. Volumes of 10 mL, 20 mL, or 50 mL of methylene chloride were added to the jars using volumetric pipets. The jars were closed, sealed with wax film and then placed on a shaker table for 15 min. 70 µL of the extract was transferred (without filtering) to a SPME vial for analysis using the optimized TV-SPME/GC/MS method.

3.3 Results and Discussion

In the discussion that follows, NG, DPA and EC were analyzed under various conditions. However, there will be an inherent emphasis on the determination of nitroglycerin based upon the focus of forensic science laboratories. Under most forensic protocols, identifying NG on post-blast debris is required in order to report that residues of double-base smokeless powder were present. In contrast, the stabilizers and other compounds in smokeless powder can help identify the brand of the powder, but they are not unique to the explosive.

Prior to systematically gathering data, several internal standards were considered for use in the quantitation of nitroglycerin. The candidates included nitropropane (b.p. 131-132°C), nitrobenzene (b.p. 210-212°C), and triacetin (b.p. 257-259°C). The relative response of nitropropane was very low, whereas the response of nitrobenzene and triacetin were not sufficiently reproducible between runs.

The use of external standardization was further justified by determining the extraction efficiency of the method. Extracting three post-blast fragments twice in

succession proved that the first extraction was exhaustive and the mean recovery was 99.9% of the NG present. Lastly, the accuracy of external standardization was confirmed by using a 0.1 ppm test mix to challenge the calibration curve ranging from 3 ppb to 1 ppm. The mix was calculated experimentally to be 0.102 ppm, representing a 2% error.

3.3.1 Effect of Fiber Chemistry

The results of a SPME fiber comparison are summarized in Table 3-1. By far, the more polar fibers (PA and PEG) exhibited the greatest sensitivity, exceeding that of the PDMS and PDMS-DVB fibers by almost two orders of magnitude. The PEG fiber was ultimately selected as it also exhibited the widest linear range, spanning three orders of magnitude.

Table 3-1 Effect of fiber chemistry on the linear range, sensitivity, and linearity of TV-SPME for nitroglycerin.

Fiber	**Linear Range**	**Slope**	**R^2**
PDMS	50 ppb – 5 ppm	2.47×10^6	0.987
PDMS-DVB	10 ppb – 5 ppm	1.84×10^6	1.000
PA	50 ppb – 5 ppm	1.18×10^8	0.998
PEG	5 ppb – 5 ppm	1.26×10^8	0.997

3.3.2 Effect of Sample Volume

Various volumes of NG, DPA and EC standards in methylene chloride were analyzed using a PEG fiber at 60^{o}C. In this case, one set of calibrants had the same concentration for all analytes (0.5 ng/µL) whereas the other set of calibrants had differing

concentrations so that the total amount of each analyte in the vial was fixed at 50 ng. The calculated maximum volume of methylene chloride that can be vaporized at 60°C in a SPME vial was 95 µL. This is based upon Equation 3-5 and a calibration of the volume of the SPME vials using water (20.9 ± 0.1 mL).

As shown in Figure 3-3, when sample volume increased and the mass of NG was constant, the response was initially flat (as expected) followed by a rapid decrease at volumes larger than 70 µL. On the one hand, it would be expected that the response in TV-SPME would drop precipitously once the sample volume exceeded the calculated maximum. Under these conditions, some portion of the liquid sample would remain and significantly perturb the distribution of analyte. The fact that this decline actually began at much lower sample volumes may be due to the concentration of DCM vapor in the vial, which exceeds 33 ppm (v/v) with sample volumes greater than 70 µL. Given that the fiber coating does not swell (as verified by immersing the fiber in DCM), there must be a decrease in the distribution coefficient.

When sample volume increases and the mass of NG is also increasing, the response reaches a maximum at 70 µL followed by a less dramatic decline. This is consistent with the competing effects of decreased partition coefficient (as discussed above) and increasing mass of analyte. Based upon these results, the experimentally determined maximum of 70 µL for NG was used for the remainder of the study.

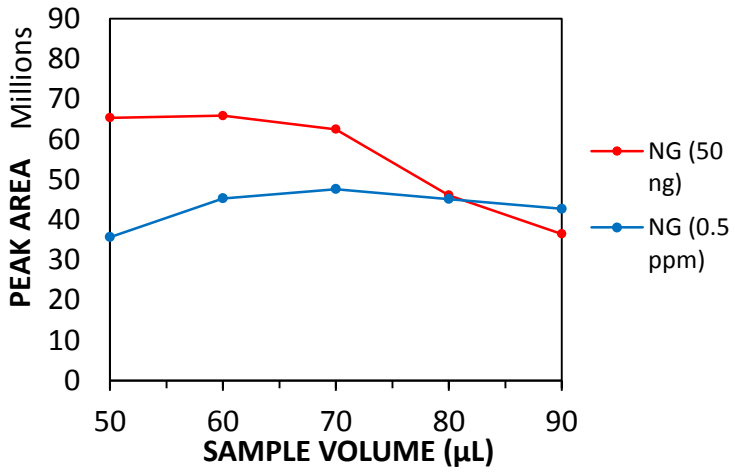

Figure 3-3 Response to nitroglycerin (m/z 62) as a function of sample volume at 60°C.

3.3.3 Optimization

In the RSM optimization, the amount of each solute was held constant in all vials by adjusting the concentration of the solutions. It became clear that the recovery of NG was much more sensitive to temperature than DPA and EC. Figure 3-3 shows three of the twenty optimization runs that utilized an extraction time of 17.5 min but with differing extraction temperatures. The peak intensities have been normalized to the response at 40^{o}C. As can be seen in Figure 3-4, NG is also exhibiting some amount of degradation in the GC inlet, resulting in two chromatographic peaks. The degradation product results from the hydrolysis of one of the nitro functional groups on trinitroglycerin to form dinitroglycerin. Additional experiments varying the inlet temperature program (data not shown) have indicated that this peak can be significantly reduced by using a lower inlet temperature.

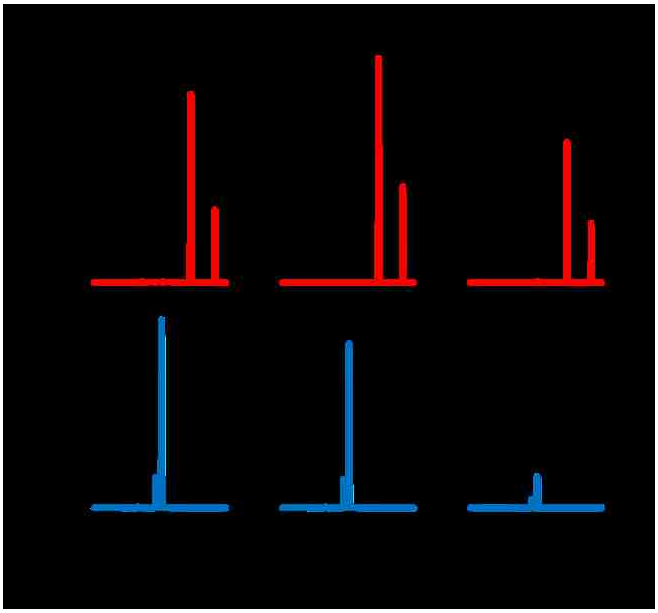

Figure 3-4 TV-SPME chromatograms of smokeless powder components using an extraction time of 17.5 min and three different extraction temperatures (Top: positive m/z 170; bottom: negative m/z 62). The peak prior to NG has been identified as dinitroglycerin (see text).

The optimized parameters for NG, DPA and EC are shown in Table 3-2 along with the overall optimum. Desirability ranges from 0 to 1 and is an indicator of how well the calculated parameters result in the optimum response. The desirability of the global optimum is noticeably lower than the optima that were found for each single component. This is primarily due to the large difference in optimal extraction temperature for NG, DPA and EC. Given the focus of this study, the optima determined for NG were used for all subsequent experiments. The ideal sample volume was determined to be 50 µL, the maximum volume investigated. Due to this, a separate volume study was done (see 3.3.2) with an expanded range to determine the optimal value.

Table 3-2 Results of the CCD optimization of TV-SPME parameters for DBSP components (R^2 = 0.81).

Analyte	**Extraction Temperature (°C)**	**Extraction Time (min)**	**Desirability (0 – 1)**
NG	60	20	0.990
DPA	80	20	0.974
EC	108	22	0.903
All	80	20	0.756

Figure 3-5 shows the results of a separate extraction time study spanning the same range as the optimization, 5-30 minutes. For extraction times up to 20 minutes, the signal for all three components increased. However, by 30 minutes, the signal for NG had significantly decreased, whereas the signal for DPA and EC leveled off. Based on these results as well as those obtained during the optimization, a 20 minute extraction time was used for the remainder of this project.

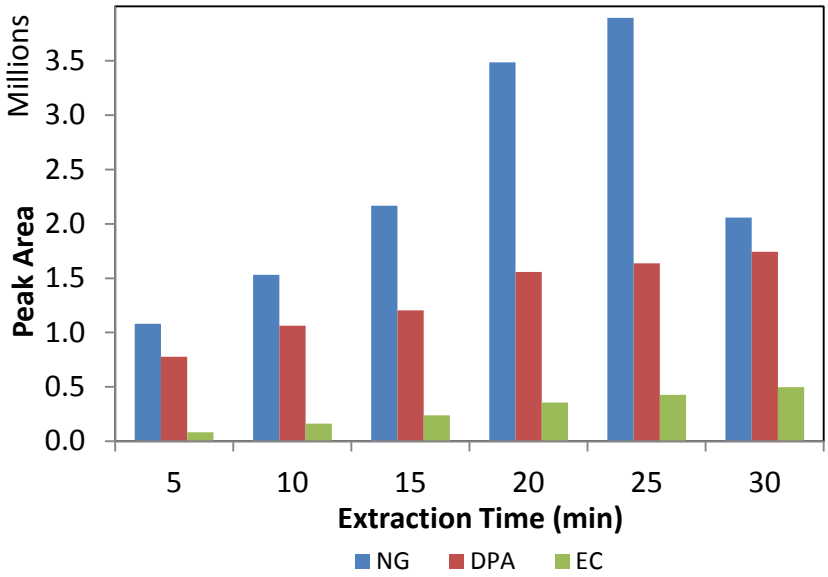

Figure 3-5 Comparison of peak area relative to extraction time for three double base smokeless powder components.

3.3.4 Sensitivity

The current "gold standard" for determining smokeless powder residues on bomb fragments is liquid injection GC/MS. Calibration curves were generated for nitroglycerin ranging from 10 ng/mL to 1 µg/mL using both liquid injection and SPME injection. The slope was calculated for both plots, and the sensitivity for TV-SPME was more than an order of magnitude larger than liquid injection. Furthermore, the signal to noise for the 10 ng/mL calibrant was over an order of magnitude higher using TV-SPME (Table 3-3). The estimated limit of detection for NG using the TV-SPME method is 100 pg/mL (S/N = 5).

Table 3-3 Sensitivity and linearity for nitroglycerin by liquid and TV-SPME injection.

Method	**Slope**	**R^2**	**S/N (10ng/mL)**
Splitless (1 µL)	2.05×10^6	1	37
TV-SPME (70 µl)	2.52×10^7	0.98	399

3.3.5 Analysis of Pipe Bomb Fragments

The optimized TV-SPME method was then applied to real post-blast pipe bomb fragments. A summary of the masses of the container, propellant and residues is shown in Table 3-4.

Table 3-4. Summary of results for the steel pipe bombs.

	Device	**1**	**2**	**3**	**4**	**5**
Pipe	**Initial Mass (g)**	724.93	740.71	737.96	738.44	744.83
	Mass Recovered (g)	617.465	489.59	437.624	729.209	505.689
	% recovery	85	66	59	99	68
	# fragments	37	54	50	36	47
Smokeless Powder	**Total (g)**	52.08	52.10	52.03	52.02	52.03
	NG (g)	9.37	9.38	9.37	9.36	9.37
Post-Blast Residues	**NG (mg)**	1.14	0.61	0.47	2.20	0.61
	DPA (µg)	-	22.42	11.99	12.90	2.00
	EC (µg)	-	3.61	3.89	-	-

Figure 3-6 shows a sample chromatogram for a galvanized steel pipe bomb fragment. Nitroglycerin and diphenylamine were able to be quantified. Ethyl centralite was present in a few extracts, but in others it was below the limit of quantitation.

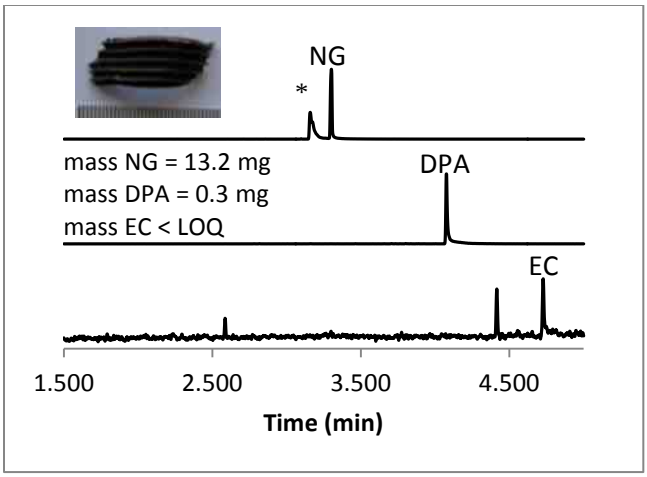

Figure 3-6 Photo (scale in mm) and chromatogram for a post-blast steel fragment (Top: negative m/z 62; middle: positive m/z 170; bottom: positive m/z 269). The peak marked with a star (*) has been identified as dinitroglycerin (see text).

The mass of NG recovered from different locations on the devices is shown in Figure 3-7 as a color-coded "heat map". In all five devices, the highest mass of NG was located on the endcap. The star represents where intact DBSP particles were found, leading to a higher recovery of NG in that location.

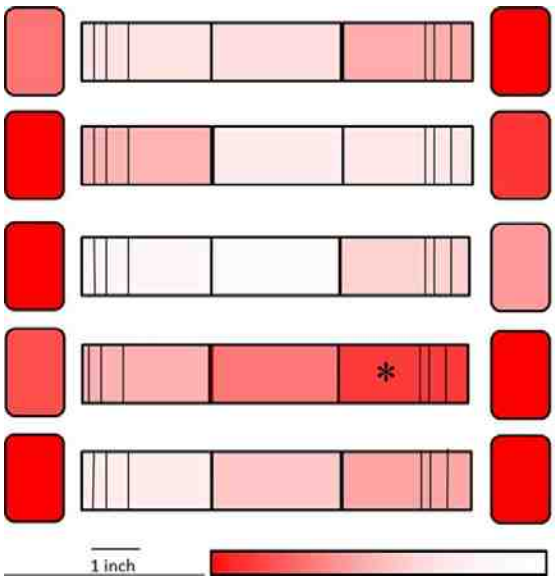

Figure 3-7 Heat maps of the five devices showing the NG distribution. The color scale is normalized to the highest amount of NG within each device (* indicates the location of the intact DBSP particles).

In similar fashion to NG, the highest concentrations of DPA were located on or near the endcaps (data not shown). The total amount of DPA recovered was much lower than NG, averaging 12.3 µg. The devices yielded a total of 7.5 µg of EC.

The extent to which explosives residues accumulate preferentially on the end caps of a pipe bomb has not been reported previously. High speed video footage of pipe bomb explosions has shown that steel devices rupture first at one of their end caps[74,75]. Therefore, the end cap regions of a pipe bomb may inherently capture and/or shield the explosives residue from the heat of the blast regardless of how the device container initially fails. This trend will need to be further confirmed in additional devices.

3.4 Conclusions

A TV-SPME method has been designed, characterized and optimized for the analysis of explosive residues on pipe bomb fragments. In this work, sample volume, incubation temperature, and extraction time of the TV-SPME method were optimized. Optimized parameters for nitroglycerin were a 60°C incubation temperature, a 20 minute extraction time, and a 70 µL sample volume. Additionally, sensitivity was compared to liquid injection, and TV-SPME was more than 12-fold more sensitive with lower detection limits (i.e., less than 1 ng/mL).

When applied to actual pipe bombs, this method determined that the mean concentration of nitroglycerin on the steel fragments was 0.25 ppm (w/w) and the mean mass of NG recovered was 1.0 mg. Fragments from the end caps yielded the highest amount of NG and DPA. These results add to the understanding of how small IEDs function as well as inform analysts regarding the sensitivity that is required for post-blast analysis of smokeless powder. In the future, other types of smokeless powder (single and triple based) could be investigated. Additionally, this technique could be applied to other container types, such as PVC.

CHAPTER 4. COMPARISON OF THE DISTRIBUTION OF POST-BLAST SMOKELESS POWDER RESIDUE IN STEEL AND PVC PIPE BOMBS USING TOTAL VAPORIZATION SOLID PHASE MICROEXTRACTION GAS CHROMATOGRAPHY MASS SPECTROMETRY (TV-SPME/GC/MS)

4.1 Introduction

It is not commonly known among the general public that criminal bombings occur daily in the United States. For example, over 36,000 illegal bombing incidents occurred in the United States between 1983 and 2002 leading to over 5,900 injuries and 699 deaths[76]. The most recent statistics from the U.S. Bomb Data Center show that the number of reported explosive incidents in the U.S. has been steadily increasing since 2009. Although the number of people that were injured and killed declined between 2004 and 2007, a large increase is seen in 2013 due to the Boston Marathon Bombing (Figure 4-1).

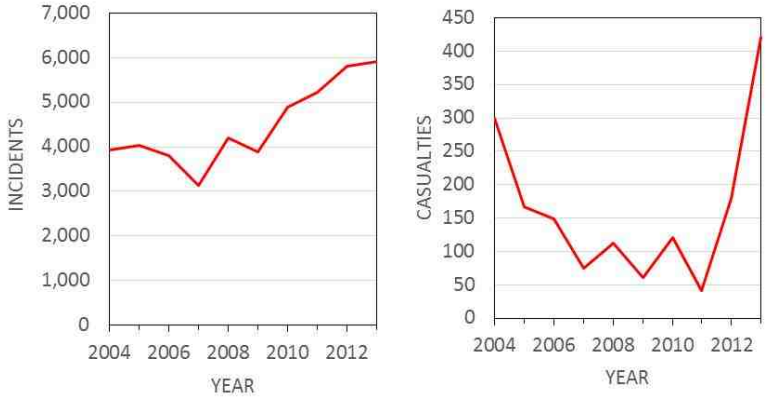

Figure 4-1 Bombing incidents and causalities from 2004 to 2013.

Post-blast analysis of various explosives is an established practice in explosives investigation. For example, nitroaromatics have been extracted from aqueous samples using a molecularly imprinted silica sorbent and analyzed using liquid chromatography[77]. Direct immersion solid phase microextraction (SPME) coupled with gas chromatography with electron capture detection was utilized to quantitatively and qualitatively identify 2,6-dinitrotoluene, trinitrotoluene, and pentaerythritol tetranitrate from aqueous solutions[59]. Additionally, triacetone triperoxide residue from various witness materials was analyzed using headspace SPME with gas chromatography mass spectrometry[78].

Among the various types of Improvised Explosive Devices (IEDs), pipe bombs are easily constructed from readily available materials. Materials such as pipes and endcaps are found in hardware stores, and low explosives are available at sporting goods stores. For example, double base smokeless powder (DBSP) is a deflagrating low explosive that will cause an explosion if contained. DBSP contains the energetic compound nitroglycerin (NG), as well as stabilizers and plasticizers such as diphenylamine (DPA) and ethyl centralite (EC). Traditionally, analysis of post-blast pipe bomb fragments is limited to qualitative identification of the explosive, due to legal issue being what, not how much of an explosive is present[4]. However, there is value to quantitation in explosives research, as it provides information on the manner by which devices explode, the amount of explosive residue remaining, as well as what instrumental sensitivity is required for analysis. Additionally, mapping of the residue will shed light on distribution and location of fragments with the highest concentration.

There are many analytical techniques that can be used to detect smokeless powder constituents, including liquid chromatography mass spectrometry[68], gas chromatography coupled with thermal energy analysis as well as mass spectrometry[69], and capillary zone electrophoresis[70,79]. The National Center for Forensic Science's Smokeless Powder Database lists standard operating procedures and instrumental methods for the analysis of smokeless powder [34]. Additionally, the Technical Working Group for Fire and Explosions Analysis (TWGFEX) released a guide in 2009 for the forensic identification of post-blast residues using categorized analytical techniques[80]. Recently, a total vaporization technique coupled with solid phase microextraction (SPME) has been

applied to the analysis of nicotine and cotinine in human hair[25] and the analysis of post-blast smokeless powder residue[81]. TV-SPME/GC/MS completely vaporizes the liquid extract which simplifies the thermodynamic equilibria. This increases the sensitivity of the pre-concentration technique, allowing lower concentrations and larger volumes to be analyzed. In this chapter, total vaporization solid phase microextraction gas chromatography mass spectrometry was used to detect smokeless powder components such as nitroglycerin (NG), diphenylamine (DPA) and ethyl centralite (EC) from extracts of both galvanized steel and PVC post-blast fragments. The goal was to quantitatively map the distribution of nitroglycerin and diphenylamine. This chapter expands on the proof of concept detailed in chapter 3. The data related to the steel devices was presented first in chapter 3 and is being repeated here in comparison to the PVC data.

4.2 Materials and Methods

4.2.1 Materials

Galvanized steel and PVC pipe (8” x 1”diameter) and cast iron and PVC endcaps (1” diameter) were purchased at Home Depot, and the Alliant Red Dot double base smokeless powder was obtained from Gander Mountain. Methylene chloride (HPLC grade) was purchased from Fisher Scientific. SPME vials and PTFE caps were acquired from Gerstel. Polyethylene glycol SPME fibers, ethyl centralite (99%), and acetone were obtained from Sigma Aldrich. Standards of nitroglycerin (1 mg/mL) and diphenylamine (ACS grade) were purchased from Restek and Acros Organics respectively.

4.2.2 Pre and Post Pipe Bomb Initiation

The constructed pipe with endcaps were divided into 5 sections; left endcap (4.57 cm x 3.05 cm), three sections along the pipe body (each 3.05 cm x 6.78 cm), and right endcap (4.57 cm x 3.05 cm). Each section was color coded with white, black, or orange paint. In the steel devices, the endcap overlapped the threaded portion of the pipe by

0.889 cm. Cages constructed of a welded steel frame and two layers of metal grating were used to contain the fragments post blast. The setup is shown in Figure 4-2.

Figure 4-2 Depiction of the experimental setup.

Approximately 50 g of DBSP was used in each device. A time fuse was used as the initiation mechanism (inserted into the white endcap). The eight devices (five galvanized steel and three PVC) were assembled, suspended, and initiated by the Indiana State Police Bomb Squad. After the explosions, fragments from within the cages were collected by gloved personnel and placed in paint cans specific to each device.

4.2.3 Cataloging Fragments

The fragments were first photographed as a whole. Then, the pipe bomb fragments were sorted by pipe location/color. Each fragment was assigned an identification number according to the convention, device number – location – number. Fragments were photographed individually, weighed, and placed in plastic bags.

4.2.4 Preparation of Standards and Extraction of Fragments

Calibrants were prepared in concentrations ranging from 25 ppb to 1 ppm containing nitroglycerin, diphenylamine, and ethyl centralite in methylene chloride. Recoveries were prepared in concentrations of either 0.1 ppm or 0.2 5ppm with the three components in DCM for the steel devices and acetone for PVC. The solutions were placed in the three jars used for fragment extraction, shaken for 15 min, and then 70 µL of DCM or 55 µL of acetone extract was transferred to a SPME vial.

Pipe bomb fragments were placed in one of three extraction jars based on fragment size. The appropriate extraction solvent, in a volume of 50 mL, 20 mL, or 10 mL, was used to extract the analytes. The jars were sealed and placed on a shaker table for 15 min. Then, 70 µL of methylene chloride or 55 µL of acetone extract, was transferred to a SPME vial for analysis.

4.2.5 Chemical Analysis

Samples were incubated at 60°C for 5 min. A polyethylene glycol fiber was then exposed inside the SPME vial for 20 min. These parameters were optimized as described previously[81]. After sample extraction, the SPME fiber was inserted into the inlet of the GC and desorbed for 1 min. The GC inlet was operated in PTV mode with an initial temperature of 200°C held for 0.21 min, ramped 10°C/s to 250°C and held for 0.21 min with a splitless injection of 1 min to correspond to the SPME desorption time. After desorption, the SPME fiber was then conditioned for 3 min at 240°C. Analytes were separated on a ZB-5MS column (10 m x 0.18 mm x 0.18 µm) using helium as the carrier gas at a flow of 1.5 mL/min. The oven program began at 40°C for 1 min, ramped at 45 °C/min to 220°C, ramped infinitely to 300°C, and held for 1 min. The transfer line to the MS was held at 250°C. Pulsed positive ion negative ion chemical ionization was used as the ionization technique. Methane was the carrier gas used for chemical ionization (1.3 mL/min). Selected ion monitoring (SIM) was used for analyte detection, with positive ions of m/z 170 and 269 and a negative ion of m/z 62.

4.3 Results and Discussion

4.3.1 Macroscopic Examination

Fragments were first sorted by color, corresponding to their initial pipe location (Figure 4-3). The number of recovered fragments ranged from 32-56 for the five galvanized devices and 757–864 for the three PVC devices. Each piece was examined macroscopically for intact smokeless powder particles, which were found on one steel device on the endcap and pipe body. This resulted in an abnormally high concentration of NG as expected, which will be discussed later. No intact particles were found on PVC fragments. Additionally, fracture matches were observed between both endcap and pipe body fragments on multiple steel devices. No fracture matches were apparent with the PVC fragments. Individual fragment masses were summed for the aggregate total. The average recovery by mass was 76% for galvanized and 56% for PVC. Many of the pipe body fragments contained several colors as shown in Figure 4-3.

Figure 4-3 Reconstruction of both device types (L: steel; R: PVC).

Since the goal is to map the concentration distribution based on color, galvanized fragments with multiple colors were separated with a handheld rotary tool prior to extraction. PVC fragments containing two colors were placed into the majority color's category.

4.3.2 Quantitative Mapping of Smokeless Powder Constituents

The performance of this analytical method is summarized elsewhere[81], but a few key parameters are highlighted here. Using a PEG fiber, the linear range spanned three orders of magnitude, from 5 ppb to 5 ppm with a linearity of 0.997. Compared to liquid splitless injection on the same sample solution, the TV-SPME method was an order of magnitude more sensitive. Additionally, the recovery of NG from PVC was quite good, 99 ± 6%, and the recovery from steel was lower but reproducible at 72 ± 2%.

The average quantity of NG recovered from each of the five steel devices was 1 mg. Although the total mass of the container recovered from the PVC devices was lower, the amount of NG recovered from each device also averaged 1 mg. Masses recovered by location are shown in Table 4-1, and heat map distributions of these values are depicted in Figure 4-4. In all cases, the highest masses were located on the endcaps; five on the fused side and three on the opposite end cap. This corresponds with the point of first failure of steel devices as shown in high speed video[71,72]. In all cases, the endcap amounts were considerably higher (~3 fold) than those of the pipe body. Note the seemingly high totals for the right side of device 4 (Figure 4-4). This is due to the intact particles that were found on the rim of the endcap and in the threads of the pipe body.

Table 4-1 Summary of NG recovered per device section.

Device	**Endcap 1 Mass (µg)**	**Pipe Body 1 Mass (µg)**	**Pipe Body 2 Mass (µg)**	**Pipe Body 3 Mass (µg)**	**Endcap 2 Mass (µg)**	**Total Mass (mg)**
Steel 1	295.6	58.5	64.6	173.9	543.5	1.1361
Steel 2	292.2	56.9	19.7	26.9	209.4	0.6051
Steel 3	289.0	8.7	2.5	52.9	116.5	0.4696
Steel 4	461.9	199.8	354.8	515.9	669.5	2.2018
Steel 5	234.5	15.5	49.3	82.5	231.1	0.6129
PVC 1	245.0		118.2	602.9		0.9661
PVC 2	559.1		65.8	600.2		1.2251
PVC 3	297.0		70.1	659.5		1.0266

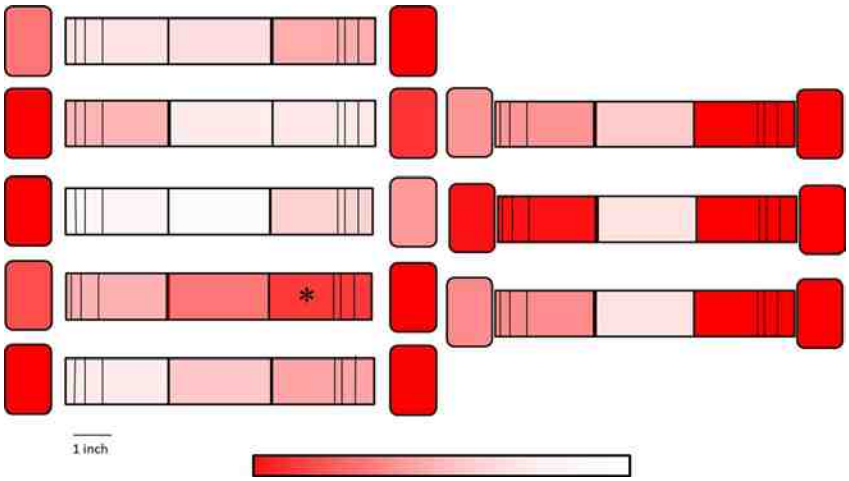

Figure 4-4 Heat maps depicting mass distribution of NG (* shows location of intact DBSP particles).

In Figure 4-4, each device has been normalized to the highest concentrated segment. This shows intra device relationships. Figure 4-5 below shows devices that have been normalized to the highest value from all devices, 669.5 µg. By doing so, the inter device distributions are highlighted. Once again, the endcaps are still more concentrated than the pipe body. The PVC devices also appear to be more concentrated relatively than most of the steel devices.

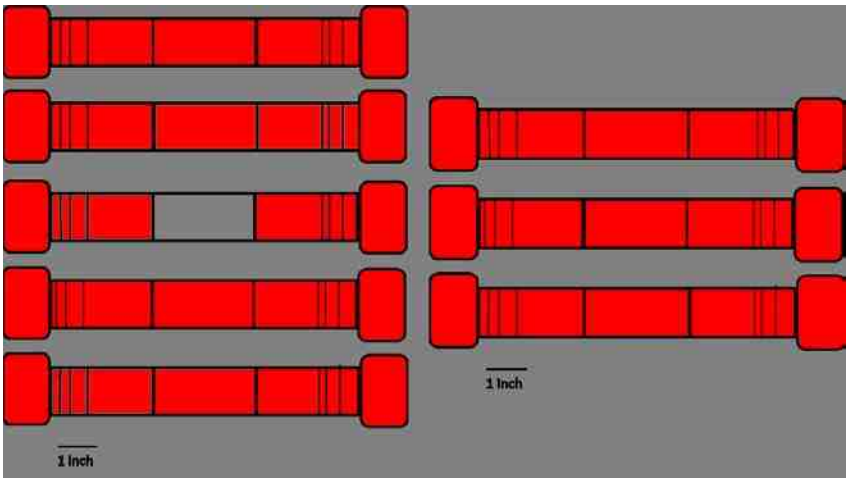

Figure 4-5 Heat maps depicting mass distribution of NG normalized to the highest value from all devices (669.5 µg).

Similar to NG, the most concentrated areas of DPA were also the endcaps, once again corresponding to the location of first failure of the steel devices (Figure 4-6). The total mass recovered for DPA was much lower than NG, only averaging 12 µg and 24 µg for steel and PVC respectively. Finally, three devices had levels of EC that were above the LOD resulting in a total mass of 8 µg.

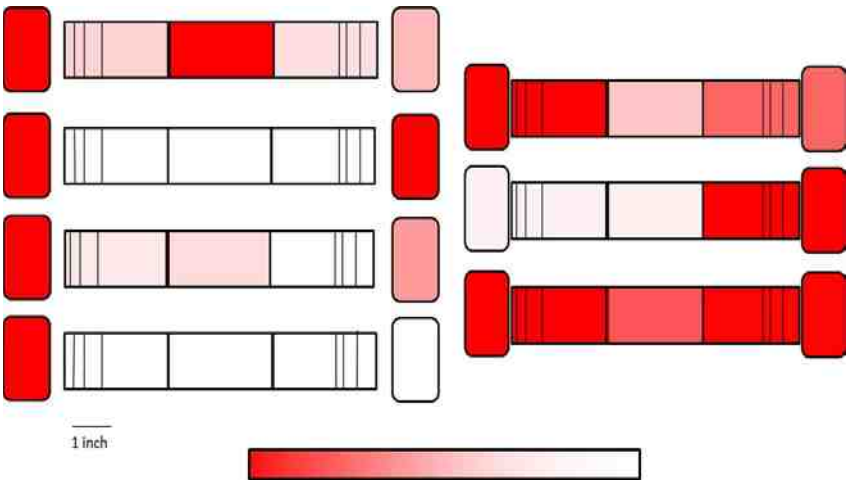

Figure 4-6 Heat maps showing DPA distribution.

Histograms were generated to depict the total mass of NG recovered as well as the ratio of mass of NG to the mass of the respective fragment (Figures 4-7 and 4-8). The range of NG found on individual steel fragments spanned from 0-516 µg, with the most common being between 50 and 100 µg. PVC range was narrower, covering 0-216 µg, with the most common under 25 µg.

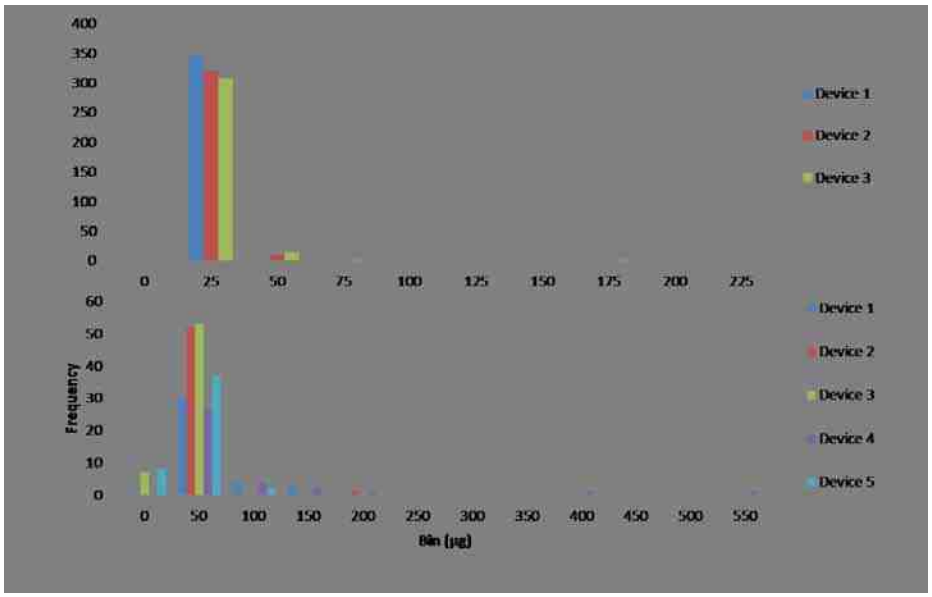

Figure 4-7 Distribution of the mass of NG recovered per fragment (Top: PVC; Bottom: steel).

The ranges of concentrations were 0-151 µg NG/g fragment and 0-114 µg NG/g fragment for galvanized and PVC respectively. In both cases, the most common range centered around 15 µg/g. Both histograms exhibit a Gaussian distribution.

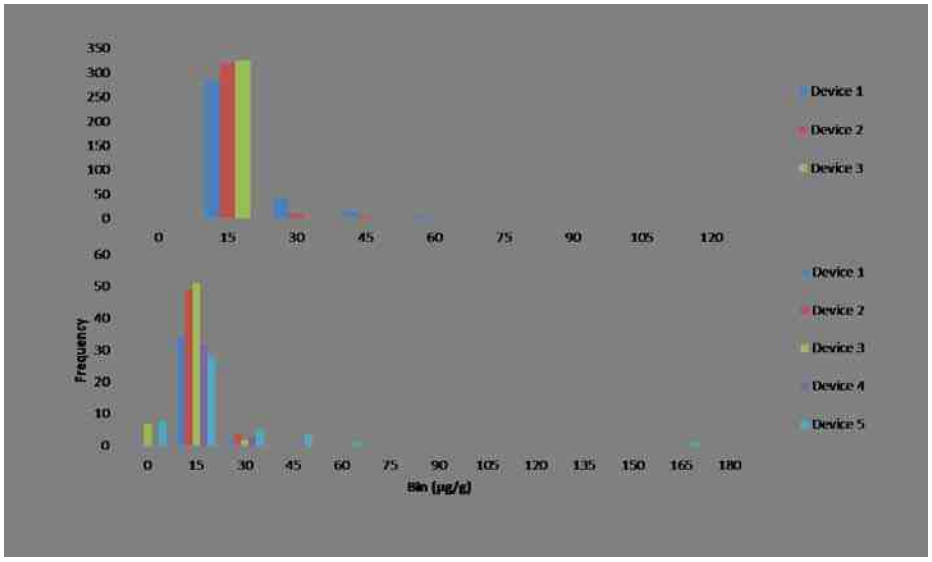

Figure 4-8 Distribution of NG concentration (µg/g) per fragment (Top: PVC; Bottom: steel).

It was also determined that there was no correlation between fragment mass and mass of NG. This is not surprising as the distribution of NG on the fragments is not homogenous during the explosion.

4.4 Conclusions

Overall, the amount of explosive residue left on fragments is small, 0.5-2 mg for NG and 2-24 µg for DPA, but not inconsequential. Both NG and DPA concentrations are the highest on the endcaps, corresponding to the location of first failure on the galvanized device. The concentration of NG was as high as 151 ppm (w/w), indicating the instrumental sensitivity required. Explosive residues are not uniformly distributed, which is expected. This is confirmed by the lack of correlation between the mass of residue and mass of fragment.

CHAPTER 5. CHEMICAL ANALYSIS OF RACING FUELS AND TRACK ADHESIVES USING TOTAL VAPORIZATION AND GAS CHROMATOGRAPHY MASS SPECTROMETRY (GC/MS)

5.1 Introduction

The National Hot Rod Association (NHRA) is the governing body of North American drag racing and is the largest motorsports sanctioning body in the world. Since it was founded in 1951, the NHRA has grown to over 20 categories of competition, including top fuel, funny car, pro stock, and pro stock motorcycle[82]. One of the duties of the NHRA is safety, therefore monitoring the consistency of the adhesives used to prepare the dragstrip is vital. Factors such as geographical region, humidity, and ambient temperature can affect the performance of the adhesive. Additionally, race teams are required to purchase approved fuel for their vehicles. This is the only fuel allowed and any adulteration is prohibited. The NHRA is responsible for post-race fuel testing as well. Precise analyses are required due to stiff monetary and performance penalties that can be imposed on the race teams as a result of the laboratory findings.

One type of fuel that is used is based upon nitromethane. However, the maximum percentage of nitromethane allowed in the blend is 90% by volume, with the remainder consisting of methanol. Due to the oxygen contained with the nitromethane structure, the power output when burned is higher than that of regular gasoline. In this study, total vaporization headspace gas chromatography mass spectrometry was used to quantitate the percentage of methanol in nitromethane fuels. Total vaporization is a technique used to fully vaporize a liquid sample, forcing all of the analytes into the headspace. The volume that can be vaporized is dependent on the solvent properties and temperature, and is shown in Equation 3-5[25].

Nitromethane has been analyzed using headspace GC/MS for the purpose of canine explosive detection[83]. Quantitation of nitromethane in human blood for the purpose of assessing toxicity was done using solid phase microextraction with GC high resolution mass spectrometry[84]. Another study used activated carbon with gas chromatography flame ionization detection to sample and test nitromethane in air[85].

In addition to nitromethane-based fuels, racing gasolines are also used. Gasoline contains a mixture of hydrocarbons and additives. For example, lead is added in the form of tetraethyllead and serves as an octane booster. Gasoline has been analyzed using a variety of methods, such as GC/MS for the detection of added organic solvents[86], near infrared along with multivariate statistical analysis for the classification of gasoline[87], and high performance liquid chromatography with a UV-diode array detector for the measurement of benzene and the total aromatic fraction in gasoline[88]. In this study, total vaporization solid phase microextraction with gas chromatography mass spectrometry will be used to analyze racing gasoline. This technique has been used to analyze nicotine in hair and post-blast explosive residue on bomb fragments[25,81].

In order to ensure the safety of the racers as well as the uniformness of the racing surface from event to event, several adhesive samples were also analyzed. The process of preparing a track involves a multistep procedure of scraping, cleaning, dragging, spraying diluted adhesive, and curing. Environmental factors, such as temperature and humidity, must be taken into consideration when preparing the track for each event. To our knowledge, there are no current methods of analysis for this specific product. A suite of techniques including liquid injection GC/MS, infrared spectroscopy, and gravietry to determine evaporation rate were used to evaluate the performance of the adhesive.

Racing gasolines have never been analyzed using TV-SPME/GC/MS and no literature has been published on track adhesive analyses either. All analyses related to NHRA samples are novel. The overall aim of this work is to design and implement a protocol for fuel and adhesive analysis that can be used for future testing.

5.2 Materials and Methods

5.2.1 Chemicals and Reagents

HPLC grade nitromethane (NM, ≥96%) and HPLC grade methanol (MeOH, ≥99.9%) were purchased from Sigma-Aldrich (St. Louis, MO). SPME vials and PTFE lined caps were purchased from Gerstel (Linthicum, MD).

5.2.2 Nitromethane Standard Preparation

Five calibrants ranging in concentration from 0-20% v/v methanol in nitromethane were prepared. Two test mixes were prepared at 8% and 12% methanol in nitromethane. Twenty microliters of calibrant were transferred to 20mL headspace vials.

5.2.3 Nitromethane GC/MS Instrumental Parameters

A Thermo Scientific Trace Ultra GC, DSQII, and Triplus autosampler were used for all analyses (Waltham, MA). The sample vials were incubated for 5 minutes at 80°C so that they totally vaporized. The headspace syringe was heated to 85°C and injected a sample volume of 1 mL. The sample was split 100:1. Hydrogen was the carrier gas, held at 1 mL/min. The inlet temperature was 220°C and the oven was held at 35°C for 4.5 min. The column used was a Zebron ZB-5MS with dimensions of 60 m x 0.25 mm x 0.25 µm (Phenomenex, Torrance, CA). The transfer line temperature was 280°C and the ion source was 200°C. The mass spectrometer was operated in electron impact mode with no solvent delay, scanning a range of m/z 29-100.

5.2.4 Racing Gasoline GC/MS Instrumental Parameters

The racing gasoline samples (VP C-25, VP C-23, Sunoco SR-18) were transferred to 20 mL SPME vials (80 µL). The samples were incubated for 5 min at 100°C and

extracted for 20 min at 100°C using a polyethylene glycol (PEG) fiber. The fiber was desorbed in the inlet in splitless mode for 1 min at 240°C, and conditioned for 3 min at 240°C. Helium was the carrier gas at 1.5 mL/min. The oven program began at 40°C and was held for 2.5 min. It was then ramped 10°C/min to 280°C and held for 3 min. The column used was a Zebron ZB-5MS with dimensions of 10 m x 0.18 mm x 0.18 µm. The transfer line and ion source were both 250°C. The mass spectrometer was operated in electron impact mode with no solvent delay, scanning a range of m/z 30-500.

5.2.5 Track Adhesive GC/MS Instrumental Parameters

The track adhesive samples (100% adhesive, diluted adhesive, and methanol) were transferred to 2 mL autosampler vials. Samples were injected (0.1 µL) into a 280°C inlet with a split ratio of 100:1. The carrier gas was helium at 1.5 mL/min. The oven started at 40°C and was held for 2 min. It was then ramped 20°C/min to 300°C where it was held for 3 min. The transfer line was 300°C and the ion source was 200°C. The mass spectrometer was operated in electron impact mode with no solvent delay, scanning a range of m/z 24-300 for the first 2 min, and m/z 22-300 for the remainder of the run.

5.2.6 Track Adhesive ATR-FTIR Instrumental Parameters

A Perkin Elmer Spectrum 1 infrared spectrometer was used for all analyses (Waltham, MA). A drop of the undiluted adhesive was placed on the crystal and the solvent was allowed to evaporate. Four scans were acquired with a resolution of $4cm^{-1}$, scanning a range of $4000\text{-}650cm^{-1}$.

5.2.7 Track Adhesive Evaporation Study

Several milliliters of adhesive sample were added to a tared tin on an analytical balance. The mass of the adhesive was recorded every 15 seconds for 5 minutes. The

mass vs time values were plotted, and the first five points were used to calculate the slope, which is equivalent to the evaporation rate. The tins were allowed to dry overnight, and the final mass along with the initial were used to calculate the percent residual solid by mass.

5.3 Results and Discussion

5.3.1 Nitromethane

The maximum volume of nitromethane that can be vaporized at a given temperature can be calculated using Equation 3-5. The maximum sample volumes as a function of temperature, ranging from 55 – 90°C, are shown in Figure 5-1 for nitromethane.

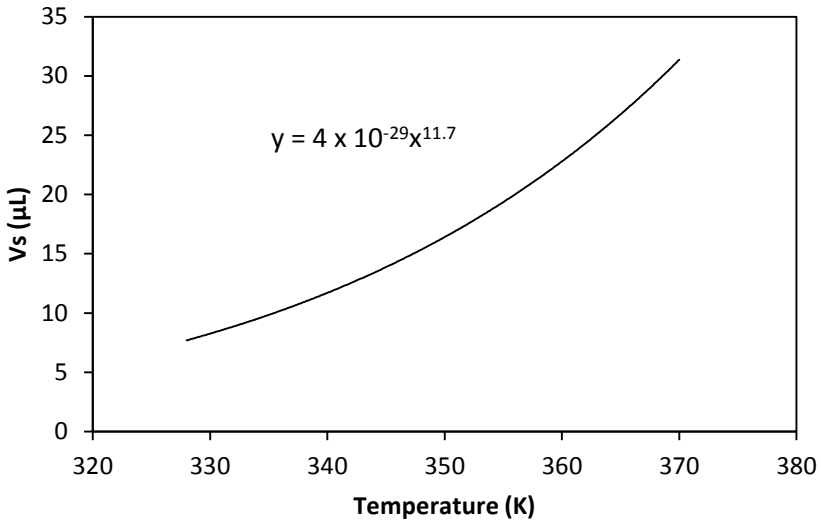

Figure 5-1 Theoretical volume of nitromethane that can be vaporized as a function of temperature.

In this method, the incubation temperature is 80°C which corresponds to a calculated maximum volume of 19 µL. A volume study was performed to evaluate this number, with volumes ranging from 12 – 24 µL (Figure 5-2). The optimal volume was

determined to be 20 µL, with larger volumes plateauing in peak area response. These experimental results agree with the theoretical value.

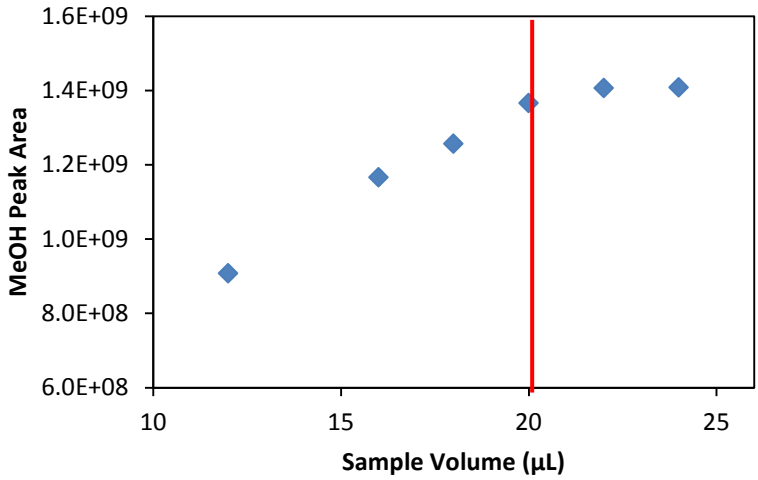

Figure 5-2 Volume study results showing methanol peak area as a function of sample volume.

Following the volume study, a calibration curve was made by preparing standards ranging from 0 – 20% methanol in nitromethane (v/v). The linearity was excellent, with a R^2 value of 0.996. The two test mixes of 8% and 12% methanol in nitromethane were determined experimentally to be 8.8% and 13.4% using this method. This corresponds to a relative error of 10% and 12%, respectively.

5.3.2 Racing Gasoline

The major component of the racing fuels tested is isooctane. Using Equation 3-5, the theoretical maximum volume of isooctane that can be vaporized at 100°C is 109 µL. To be conservative, 80 µL of fuel was used for analysis. Three racing gasolines from the manufacturer VP Racing (C25, C23, and C11) and one from Sunoco (SR18) were analyzed. It was determined that the fuels contained both branched and aromatic hydrocarbons, along with tetraethyllead. Tetraethyllead was present in all racing fuels tested and is an anti-knock, octane boosting additive.

In one instance, a fuel sample from a car looked noticeably different than the C25 reference (Figure 5-3). The car fuel had a mixture of straight and branched hydrocarbons with boiling points between eicosane ($C_{20}H_{44}$) and tetracosane ($C_{24}H_{50}$). Examples of products that fall in this range are heavy fuel oils, lubricating oils, and waxes[15]. Therefore it is thought that other compounds from the automobile made their way into the fuel.

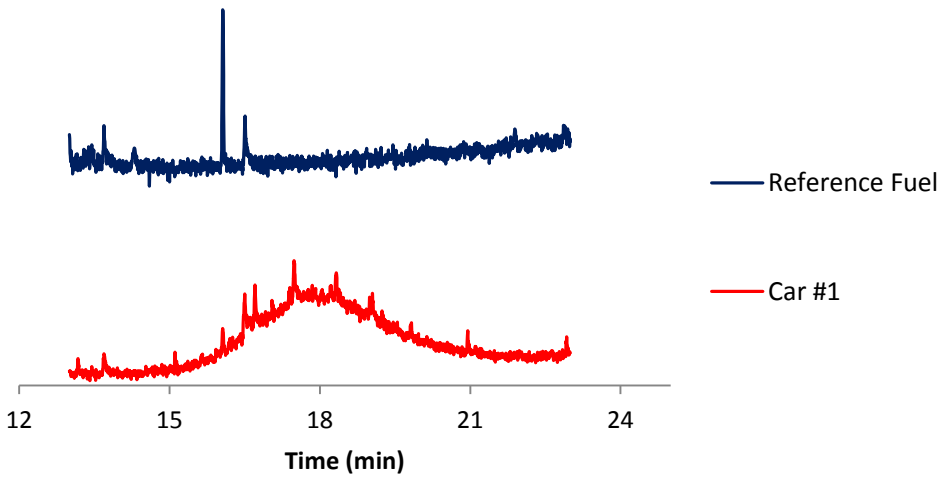

Figure 5-3 Comparison of a C25 reference fuel to a car fuel sample.

The second VP fuel, C23, had similar components, with the addition of toluene. An example chromatogram is shown in Figure 5-4.

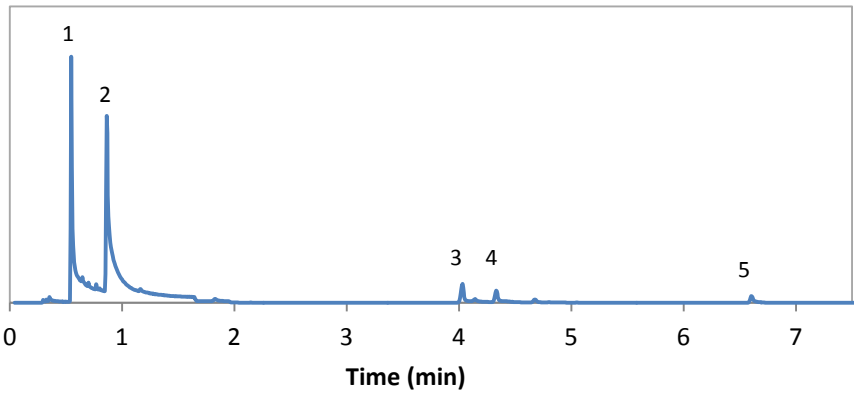

Peaks: 1) isooctane, 2) toluene, 3) 2,2,4,6,6-pentamethylheptane, 4) 2,2,4,4-tetramethyloctane, 5) tetraethyllead

Figure 5-4 Example chromatogram of VP C23 fuel.

In 2015, the NHRA switched fuel suppliers from VP to Sunoco. The Sunoco SR18 racing gasoline had similar components to VP C25, along with the presence of toluene. The major difference is that VP C25 had three unique components, 2,2-dimethylbutane, 2,2,4,4-tetramethyloctane, and 2,2,7,7-tetramethyloctane that are not present in Sunoco SR18. NHRA officials suspected race teams of adulterating their fuel with last year's brand, since it performs better according to the teams. A questioned fuel was analyzed along with standards of fuel. The results are shown in Figure 5-5 below. Peak 3, 2,2-dimethylbutane is unique to C25, and it is present in the questioned car sample (17) although it shouldn't be. The tetramethyloctane isomers not shown in the chromatogram were also present in the car sample, therefore it was concluded that the fuel was illegally adulterated. The three compounds unique to C25 all act as octane boosters in the fuel. This means the gasoline is able to be compressed more before auto-ignition, decreasing engine knock caused by the spontaneous combustion. Since more of the fuel is ignited by the proper method, the spark plug, more horsepower is generated leading to higher performance of the vehicle. Based on this knowledge, the claim made by the race teams that C25 has superior performance is confirmed and explained using this method.

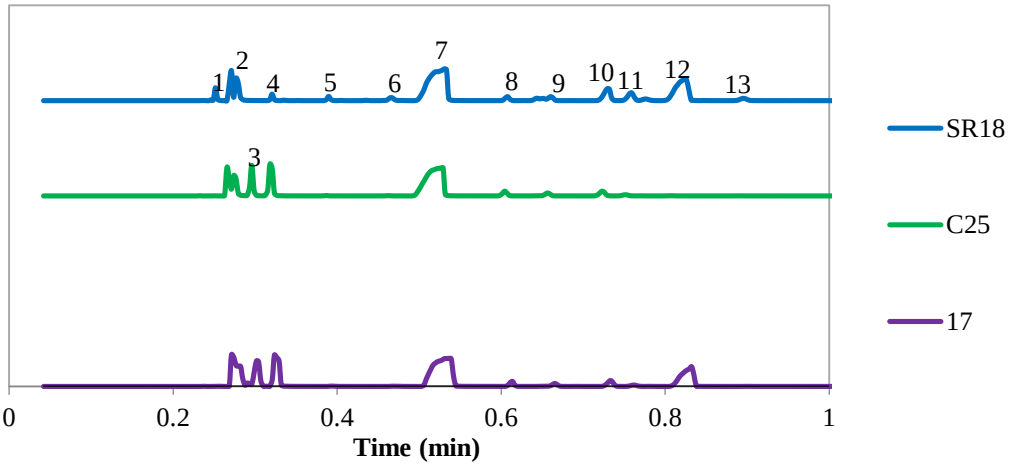

Peaks: 1) butane; 2) isopentane; 3) 2,2-dimethylbutane; 4) isohexane; 5) 2,4-dimethylpentane; 6) 2,3-dimethylpentane; 7) isooctane; 8) 2,2-dimethylhexane; 9) 2-methylheptane; 10) 2,3,4-trimethylpentane; 11) 2,3-dimethylhexane; 12) toluene; 13) 2,2,4-trimethylhexane

Figure 5-5 Chromatograms of reference racing gasolines and a questioned car sample labelled 17.

Since the fuels appeared different, specific gravity measurements were calculated. Specific gravity is a ratio of the density of a substance to the density of a reference, in this case HPLC water. Specific gravity is used as a tool in fuel monitoring since it can be an indicator of composition. The reported value for the Sunoco SR18 was 0.70. The experimentally determined specific gravity values ranged from 0.697 – 0.709 for all fuels with a precision of 0.2% - 0.5%. Acceptable limits have not been set by the NHRA and additional testing is required to determine at what concentration adulteration can be detected using this technique. The questioned fuel in Figure 5-5 had an experimentally determined specific gravity of 0.7006. Therefore, the presumptive specific gravity test was not enough to detect the additional fuel, the confirmatory TV-SPME/GC/MS analysis was required.

5.3.3 Track Adhesive

Track adhesives were analyzed first by GC/MS. An example chromatogram is shown in Figure 5-6. Identified components include isopropanol, methylene chloride, 2-methylpentane, 3-methylpentane, hexane, 2,2-dimethylpentane, 2,4-dimethylpentane, methylcyclopentane, 3,4-dimethylbutane, 3,3-dimethylpentane, cyclohexane, heptane, 1,1-diethoxythane, toluene, d-limonene, and p-tertbutylphenol.

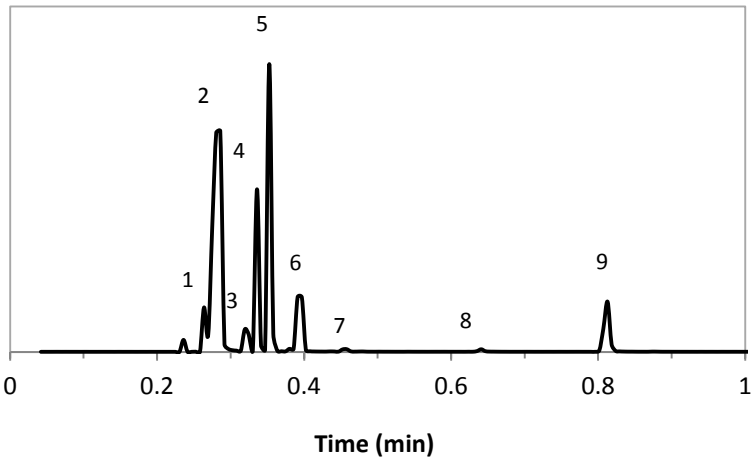

Peaks: 1) ethanol; 2) acetone, syringe wash; 3) 2-methylpentane; 4) 3-methylpentane; 5) hexane; 6) methylpentane, 7) cyclohexane, 8) 1,1-diethoxyethane, 9) toluene

Figure 5-6 Example chromatogram of a track adhesive sample.

Infrared analysis yielded visually similar spectra, with the library hit being poly (vinyl ethyl ether). There is an additional peak at 1780 cm^{-1} in the library that is not present in the sample. This represents a carbonyl group. Poly (vinyl ethyl ether) does not have a carbonyl in its structure, and therefore should not have this peak in the spectrum. Example spectra are shown in Figure 5-7. Poly (vinyl ethyl ether) is commonly found in pressure sensitive tapes, due in part to their resistance to sunlight and transparent nature[89]. These adhesives contain poly (vinyl ethyl ether) as the base adhesive, along with other tackifiers, plasticizers, and antioxidants[89].

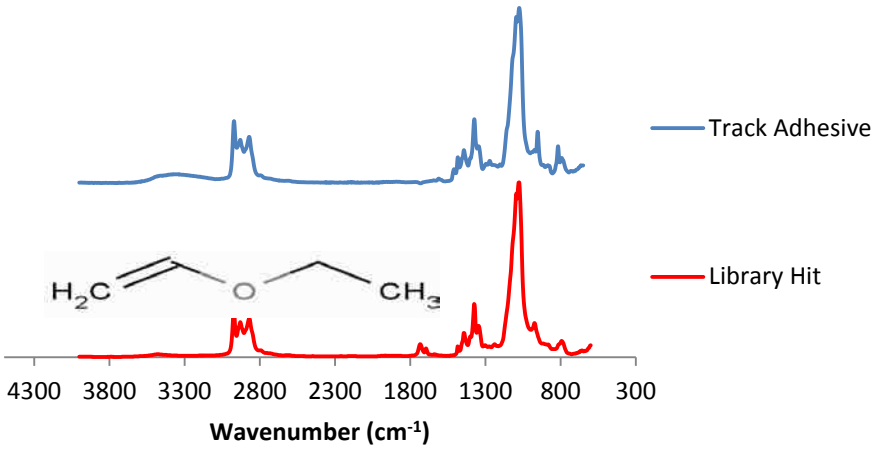

Figure 5-7 Example IR spectrum of a track adhesive sample and the library hit with the structure of poly vinyl ethyl ether.

In addition to chemical analysis by GC/MS and IR, the evaporation rate and percent residual solid of the track adhesives were calculated. The results for one set of samples are shown in Table 5-1. The average evaporation rate was 29 mg/min, which was calculated from the slope of the linear trendline on the mass vs time plot. The average percent residual solid was 18%, signifying the amount of adhesive left after the solvent has fully evaporated. These samples are listed in the order in which they were collected over a five month period. There is a clear trend as the summer progresses; the residual mass of the adhesive decreases and the evaporation rate increases. Diluted samples (75% v/v) of track adhesive were also submitted. In this case, the actual dilution factor was determined based on the residual solids. The average dilution factor was 75 ± 4%. After discussion with the NHRA, some races required a higher dilution since the adhesive was too sticky due to environmental conditions. This accounts for some of the error in precision.

Table 5-1 Track adhesive evaporation rates and residual solid masses.

Sample	Evaporation Rate (mg/min)	Mass % of 100% Adhesive	Percentage of 75% to 100% Adhesive
1	20.9	20.6	70
2	24.2	20.0	72
3	24.5	19.4	69
4	31.3	19.2	73
5	26.5	18.9	74
6	26.5	17.7	79
7	28.3	17.4	75
8	29.6	17.5	73
9	30.8	16.7	76
10	30.8	16.4	78
11	32.0	15.4	80
12	33.6	14.8	77
13	33.6	14.6	78

Another set of track adhesives were analyzed using the same technique. The range of percent residual solid was rather wide (11-22%) compared to previous samples. When plotted chronologically, the first three races appear to have higher values than subsequent races (Figure 5-8). NHRA officials later informed us that the manufacturer cut the amount of adhesive within the mix due to some of the components being backordered. This could account for the apparent decrease after the third race.

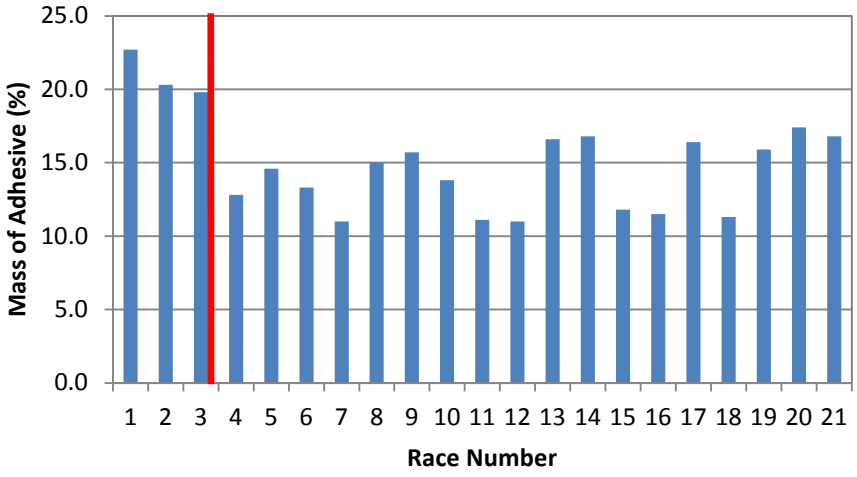

Figure 5-8 Percent residual solid of track adhesives in chronological order.

5.4 Conclusions

Multiple GC/MS methods, including two based upon total vaporization, have been developed to identify compounds in racing fuels and track adhesives. These results, along with IR data, provide a comprehensive picture of normal/abnormal fuel compositions as well as the extent of quality control of track adhesives. All methods have been validated for the application to NHRA related standards and samples. These methods and protocols will be used for future quality control testing.

CHAPTER 6. FUTURE DIRECTIONS

6.1 Characterization of Pipe Bomb Fragments

As mentioned previously, the lethality of pipe bomb shrapnel is not fully recognized. A study could be designed using high speed video that includes information on velocity, mass, momentum, kinetic energy, standoff distance and perforation potential. Only one camera was used in the previous study, meaning a two dimensional image of a three dimensional event was generated. Because the third dimension was not accounted for, the velocities that were calculated from the footage were minimum estimates. A second camera placed at a 90° angle to the first (Figure 6-1) would allow a three dimensional representation of the event to be captured. ProAnalyst software has the capability to combine the two videos and generate one velocity measurement for each fragment. This will provide more accurate velocity measurements than only using one camera.

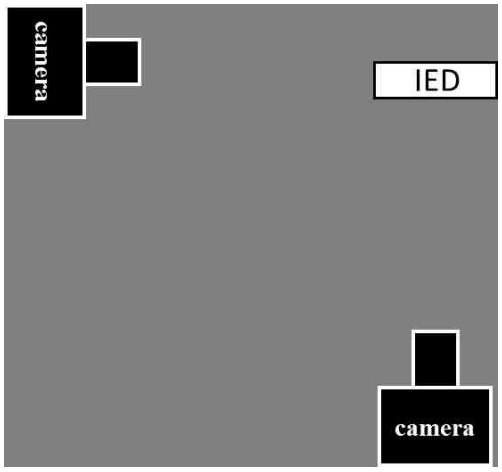

Figure 6-1 Schematic of the two camera setup for capturing pipe bomb explosions

Also in the previous study, only three fragments were able to be identified conclusively in the video footage. Therefore, advanced information (momentum and kinetic energy) was only able to be calculated for three out of hundreds of fragments. In the proposed study, devices would be color coded and color video would be used to enhance the probability that individual fragments can be identified. By doing so not only would the mass and velocity be known, but momentum and kinetic energy could be calculated as well, further demonstrating the damage potential of bomb fragments.

Although the size of a device may be rather small, a 20.32 cm long by 2.54 cm diameter pipe for example, the explosion can cause the fragments to travel long distances at impressive speeds. The fragmentation safety distance for a single ammunition item is described by the following equation[90]:

$$D = 370W^{\frac{1}{5}} \qquad \text{(Equation 6-1)}$$

Where D is the distance in meters and W is the mass of the item being destroyed including case and charge. For example, in the bomb study that was completed for this project, a PVC device would require a distance of 271 m and a steel device would require 362 m.

In addition to standoff distance, the likelihood of penetration by fragments can also be calculated. The V_{50} represents the striking velocity for which half of the impacting projectiles will perforate an object. An equation was experimentally derived using steel projectiles of various shapes and masses as well as human and goat skin[91].

$$V_{50} = 1247.1\,\frac{kg}{m*s}\left(\frac{A}{M}\right) + 22.03\,\frac{m}{s} \qquad \text{(Equation 6-2)}$$

Where A is the cross-sectional area of the projectile along the trajectory and M is the mass of the projectile. This equation was applied to two steel fragments of varying shapes and sizes, shown in Figure 6-2. The larger fragment has a V_{50} value of 23 m/s while the smaller fragment's velocity is 30 m/s. The average velocity of steel fragments immediately following a device rupture was 234 m/s in one blast. At this velocity, fragments would puncture skin and cause serious injury.

Figure 6-2 Fragments used to calculate V_{50} velocities.

The proposed study would test the theoretical calculated velocities. The mass and area of the post-blast fragments would allow a direct comparison of the experimental and theoretical values. By investigating the mass, velocity, momentum, kinetic energy, potential distance traveled, and the velocity required for perforation, the destructiveness of pipe bomb fragments will become apparent.

6.2 Chemical Analysis of Explosive Residue

In regard to mapping explosive residue, several modifications and additional experiments could be done in order to extract more information from the results. First, prior to initiation, the PVC devices should be colored using five different colors opposed to three. The endcaps and pipe body were indistinguishable post-blast for PVC, therefore only three device sections were able to be used compared to five for the steel devices. Using five distinct colors will allow a more specific breakdown of the residue distribution, as well as a direct comparison to the steel data.

Another improvement to the real world device initiation procedure would be to enhance the durability of the bomb containment structure. The goal would be to design a cage that would allow the blast pressure to escape without destruction and to contain as many of the fragments as possible. Multiple containment structures were tested before the final one was decided upon, including wood, plastic lined wood, wood with metal

grating, and perforated metal grating surrounding a steel frame. The perforated steel design allowed the pressure to escape and contained the fragments to a degree, but repeated use led to large holes as shown in Figure 6-3.

Figure 6-3 Containment structure after multiple initiations of steel devices.

On average, 76% of PVC fragments were recovered, while only 56% of steel fragments were recovered. This recovery was able to lead to definitive conclusions on the distribution and amount of explosive residue, however a higher recovery of fragments would bolster the results. Additional layers of perforated grating would create a stronger barrier, effectively increasing the overall recovery. The closer the recovery to 100%, the more representative the quantitative residue results will be. A larger structure would not be beneficial, since the initial velocity value only has only decreased 4 m/s at a distance of 100 m based on the following equation[14]:

$$V_s = V_o e^{\frac{-\rho C_d A s}{2m}} \qquad \text{(Equation 6-1)}$$

Figure 6-4 shows the relationship between the estimated velocity of a specific fragment as a function of distance. The containment structure would need to be extremely large to allow for the fragments to decrease velocity before impacting the barrier.

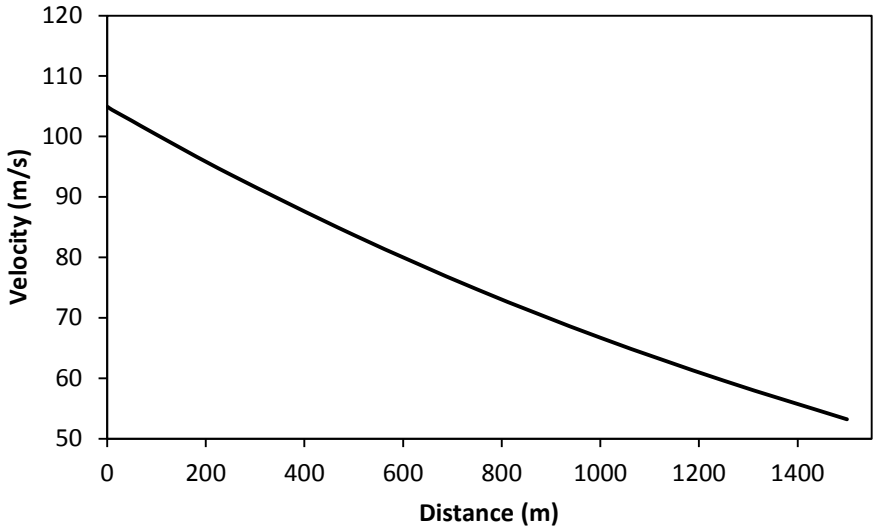

Figure 6-4 Fragment velocity as a function of distance for a black steel double base smokeless powder fragment.

In regard to the chemical analysis of explosive residue, the aforementioned nitroglycerin degradation peak could be investigated in order to decrease or eliminate it. The degradation peak was present in all samples and standards, and was not included in any calculations. It is known that NG decomposes near 220°C, and the inlet program began at 200°C and ended at 250°C. An inlet program was used to assist in the desorption of the three analytes, NG, DPA, and EC, which have boiling points ranging from 50-325°C. Lower inlet temperatures showed a decrease in degradation peak intensity, with a 100°C isothermal inlet temperature eliminating the peak altogether. A drawback to using such a low inlet temperature for this study is that the sensitivity of DPA and EC decreases dramatically. This is due to those compounds having much higher boiling points than NG.

The sensitivity of TV-SPME is much higher than traditional liquid injection. This is due in part to the ability of TV-SPME to analyze larger sample volumes, 70 μL in this case. TV-SPME at this volume has been directly compared to a 1 μL liquid injection, with TV-SPME sensitivity being an order of magnitude higher (Table 3-3). To further compare the two techniques, the same sample volume (1 μL) could be analyzed using both methods. Based on the values in Table 3-3, the extrapolated response from NG using

TV-SPME at a volume of 1 µL would be 3.6 x 10^5. This value is less sensitive than liquid injection at the same volume, however this shows the advantage to using TV-SPME; larger volumes are able to be used, yielding higher sensitivity.

Quantitative mapping of explosive residue was done for two container types but only one explosive filler, a double base smokeless powder. Additional fillers could be investigated to see if the resulting distribution is similar in that the endcaps are highly concentrated compared to the pipe body. A filler that could be tested is Pyrodex, a black powder substitute. Pyrodex is also a low explosive, like double base smokeless powder, however it is lower energy. By comparing various energetic fillers, additional information into the residue distribution and deflagration process will be known.

TV-SPME is a novel technique used to analyze explosive residue in this case, but in the future another recently developed technique could be investigated. Ambient ionization generates charged analytes outside the mass spectrometer and does not need prior extraction or separation. This allows for *in situ* analysis and enhances throughput. A specific type of ambient ionization is desorption electrospray ionization or DESI. A nebulizing gas carries a charged solvent spray which ionizes and desorbs analytes from the substrate, then the ions are drawn into the mass spectrometer[92] (Figure 6-5). DESI has been used to analyze high explosives, TNT, RDX, HMX, Composition C-4, and PETN from a variety of surfaces such as metal, plastic, paper, and human skin[93-95].

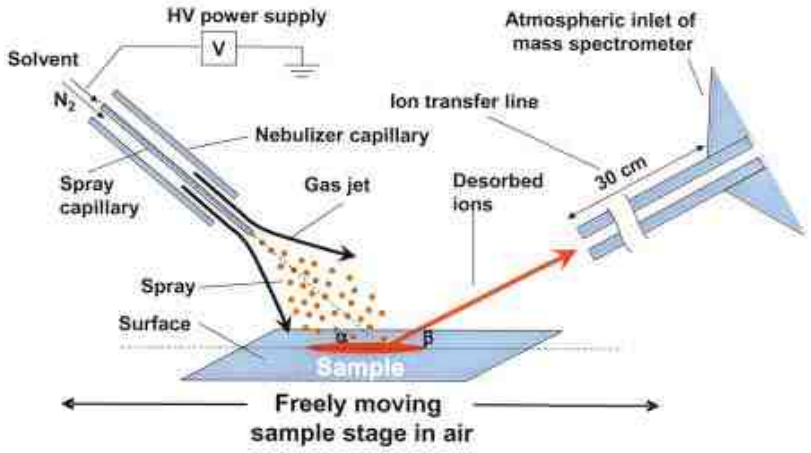

Figure 6-5 Schematic of desorption electrospray ionization[92].

By using DESI, the extraction step would be eliminated as fragments could be directly analyzed. DESI can generate images based on the abundance and location of certain ions. This would be beneficial in mapping the concentration of the smokeless powder components, as well as overcome the fact that only a small spot is analyzed at a given time. Not only would an overall device map be created, but the distribution on each fragment could also be diagrammed. A potential issue is the capability of DESI to analyze curved surfaces, like many metal pipe bomb fragments are (Figure 6-1). The 3D DESI systems are able to move the sample stage in three dimensions, which is beneficial to keeping the sampling distance consistent and to analyzing the entire curved surface. If this is not sufficient, the twisted fragments could be flattened as much as possible prior to analysis.

6.3 NHRA Samples

A TV-SPME method was developed for the racing gasoline samples, but not for the track adhesives. In the future, a TV-SPME method will be beneficial since the adhesives contain a variety of solvent. TV-SPME is a technique ideal for the analysis of volatile and semi-volatile compounds. An advantage of TV-SPME is the elimination of matrix effects. The adhesive polymer present in the adhesive solution could interfere with the volatile compounds transitioning into the headspace. To test this, a matrix recovery study could be done in order to calculate the known concentration of the analyte in solvent alone, as well as the analyte in a polymer matrix. The calculated recoveries will indicate the presence of any matrix effects, however with TV-SPME these are minimized if not eliminated.

Due to the inconsistencies in the track adhesive in varying ambient temperature, other base adhesives will be investigated. Those with a broader temperature range where adhesive strength remains steady would provide a more stable racing surface throughout the season. The current adhesive is in the poly (ethyl ether) class. Another commercial option is a fatty acid based adhesive. Preliminary results show that a commercially

available fatty acid based adhesive evaporates at least two times slower and has less adhesive by mass. Additionally, after the solvents have evaporated, a cloudy oily type substance remains, compared to a clear thin film left by the ethyl ether adhesive (Figure 6-6).

Figure 6-6 Post evaporation of commercially available track adhesives (Left: poly (ethyl ether) based; right: fatty acid based).

Since the fatty acid based does not appear to out-perform the current adhesive, others should be tested, such as solvent acrylic based and polychloroprene based. These two adhesives have a wide operating temperature range and have a high tack, both of which are important in preparing a race track across the United States.

LIST OF REFERENCES

LIST OF REFERENCES

(1) Lucas, J.; Crane, J. *The American Journal of Forensic Medicine and Pathology* **2008**, *29*, 93-98
(2) Lardner, G.; Adams, L. In *Washington Post*, 1996.
(3) ATF. 2011.
(4) Beveridge, A. In *International Forensic Science and investigation Series*; CRC Press, 2011, p 792.
(5) Midkiff, C. In *Forensic Science Handbook*, Saferstein, R., Ed.; Prentice Hall, 2002.
(6) Marshall, M.; Oxley, J. *Aspects of Explosives Detection*; Elsevier: New York, 2009.
(7) Yinon, J. In *Advances in Forensic Applications of Mass Spectrometry*, J, Y., Ed.; CRC Press: New York, 2004, pp 243-286.
(8) Taylor, G. I. *Scientific Papers* **1944**, *3*, 387-390.
(9) Al-Hassani, S. T. S.; Hopkins, H. G.; Johnson, W. *International Journal of Mechanical Sciences* **1969**, *11*, 545-549.
(10) Hoggatt, C. R.; Recht, R. F. *Journal of Applied Physics* **1968**, *39*, 1856-1862.
(11) Anderson, C. E.; Predebon, W. W.; Karpp, R. R. *International Journal of Engineering Sciences* **1985**, *23*, 1317-1330.
(12) Taylor, G. I. *Scientific Papers* **1941**, 277-286.
(13) Beveridge, A. In *Forensic Science Series*; Taylor and Francis: Bristol, PA, 1998.
(14) 01.80:2011[E], I., Formulae for Ammunition Management; UNODA 2011.
(15) Oxley, J. C.; Smith, J. L.; Resende, E.; Rogers, E.; Strobel, R. A.; Bender, E. C. *Journal of Forensic Sciences* **2001**, *46*, 510-534.
(16) R. Dean, M. R. E. *Practical Failure Analysis* **2002**, *2*, 33-40.
(17) Held, M.; Kuhl, P. *Propellants and Explosives* **1976**, *1*, 20-23.
(18) Graham A. Walsh, O. T. I., Van D. Romero. *Journal of Forensic Sciences* **2003**, *48*, 945-960.
(19) Otto Gregory, J. O., James Smith, Michael Platek, Hamouda Ghonem, Evan Bernier, Markus Downey, Christopher Cumminskey. *Materials Characterization* **2010**, *61*, 347-354.
(20) Germain, Y. *Polymer Engineering & Science* **1998**, *38*, 657-661.
(21) Merah, N.; Saghir, F.; Khan, Z.; Bazoune, A. *Plastics, Rubber and Composites* **2006**, *35*, 226-230.
(22) Merah, N.; Al-Qahtani, T.; Khan, Z. *Plastics, Rubber and Composites* **2008**, *37*, 353-358.
(23) Merah, N.; Irfan-ul-Haq, M.; Khan, Z. *Journal of Materials Processing Technology* **2003**, *142*, 247-255.

(24) McAbee, E.; Chmura, M. *Journal of Applied Polymer Science* **1964**, *8*, 3-24.(25) Rainey, C. L.; Bors, D. E.; Goodpaster, J. V. *Analytical Chemistry* **2014**, *86*, 11319-11325.
(26) 2008, p Weather History: Past Weather Reports.
(27) Bors, D.; Cummins, J.; Goodpaster, J. *Journal of Forensic Sciences* **2014**, *59*, 42-51.
(28) Pawliszyn, J. *Solid Phase Microextraction Theory and Practice*; Wiley-VCH, Inc: Canada, 1997.
(29) Pawliszyn, J. *Applications of Solid Phase Microextraction*; The Royal Society of Chemistry, 1999.
(30) Zhang, Z.; Pawliszyn, J. *Analytical Chemistry* **1993**, *65*, 1843-1852.
(31) Zhang, Z.; Yang, M. J.; Pawliszyn, J. *Analytical Chemistry* **1994**, *66*, 844A-853A.
(32) Kolb, B.; Ettre, L. *Static Headspace-Gas Chromatography*; Wiley-VCH, 1997.
(33) Hu, H.-C.; Chai, X.-S. *Journal of Chromatography A* **2012**, *1222*, 1-4.
(34) Li, H.; Chai, X.-S.; Deng, Y.; Zhan, H.; Fu, S. *Journal of Chromatography A* **2009**, *1216*, 169-172.
(35) Schuberth, J. *Journal of Chromatographic Science* **1996**, *34*, 314-319.
(36) Ochiai, N.; Sasamoto, K.; Hoffmann, A.; Okanoya, K. *Journal of Chromatography A* **2012**, *1240*, 59-68.
(37) Haddadi, S. H.; Niri, V. H.; Pawliszyn, J. *Analytica chimica acta* **2009**, *652*, 224-230.
(38) Guo, J.; Jiang, R.; Pawliszyn, J. *Journal of Chromatography A* **2013**, *1307*, 66-72.
(39) Martendal, E.; Carasek, E. *Journal of Chromatography A* **2011**, *1218*, 1707-1714.
(40) Staerk, U.; Kulpmann, W. R. *J Chromatogr B Biomed Sci Appl* **2000**, *745*, 399-411.
(41) Robertson, J.; Grieve, M. *Forensic Examination of Fibres*; CRC Press, 1999.
(42) Sinnott, R. K. *Chemical Engineering Design: Chemical Engineering*; Elsevier Science, 2005.
(43) Bezerra, M. A.; Santelli, R. E.; Oliveira, E. P.; Villar, L. S.; Escaleira, L. A. *Talanta* **2008**, *76*, 965-977.
(44) Stalikas, C.; Fiamegos, Y.; Sakkas, V.; Albanis, T. *Journal of Chromatography A* **2009**, *1216*, 175-189.
(45) Vera-Candioti, L.; Gil García, M. D.; Martínez Galera, M.; Goicoechea, H. C. *Journal of Chromatography A* **2008**, *1211*, 22-32.
(46) Montgomery, D. *Design and Analysis of Experiments*, 6 ed.; John Wiley & Sons, Inc., 2005.
(47) Bradley, N. *The Response Surface Methodology*. Indiana University2007.
(48) Lai, H.; Leung, A.; Magee, M.; Almirall, J. *Anal Bioanal Chem* **2010**, *396*, 2997-3007.
(49) Kirkbride, K. P.; Klass, G.; Pigou, P. E. *Journal of Forensic Sciences* **1998**, *43*, 76-81.
(50) Chang, K. H.; Yew, C. H.; Abdullah, A. F. L. *Journal of Forensic Sciences* **2014**, *59*, 1100-1108.
(51) Kranz, W.; Kitts, K.; Strange, N.; Cummins, J.; Lotspeich, E.; Goodpaster, J. *Forensic Sci. Int.* **2014**, *236*, 157-163.
(52) Kranz, W. D.; Strange, N. A.; Goodpaster, J. V. *Analytical and Bioanalytical Chemistry* **2014**, *406*, 7817-7825.

(53) Furton, K. G.; Myers, L. J. *Talanta* **2001**, *54*, 487-500.(54) Lorenzo, N.; Wan, T.; Harper, R. J.; Hsu, Y.; Chow, M.; Rose, S.; Furton, K. *Analytical and Bioanalytical Chemistry* **2003**, *376*, 1212-1224.
(55) Harper, R. J., J.R. Almirall, and K.G. Furton. *Talanta* **2005**, *67*, 313-327.
(56) Barshick, S.-A.; Griest, W. H. *Analytical Chemistry* **1998**, *70*, 3015-3020.
(57) Monteil-Rivera, F.; Beaulieu, C.; Hawari, J. *Journal of Chromatography A* **2005**, *1066*, 177-187.
(58) Calderara, S.; Gardebas, D.; Martinez, F. *Forensic science international* **2003**, *137*, 6-12.
(59) Ahmad, U. K.; Kiu, K. H. *Jurnal Teknologi* **2012**, *46*, 59–74.
(60) Furton, K. G.; Wu, L.; Almirall, J. R. *Journal of Forensic Sciences* **2000**, *45*, 857-864.
(61) Beveridge, A. *Forensic Investigation of Explosions, Second Edition*; Taylor & Francis, 2011.
(62) TWGFEX. In *Recomended Guidelines For Indetification of Post-Blast Explosives Residue*, 2007.
(63) TWGFEX. In *Recomended Guidlines for Forensic Identification of Intact Explosives*, 2007, pp 1-4.
(64) Furton, K. G.; Wang, J.; Hsu, Y.-L.; Walton, J.; Almirall, J. R. *Journal of Chromatographic Science* **2000**, *38*, 297-306.
(65) Burleson, G. L.; Gonzalez, B.; Simons, K.; Jorn, C. *Journal of Chromatography A* **2009**, *1216*, 4679-4683.
(66) Wu, L.; Almirall, J. R.; Furton, K. G. *J. High Resol. Chromatogr.* **1999**, *22*, 279-282.
(67) Bender, E. C.; Beveridge, A. In *Forensic Investigation of Explosions*, Beveridge, A., Ed.; CRC Press: Boca Raton, 2012, pp 429-491.
(68) Mathis, J. A.; McCord, B. R. *Forensic Science International* **2005**, *154*, 159-166.
(69) Muller, D.; Levy, A.; Vinokurov, A.; Ravreby, M.; Shelef, R.; Wolf, E.; Eldar, B.; Glattstein, B. *Journal of forensic sciences* **2007**, *52*, 75-78.
(70) Hopper, K. G.; McCord, B. R. *Journal of forensic sciences* **2005**, *50*, 307-315.
(71) Bors, D.; Cummins, J.; Goodpaster, J. *Journal of forensic sciences* **2014**, *59*, 42-51.
(72) Bors, D.; Cummins, J.; Goodpaster, J. *Forensic Science International* **2014**, *234*, 95-102.
(73) Furton, K. G.; Almirall, J. R.; Bi, M.; Wang, J.; Wu, L. *Journal of Chromatography A* **2000**, *885*, 419-432.
(74) Bors, D.; Cummins, J.; Goodpaster, J. *J Forensic Sci* **2014**, *59*, 42-51.
(75) Bors, D.; Cummins, J.; Goodpaster, J. *Forensic Sci. Int.* **2014**, *234*, 95-102.
(76) Kapur, G. B.; Hutson, H. R.; Davis, M. A.; Rice, P. L. *Journal of Trauma and Acute Care Surgery* **2005**, *59*, 1436-1444.
(77) Lordel-Madeleine, S.; Eudes, V.; Pichon, V. *Anal Bioanal Chem* **2013**, *405*, 5237-5247.
(78) Stambouli, A.; El Bouri, A.; Bouayoun, T.; Bellimam, M. A. *Forensic Science International* **2004**, *146, Supplement*, S191-S194.
(79) Smith, K. D.; McCord, B. R.; MacCrehan, W. A.; Mount, K.; Rowe, W. F. *Journal of forensic sciences* **1999**, *44*, 789-794.

(80) TWGFEX. *Recommended Guidelines for Forensic Identification of Post-Blast Explosive Residues* **2009**.
(81) Bors, D.; Goodpaster, J. *Analytical Methods* **2015**, *7*, 9756-9762.
(82) Dean, R.; Edwards, M. *Practical Failure Analysis* **2002**, *2*, 33-40.
(83) Lotspeich, E.; Kitts, K.; Goodpaster, J. *Forensic science international* **2012**, *220*, 130-134.
(84) Alwis, K. U.; Blount, B. C.; Silva, L. K.; Smith, M. M.; Loose, K.-H. *Environmental science & technology* **2008**, *42*, 2522-2527.
(85) Takeuchi, A.; Nishimura, Y.; Kaifuku, Y.; Imanaka, T.; Natsumeda, S.; Ota, H.; Yamada, S.; Kurotani, I.; Sumino, K.; Kanno, S. *Journal of occupational health* **2010**, *52*, 194-197.
(86) Moreira, L.; d'Avila, L.; Azevedo, D. *Chromatographia* **2003**, *58*, 501-505.
(87) Balabin, R. M.; Safieva, R. Z.; Lomakina, E. I. *Analytica Chimica Acta* **2010**, *671*, 27-35.
(88) Zoccolillo, L.; Alessandrelli, M.; Felli, M. *Chromatographia* **2001**, *54*, 659-663.
(89) 1967.
(90) Jones, D.; Kemister, G., Safety Distance Calculations for Multi-Item Fragmenting Munitions; DTIC Document1997.
(91) Sperrazza, J.; Kokinakis, W. *Annals of the New York Academy of Sciences* **1968**, *152*, 163-167.
(92) Z Takats, J. W., B Gologan, RG Cooks. *Science* **2004**, *306*, 471-473.
(93) Cotte-Rodríguez, I.; Takáts, Z.; Talaty, N.; Chen, H.; Cooks, R. G. *Analytical Chemistry* **2005**, *77*, 6755-6764.
(94) Cotte-Rodríguez, I.; Cooks, R. G. *Chemical Communications* **2006**, 2968-2970.
(95) Justes, D. R.; Talaty, N.; Cotte-Rodriguez, I.; Cooks, R. G. *Chemical Communications* **2007**, 2142-2144.

VITA

VITA

Dana Bors, Ph.D.
Purdue University

Education:

Doctorate of Philosophy in Analytical Chemistry, IUPUI, 2015
- GPA: 3.964
- Advisor: John V. Goodpaster

Bachelor of Science in Forensic Chemistry, Thomas More College, 2011
- GPA: 3.6 *cum laude*

Employment:

PhD Candidate, Indiana University Purdue University Indianapolis, Indianapolis, IN
- Perform research on multiple projects: analyze pipe bomb fragmentation patterns based on ambient temperature, container type, and explosive filler; analyze post-blast explosive residue on pipe bomb fragments; develop instrumental methods
- Analyze racing fuels and track adhesives for regulatory compliance and safety (sponsored by the National Hot Rod Association)
- Gain universally practiced laboratory skills and efficiency using instrumental methods such as gas chromatography/mass spectrometry, liquid chromatography/mass spectrometry, infrared spectroscopy, UV/visible spectroscopy, Raman spectroscopy, and microspectrophotometry

Physical Science Technician, US Environmental Protection Agency, Cincinnati, OH
- Gained experience on various instruments: gas chromatograph-tandem mass spectrometer and liquid chromatograph- tandem mass spectrometer
- Performed solid phase extraction on large river water and effluent sample sets as part of an ongoing national study
- Assessed stream habitats in the field and graphically modeled the East Fork Watershed

Laboratory Intern, Northern Regional Forensic Laboratory, Cold Spring, KY

- Analyzed illicit drugs, blood alcohol samples, and biological specimens
- Followed proper chain of custody and evidence handling protocols
- Observed expert witness testimony

Activities and Honors:

- IUPUI Dept. of Chemistry and Chemical Biology Graduate Dissertation Award (2015)
- Graduate Assistance in Areas of National Need Fellowship (2013-2015)
- IUPUI School of Science Graduate Student Council Travel Grant (2013)
- Charles B'Hymer Chemistry Scholarship (2009-2011)
- TMC Chemistry Club Secretary (2010-2011)
- TMC Leadership Award (2008-2011)
- Member of TMC Softball Athletics (2007-2011)
- President's Athletic Conference Softball Player of the Year (2009)
- Member of TMC Women's Basketball Athletics (2007-2011)
- TMC Scholar Athlete (2007-2011)

Teaching Experience:

- Mentor for ACS Project SEED high school student, June 2014 - July 2014
- Instructor for General Chemistry II lab, January 2014 – May 2014
- Instructor for Forensic Chemistry I lab, August 2013 – December 2013
- Instructor for General Chemistry I lab, January 2013 – May 2013
- Instructor for Instrumental Analysis lab, August 2011 – December 2011

Research Presentations:

February 2015: American Academy of Forensic Science National Meeting
Oral: "Quantitative mapping of post-blast nitroglycerin residues on pipe bomb fragments using total vaporization solid phase microextraction-gas chromatography/mass spectrometry (TV-SPME-GC/MS)"

December 2014: IUPUI Department of Chemistry and Chemical Biology Annual Poster Session

Poster: "Quantitative Mapping of Post-Blast Nitroglycerin Residues on Galvanized Pipe Bomb Fragments Using Total Vaporization Solid Phase Microextraction-Gas Chromatography/Mass Spectrometry (TV-SPME-GC/MS)"

September 2014: Purdue University Center for Analytical Instrument Development 7th Annual Workshop: Instrumentation for Forensics, Nanoscience, and Pharmaceutical Science

Lab Co-Leader: "Analysis of Pipe Bomb Fragments Using DESI-MS"

March 2014: IUPUI Women in STEM Poster Session

Poster: "Quantitative Mapping of Post-Blast Nitroglycerin Residues on Pipe Bomb Fragments Using Total Vaporization Headspace (TV-HS) Solid Phase Microextraction-Gas Chromatography/Mass Spectrometry (SPME-GC/MS)"

February 2014: American Academy of Forensic Science National Meeting

Poster: "Quantitative Mapping of Post-Blast Nitroglycerin Residues on Pipe Bomb Fragments Using Total Vaporization Headspace (TV-HS) Solid Phase Microextraction-Gas Chromatography/Mass Spectrometry (SPME-GC/MS)"

September 2013: American Chemical Society National Meeting

Poster: "Quantitative Mapping of Post-Blast Nitroglycerin Residues on Pipe Bomb Fragments Using Solid Phase Microextraction-Gas Chromatography/Mass Spectrometry (SPME-GC/MS)"

November 2012: IUPUI Department of Chemistry and Chemical Biology Annual Poster Session

Poster: "The Anatomy of a Pipe Bomb Explosion: Measuring the Mass and Velocity Distributions of Container Fragments"

Publications:

Bors D, Goodpaster J. Mapping Explosive Residues on Galvanized Pipe Bomb Fragments Using Total Vaporization Solid Phase Microextraction (TV-SPME). Anal Meth. 2015; submitted.

Rainey C, Bors D, Goodpaster J. Design and Optimization of a Total Vaporization Technique Coupled to Solid-Phase Microextraction. Anal Chem.2014;86.22:11319-11325.

Bors D, Cummins J, Goodpaster J. The Anatomy of a Pipe Bomb Explosion: The Effect of Explosive Filler, Container Material and Ambient Temperature on Device Fragmentation. Forensic Sci Int. 2014;234:95-102.

Bors D, Cummins J, Goodpaster J. The Anatomy of a Pipe Bomb Explosion: Measuring the Mass and Velocity Distributions of Container Fragments. J Forensic Sci. 2014;59:42-51.